

MASTER OF SCIENCE BY RESEARCH

Mechatronics design and control of radiotherapy phantom

Augusciak, Marek

Award date:
2011

Awarding institution:
Coventry University

[Link to publication](#)

General rights

Copyright and moral rights for the publications made accessible in the public portal are retained by the authors and/or other copyright owners and it is a condition of accessing publications that users recognise and abide by the legal requirements associated with these rights.

- Users may download and print one copy of this thesis for personal non-commercial research or study
- This thesis cannot be reproduced or quoted extensively from without first obtaining permission from the copyright holder(s)
- You may not further distribute the material or use it for any profit-making activity or commercial gain
- You may freely distribute the URL identifying the publication in the public portal

Take down policy

If you believe that this document breaches copyright please contact us providing details, and we will remove access to the work immediately and investigate your claim.

MECHATRONICS DESIGN AND CONTROL OF RADIOTHERAPY PHANTOM

by
Marek Augusciak

Coventry, April 2011



The work contained within this document has been submitted
by the student in partial fulfilment of the requirement of their course and award

Coventry University
Faculty of Engineering and Computing
Control Theory and Application Centre

**MECHATRONICS DESIGN
AND CONTROL
OF RADIOTHERAPY PHANTOM**

by
Marek Augusciak

Project Supervisor: Dr Olivier CL Haas

*A thesis submitted in partial fulfilment of the University's requirements
for the Degree of Master of Science by Research in Control Engineering*

Coventry, April 2011

Contents

Contents	I
List of Symbols and Abbreviations	IV
List of Figures	VI
List of Tables	X
List of Equations	XI
Acknowledgments	XII
Abstract	XIII
Chapter 1 Introduction	1
1.1 Introduction to the cancer issue	1
1.2 The radiation therapy fundamentals	2
1.3 Aims and objectives	4
1.4 Deliverables	6
1.5 Outline of approach	7
Chapter 2 Dynamic thorax phantom	8
2.1 Lung tumour motion in radiotherapy	8
2.1.1 Tumour motion – range	9
2.1.2 Tumour motion – speed	10
2.1.3 Tumour motion – simulation patterns	11
2.2 Review of phantoms for RT	14
2.2.1 Review of existing phantoms for lung cancer treatment.	14
2.2.2 Limitations of the existing phantoms	24

2.3	The MAESTRO phantom	25
2.3.1	Desirable attributes for and ART phantom	25
2.3.2	The RT thorax phantom design of the MAESTRO project	25
2.3.3	Thorax phantom operating principles	28
2.3.4	Limitations	32
2.4	Conclusions	33
Chapter 3 LabVIEW Motion Control of Radiation Therapy Phantom		35
3.1	Resources for stepper motor control – electrical design and LabVIEW implementation	35
3.1.1	LabVIEW software environment	36
3.1.2	Data acquisition hardware	37
3.1.3	Stepper motor drives	40
3.1.4	Sequence control	41
3.1.5	Bi-polar stepper motor control	43
3.2	Sequence motion control	45
3.2.1	Hardware components	45
3.2.2	Program description – diagram, explanation of program	45
3.3	Frequency motion control	59
3.3.1	Used hardware	59
3.3.2	Program description - diagram, explanation of the program	60
3.3.3	Evaluation of motor drive implementations	64
3.4	Video tracking of the thorax phantom motion	71
3.4.1	Used hardware	72
3.4.2	The program description.	74
3.5	Difficulties associated with LabVIEW programming	79
3.6	Conclusions	80
Chapter 4 Experimental evaluation		81
Chapter 5 Propositions to the thorax phantom development		87

5.1	Propositions of rib-cage lateral movement	87
5.2	Improvement of mechanical phantom's protection	92
5.3	Suggestion of the rod redesigning and X-ray sensor's shaking reduction.	93
5.4	Proposal of the unification stand for CCD camera	96
5.5	Facility calibration of the camera for video tracking system	98
5.6	Safety implementation against stepper motors overheating	98
Chapter 6 Conclusions and future work		100
Chapter 7 References		103
Chapter 8 Appendices		107
Appendix 1	Program code – motion control by frequency modulated signal	109
Appendix 2	Program code – motion control by sequence signal	116
Appendix 3	High performance size 23 hybrid stepper motors of the HSX series	121
Appendix 4	MSE570 Evo2; Bi-polar 3.5 [A] stepper motor drive	124
Appendix 5	NI M Series multifunction DAQ for USB 6229	130
Appendix 6	NI DAQ Card PCI-6229	134
Appendix 7	NI DAQ Card 6024E (for PCMCIA)	138
Appendix 8	NI SC 2075 Connector Card	142
Appendix 9	IEEE1394a Digital CCD Camera FOculus FO124TB	143
Appendix 10	ICSE 2009 conference paper.	145
Appendix 11	ICSE 2009 conference – poster	151

List of Symbols and Abbreviations

3D	three dimensions of movement XYZ axis
4D	four dimensions, three dimensions of movement XYZ axis and time T
AI	Analogue Input
AO	Analogue Output
AP	Anterior-Posterior
ART	Adaptive Radiation Therapy
CCD	Charge Coupled Device - image sensor convert light into electrons
CMOS	Complementary Metal Oxide Semiconductor - image sensor
CT	computed tomography
CTAC	Control Theory and Application Centre
DI	Digital Input
DIO	Digital Input /Output
DO	Digital Output
DOF	degree of freedom, e.g. 1DOF, 2DOF, 3DOF
F	'false' or logical '0', binary signal
IEC	International Electro-technical Commission
IGRT	Image-Guided Radiation Therapy
IMRT	Intensity-Modulated Radiation Therapy
LabVIEW	Laboratory Virtual Instrumentation Engineering Workbench, software developed by National Instruments
LH	left hand side
Linac	linear accelerator
LR	Lateral
MAESTRO	Methods and Advanced Equipment for Simulation and Treatment in Radiation Oncology
MRI	Magnetic Resonance Imaging
NI	National Instruments
PET	Positron Emission Tomography

PSS	Patient Support System
RH	right hand side
RT	Radiation Therapy, Radiotherapy
SI	Superior-Inferior
subVI	executable LabVIEW subprogram
T	'true' or logical '1', binary signal
UHCW	University Hospitals Coventry and Warwickshire
USB	Universal Serial Bus
VI	executable LabVIEW program
WP	Work Package
WP1	Work Package No.1
$\in \mathbb{N}$	an element of the set Natural numbers
$\in \mathbb{R}$	an element of the set Real numbers
$\in \mathbb{Z}$	an element of the set Integer numbers

List of Figures

Figure 2.1	The layout of motion direction of the thorax and internal organs, and related Cartesian coordinate system.	9
Figure 2.2	The breathing measurement from Shirato real patient data.	12
Figure 2.3	First 4 cycles of breathing measurement from Shirato (2006) data and estimated Lujan wave.....	13
Figure 2.4	Phantom built up by Jiang et al. (2003).....	15
Figure 2.5	The movable irregular breathing platform. Phantom developed by Fitzpatrick et al. (2005).	16
Figure 2.6	In-house quality assurance phantom by Hugo et al. (2002).	17
Figure 2.7	The phantom expanded by Zhou et al. (2004).	17
Figure 2.8	The breathing phantom, PULMONE. Treatment setup.....	18
Figure 2.9	A) The RPC thorax phantom with insertions includes the lungs, heart, and spinal cord, B) example of experimental set up made by researcher of the University of Texas Southwestern Medical Center at Dallas.	18
Figure 2.10	The IMRT dynamic thorax phantom built by CIRS - Model 008	19
Figure 2.11	A) The respiratory motion phantom QUASAR, B) optional insert with film and marker (Modus Medical Devices Inc., 2009).	20
Figure 2.12	The RPC thoracic phantom (The Radiology Support Device Inc., 2008).	20
Figure 2.13	The anthropomorphic MAESTRO thorax phantom and major parts (Land, 2009).....	26
Figure 2.14	Tumour movement phases during RT treatment without displacement's compensation by patient support system (PSS).	29
Figure 2.15	Experimental set-up illustration. The machine for radiotherapy treatment and PSS, phantom, camera video tracking and used coordinate system..	30
Figure 2.16	Set up of the thorax phantom model placed on the PSS couch. Preparation to the tests of the complex compensation system.....	31

Figure 2.17 Patterns of phantom respiratory motion simulated alternatively by: a) Sinusoidal wave, b) Lujan model, c) Irregular model, d) Data from patients measurements.....	32
Figure 3.1 Diagram of electrical motion systems: sequence motion control and motion control by frequency modulation.	36
Figure 3.2 I/O card: NI PCI-6024E and NI SC-2075 data acquisition module (National Instruments Corporation, 2011).	38
Figure 3.3 Decoder of the control signal for full stepper sequence: a) with NAND and NOT gates, b) alternative decoder based on EX-OR, NOT and AND gates.....	38
Figure 3.4 I/O card: NI USB-6229 data acquisition module (National Instruments Corporation, 2011).	39
Figure 3.5 Electrical cable connection (McLennan Servo Suppliers Ltd, 2009).	40
Figure 3.6 Typical performance – torque in function of angular speed (McLennan Servo Suppliers Ltd, 2009).	41
Figure 3.7 MSE570 Evo2 bi-polar stepper motor drive: a) card, b) experimental set-up during tests.	43
Figure 3.8 Set of the Current Limiter unit (upper) with Stepper Motor Drive (below).	45
Figure 3.9 Front panel of the existing program designed by PHD student (Land, 2009).	47
Figure 3.10 Front panel of the in real time working program.	49
Figure 3.11.a) Sequence motion control code – diagram.....	51
Figure 3.12 The 8 channels DO task creation with low-level functions use. Block diagram.....	53
Figure 3.13 Spreadsheet file use to read motion pattern data. Block diagram.....	54
Figure 3.14 Restoring parameters of last one position. Block diagram.	54
Figure 3.15 Set of constants and controllers for all stepper motors. Block diagram.....	55
Figure 3.16 Arrays of coded sequences for Z-axis (other axes were set as zero); the lower array represents reverse rotation.	55
Figure 3.17 Frequency of the LabVIEW code execution. Block diagram.	55
Figure 3.18 Turning ON/OFF of the stepper motors function. The users interface (LH) and block diagram (RH).....	56
Figure 3.19 The sine waveform generator; block diagram.	56
Figure 3.20 Steps synchronisation and sequence sending to DO.....	57

Figure 3.21 Comparison sizes proportion of two drivers: set of the Current limiter (upper) with Stepper motor drive to the new Card MSE570 Evo 2.....	59
Figure 3.22 Laboratory version of extending electronic board for bi-polar card.....	59
Figure 3.23 Front panel of the program used to generate phantom motion (Tassot A.).	60
Figure 3.24 Front panel of the program used to generate phantom motion.....	61
Figure 3.25.b) Frequency motion control of the phantom – diagram.....	66
Figure 3.26 The Counter Output creation with low-level functions use.....	67
Figure 3.27 Spreadsheet file used to read motion pattern data. Block diagram.	68
Figure 3.28 Set of constants and controllers for all stepper motors. Block diagram.....	69
Figure 3.29 The IEEE1394 camera and software for video tracking two targets.....	72
Figure 3.30 The calibration grid for the video tracking system with dot diameter equals 4[mm] and distance =9.5[mm] between.....	73
Figure 3.31 Marker samples of different size and contrast threshold.	74
Figure 3.32 Block diagram of the image tacking code.	75
Figure 3.33 User interface of the video tracking. Lost target visualisation.....	77
Figure 3.34 Elimination of the targets error. If false – send actual measurements, if true – send previous data. Block diagram.	78
Figure 4.1 The stepper motor with current limiter and power supply units.	81
Figure 4.2 Testing of the frequency motion control code with GW oscilloscope use...	82
Figure 4.3 The error identification with Tektronix oscilloscope use.....	82
Figure 4.4 <i>Structure of the overall control system including the phantom with markers positioned onto it being tracked by a camera. A motion predictor anticipates the motion of the markers and is used by a controller to move the PSS.</i>	83
Figure 4.5 Typical set-up for thorax phantom prototype tests.	84
Figure 4.6 Outcome of phantom and PSS controller tests.	85
Figure 4.7 VERO experimental set-up.....	86
Figure 5.1 The rib-cage lateral expansion visualisation.....	88
Figure 5.2 The thorax phantom model – bottom view.	88
Figure 5.3 Possible types of the pattern movement regulated by shaped slope.	89
Figure 5.4 The illustration of the mechanism operating principle.....	90
Figure 5.5 Top view of the rib-cage and marked by red lines the saw-tooth beam position.....	90
Figure 5.6 The illustration of strategic change points location.....	91
Figure 5.7 The rib-cage side wall model.	91

Figure 5.8 Initially designed rod and X-ray sensor's holder.....	93
Figure 5.9 The moment of inertia J_z determination: a) general beam model; b) the beam section.	94
Figure 5.10 Changed and actual sensor holder of the tumour drive unit.....	96
Figure 5.11 Previously used tripod for CCD camera holding.	96
Figure 5.12 The example of the camera stand manufactured by Manfrotto (36).....	97
Figure 5.13 The CCD camera mounted to base plate.....	97

List of Tables

Table 2.1.a	Review of phantom for IMRT research.	22
Table 2.1.b	Review of phantom for IMRT research	23
Table 2.2	The listing of the parameters of substitute materials for specified body parts (Land, 2009).	27
Table 2.3	Mechanical properties of thorax phantom movement.....	28
Table 3.1	Table of logical states to reduce number of the digital outputs (DO).....	39
Table 3.2	Table of stepper motor sequences.....	41
Table 3.3	Mechanical properties of the thorax phantom design.	42
Table 3.4	Organisation of the thorax phantom control as a function of the type of control and hardware used.	44
Table 3.5	Movement types of the program for frequency motion control.....	63
Table 5.1	The moment of inertia equation examples in relation to shape of the section.....	95

List of Equations

Equation 2.1	Sinusoidal waveform.....	11
Equation 2.2	Lujan breathing pattern.....	11
Equation 2.3	Irregular respiratory pattern.....	12
Equation 3.1	Computation of the rib-cage steps number per millimetre.....	57
Equation 3.2	Steps number per millimetre computation for tumour X, Y, Z axis.	57
Equation 3.3	The frequency computation.....	70
Equation 5.1	Moment of bending.....	94

Acknowledgments

The work presented in this master thesis was undertaken at the Control Theory and Application Centre (CTAC) at Coventry University and at the University Hospital Coventry and Warwickshire UHCW, NHS Trust (UHCW), Coventry. I have discovered these surroundings a very inspiring and I would like to express my gratitude all the people that helped me during my graduate.

The particularly gratitude I am addressing to Dr Olivier C.L. Haas, my supervisor for his establishment and research guidance.

Also I want to thank my colleagues Mr Daniel Paluszczyzyn and Mr Mariusz Ruta, for their assistance and support during research, for knowledge and cogent advices.

The overwhelmingly gratitude goes onto Prof Keith Burnham hands, the CTAC director for his unusually welcome at Coventry University and guiding through history of Coventry.

I would like to express my appreciation Dr John Mills, Dave Gill and Bob Crichton at University Hospital Coventry and Warwickshire, for all their plentiful help and kindness.

Finally, an extraordinary gratitude is dedicated to my wife Katarzyna for an extraordinary patience, support and interminable encouragement, and to my daughter Anna Helena for being my source of the enormous happiness.

Abstract

New radiotherapy treatment techniques involve complex equipment and procedures requiring the synchronisation of the treatment delivery with the patient breathing motion. To validate the effectiveness of these new radiation dose delivery techniques, new quality control and research equipment are required. Treatments are evaluated, before being delivered to actual patients, using devices referred to, as phantom.

During the MAESTRO project, a phantom was developed to evaluate the motion compensation treatments prototype being developed. The phantom comprises four motors that have to be controlled synchronously. The major part of this work aimed to investigate alternative control method to make the phantom follow required trajectories mimicking tumour and ribs motion. In addition, the sequence control and frequency control was implemented using LabVIEW and specialised drive system connected to one of the phantom motor. The resulting solution was proved accurate but suffered from high operating temperature. An alternative sequence control was also developed to attempt to improve the motor reliability and enable to change the motor velocity interactively. The latter resulted in the development of a new laboratory exercise for MSc teaching.

The second type of contribution was to improve the design and tuning of video tracking systems to address issues associated with varying lighting in the different location used by the MAESTRO team to test the patient support motion compensation system. The re-tuned and modified software was used in the final MAESTRO demonstration.

The third set of contributions was to propose mechanical based practical solutions to first simplify the set-up of video camera at each experiment, to improve the rigidity of the film holder used to mimic a cancerous tumour, and propose means to add a lateral rib motion without any additional motor.

The culmination of the practical work was to take place in the ultimate verification of the proposed patient motion compensation system being responsible for the video tracking system.

Chapter 1

Introduction

1.1 Introduction to the cancer issue

This Chapter presents a brief introduction to radiation oncology and in particular the planning, evaluation and most importantly for the scope of this work the verification of radiotherapy treatments and evaluation of new radiotherapy treatment techniques.

Cancer has an increasingly important impact on the UK population. According to Cancer Research in the UK (2011), 154,162 people died because of cancer in 2006. In 2007, it was estimated that around 43,000 deaths were caused by tobacco smoking, which states over a quarter of cancer deaths. The latest statistics from 2010 are showing that in the UK in 2008, there were 156,723 deaths caused by cancer which is 50% of the population of Coventry (Cancer Research in UK, 2011).

There are 200 recognisable types of cancer but four of them: breast, lung, large bowel and prostate cancer compose over 54% of all new cases. Mortality for those types equals 47% of all people with cancer diseases, where prostate accounts for 6%, breast 8%, bowel 10% and the lung cancer 23%. To save lives of people affected by cancer diseases it is necessary to look for new treatments and ways to modernise known treatments. Nowadays there are many cancer treatments including surgery, radiotherapy, chemotherapy, hormone therapy, immunotherapy, gene therapy or its combination. Unfortunately the knowledge gained to date is still not sufficient to win the battle against cancer. The focus of this work is in the evaluation of new radiotherapy procedure for lung cancer.

1.2 The radiation therapy fundamentals

Radiation Therapy (RT) or radiotherapy is the medical use of high energy X-ray ionizing radiation to treat cancerous cells. Since the beginning of X-radiation discovery, ionizing radiations, referred to as X-rays or Röntgen, have increasingly been used in medicine.

The X-rays radiations, discovered by German physicist Professor Wilhelm Conrad Röntgen, are electromagnetic waves. This phenomenon was recognised on 28th of December, 1895 when it was published in *Sitzungsberichte der Physikalisch-Medizinischen Gesellschaft zu Wurzburg* (French, 1968). After ten days was publicized article in the UK by the *Daily Chronicle* on 6th of January, 1896.

The X-rays are placed on the electromagnetic wave spectrum within a frequency range from 3×10^{16} to 8×10^{23} [Hz] and are emitted by braking electrons or induced atoms. The revolution of X-ray radiation in Europe resulted in many experiments. It was quickly suggested in the *British Medical Journal Nature* (1896) that application of Roentgen radiation in medicine allowed to diagnose bone structure injury.

Active research in radiotherapy resulted in the discovery of polonium and radium in 1898, which emits high-energy gamma rays naturally. The linear accelerator (Linac) of X-ray beam was invented in 1928 by Norwegian physicist Rolf Wideröe (Wideröe, 1928). This provided the means to increase energy of Roentgen generator significantly. A brief review of Linac development history shows that X-ray radiation, emitted by late 1920s generators, only reached 200kV. Substantially developed Linac in the 1950s, provided the means to generate megavoltage [MV] energy around 8 [MV]. Currently Linacs are the most common type of radiotherapy treatment machines. Nowadays a typical Linac for medical applications uses a mono-energetic electron beam with energy range between 2 and 25 [MV] (Siemens, 2010). Computed Tomography (CT) scanning was developed in 1967, magnetic resonance imaging (MRI) in the 1970s, and emission tomography (PET) in the 1980s. In the 1990s the three-dimensional conformal radiotherapy (3D-CRT) (Cancer Research in UK, 2011) was introduced in clinical practice followed by intensity modulated radiotherapy (IMRT) to optimise dose delivery to cancer tumour and minimises irradiation of surrounding healthy tissues. The latest achievement was adaptive radiotherapy (ART) (Cancer Research in UK, 2011).

Adaptive radiotherapy is a novel approach that aims to further improve tumour motion control and protect surrounding healthy tissues. ART focuses on providing more accurate dose delivery to the tumour, through adaptation of the treatment delivery to the actual variations of cancer tumour displacement in patient anatomy. For this reason, ART offers the possibility of dose escalation, and consequently more accurate tumour control during RT treatment.

Nowadays, discoveries and technological developments allow oncologists to precisely target an X-ray beam to the target volume to destroy abnormal cells that grow up and replicate in an unpredictable way.

Unfortunately, it is not a trivial task to calculate the required radiation dose. The adoption of radiotherapy depends on numerous variables such as the shape, volume and depth of the tumour, its overall location in the body, the dose sensitivity of neighbouring organs and tumour displacement due to breathing. The challenge is to balance the negative effects of radiation on healthy tissues whilst maximising their therapeutic effects on cancerous cells. Therefore treatment efficiency is never 100%. Such issue associated with radiotherapy has still not been solved, however the detrimental effect of radiation for healthy tissues is taken into account by radiologist to determine the overall effectiveness of radiotherapy cancer treatment. New research focuses on decreasing the detrimental effect of radiation leading to healthy cells destruction. Radiotherapy can be used as an individual treatment to cure cancer, or to reduce cancer before surgery. Nowadays it is often combined with other methods and their complements such as chemotherapy or hormone-therapy, or control symptoms and improves quality of life if the cancer is too advanced to cure.

Cancer treatment depends on its results and is controlled by radiologist with dose delivery and intensity. This treatment can be applied externally or internally, where external RT means cancer irradiation by use of an external X-ray beam, and internal RT or brachytherapy aims on placing the radioactive liquid or other radiation source into the treated cancerous tissue or onto it and located by orally or intravenously method.

Radiotherapy is generally delivered in small fractions over a period of weeks with a pause for regenerations of normal tissues. This fraction of therapy often comprise 30 sessions during more than 6 weeks. Brachytherapy is often used just once or for a very small number of times if needed (Demanes, 2005).

Prior to deciding on a course of treatment it is necessary to identify the location of cancerous tissues and its shape and size by the use of three dimensional (3D) imaging and more recently 4D (3D + time) imaging to visualise tumour volume motion. Usually computed tomography (CT) is used to plan therapy. New radiotherapy treatment procedures that exploit this new 4D information are also being developed to overcome issues associated with patient motion during irradiation and help reduce side effects caused by the irradiation of healthy tissues.

1.3 Aims and objectives

The work described in this thesis was a part of the WP1 of the Framework 6 European Priority Area 1 Life Sciences, Genomics and Biotechnology for Health integrated project on Methods and Advanced Equipment for Simulation and Treatment in Radiation Oncology (MAESTRO) project. This project involved 25 partners, research institutes; oncology centres and manufacturers placed in 14 European countries and began in May 2004 for a 5 years investigation period. The MAESTRO project (2010) aimed to reduce the amount of radiation dose delivered to surrounding areas of the tumour.

The work presented in this dissertation was carried out as a part of the MAESTRO project and oriented on contributing to the ART evaluation by development of a novel, dynamic three dimensional thorax phantom. In addition it involves the tuning and improvement to the LabVIEW based video tracking system, which measures the surrogates' displacement during the experimental work.

The main focus of the work was to improve the phantom control system developed by a previous researcher. The MAESTRO objectives required producing smooth movement controlled by several different signals including "Sine Wave", "Lujan Model", "Irregular Model", "Real Patient Data" with high precision and as close to real time as possible. At the start of the project the phantom was capable of generating all these motion, however some drift and lack of repeatability were observed. It was believed to be due to the LabVIEW implementation of the stepper motors control. To achieve this first aim the following objectives were considered:

- Review existing LabVIEW code
- Investigate open loop stepper motor control strategies
- Implement alternative stepper motor control systems in LabVIEW

- Evaluate the performance of the phantom
- Support the MAESTRO researchers by setting up and operating the phantom during clinical testing of the PSS motion control system at UHCW

The second area of research was to investigate alternative LabVIEW solutions for on-line video tracking with an IEEE1394 camera. This system was applied to measure position and displacement of the markers placed on the thorax phantom. At the start of the project the camera was capable of tracking one target at frame rates between 15 and 25 frames per seconds. In some circumstances loss of tracking occurred or the frame rate decreased. The aim of this part of the work was to support a team of placement students and contribute to developing alternative implementation of the vision tracking system. To achieve this aim the following objectives were investigated:

- Review existing code based on pattern matching
- Investigate alternative video tracking algorithms
- Implement and evaluate video tracking solutions
- Adapt the previously developed method to track two targets simultaneously without slowing down the frame rate too much.
- Support the MAESTRO research team by setting up and operating the vision tracking system during tests at UHCW.

The third area of work was in the field of mechanical design. It arose from the needs identified during the experimental work as well as planned phantom improvements. The planned improvements were to identify a cost effective modification to the rib motion to enable them to move in three dimensions. Unplanned modifications were:

- New camera support design to be used with a standard tripod;
- New target attachment design to hold sensors inserted in the lungs.

A significant part of the work was involved with practical work associated with the experiments carried out at UHCW, where the complex system for image guided radiation therapy was tested, and where the duties were to set up, care and control of the camera video tracking system, and the phantom motion control.

The next Section describes the content of each Chapter which reports on the approach adopted to meet the aims and objectives of the work.

1.4 Deliverables

The work carried out in this project led to the following software deliverables in order of importance:

- Sequence based stepper motor motion control software
- Frequency based stepper motor motion control software
- Improved video tracking software able to detect two targets with different characteristics.
- Identification of Lujan model from measured patient motion

In addition some mechanical components were designed with the first one realised:

- Camera support (realised and used during experiments)
- Target attachment for lung insert
- Three alternative designs to enable 3D rib cage motion

The last type of deliverable was a scientific publication and a web based publication:

- Augusciak M, Haas OCL and Land I, LabVIEW Motion of Radiotherapy Phantom, *XII International Conference on Systems Engineering, ICSE2009*, 8-10 September 2009, Coventry, UK, pp 151-156
- Haas, Olivier C.L., (2010). *Fighting Cancer with Control Theory* - Control Theory Applications Centre (CTAC), CUTV, YouTube, uploaded, 15 Mar 2010: <http://www.youtube.com/watch?v=aUVmGoLEpCI>

The recording of the video reported the last set of tests of the overall couch based motion management system developed in Coventry. These tests took several sessions during which I was either in charge of the phantom software or the image tracking software. The most important session, from the MAESTRO project perspective, was the demonstration of the MAESTRO phantom, tracking and motion compensation system to all the MAESTRO partners on the 15 Sept 2009.

1.5 Outline of approach

This thesis comprises six chapters and is organised as follows:

Chapter 2 reviews existing literature involving research and commercial products to evaluate radiotherapy treatment delivery, and describes the general background of the research. It starts with a review of information about tumour motion behaviour along the lungs volume and resultant measurements based on average patients. It is followed by a review of relevant scientific and commercial thorax phantoms used in radiotherapy cancer treatment. Alternative solutions for the control of the stepper motor are then presented. Finally, the dynamic thorax phantom in RT developed during the MAESTRO is described in terms of requirements, design operating principles, advantages and limitations.

Chapter 3 describes the Motion Control of Radiation Therapy Phantom programmed with NI LabVIEW software. It starts with an explanation of the aims of motion control and the hardware utilised. The chapter is divided into two main subsections: frequency motion control and sequence motion control. The developed programs are described and their principle of operation demonstrated. The chapter concludes with a discussion on the relative advantages and disadvantages of the proposed control schemes.

Chapter 4 describes the use of the phantom and the video tracking program during experiments at UHCW.

Chapter 5 describes and suggests some ideas to modify and improve the thorax phantom including proposals that have been realised.

Chapter 6 presents the overall conclusions and further work related to the thorax phantom design and video tracking system.

Chapter 2 Dynamic thorax phantom

Having introduced issues related to current cancer treatments, this Chapter will focus on the means to evaluate radiotherapy treatment in the context of motion management.

The Chapter starts with a presentation of typical surrogate motion in the lung and shows how existing models can be tuned to fit the data. Having evaluated the different types of motion, which should be replicated by a phantom, the next stage reviews existing phantom designs. An in depth description of the MAESTRO phantom developed is then given as it forms the basis of this work.

The initial requirements for the MAESTRO phantom are reviewed and specific requirements to this work are identified in subsection 2.3.2 below. It includes a description of the MAESTRO thorax phantom and its operating principles.

2.1 Lung tumour motion in radiotherapy

Organ motion in RT needs to be known prior to planning treatment where organ and target motion are significant such as in the lungs. To treat lung cancer using radiotherapy it is necessary to know the range and variations of the tumour position that has a significant impact on radiotherapy effectiveness. Taking motion into account enables to increase the amount of irradiation delivered to cancer cells, accelerate cure and decrease X-ray beam influence on nearby healthy tissues.

Many investigations of internal organ motion have been done, where researchers have used different imaging or tracking methods to measure the object displacement inside the lungs, e.g. CT scanning, optical tracking system for external chest motion, spirometry, four dimensional CT scan (Wilbert et al., 2008). The

motion observations have increased the amount of knowledge about tumour volume and its displacement, lung correlation to other organs e.g. diaphragm or heart, and its influence on internal tumour movement.

The thorax phantom was developed to replicate observed target motion within the lungs as well as the ribs motion. The Figure 2.1 indicates the organ movement directions and describes the Cartesian coordinate system, used for the MAESTRO thorax phantom construction.

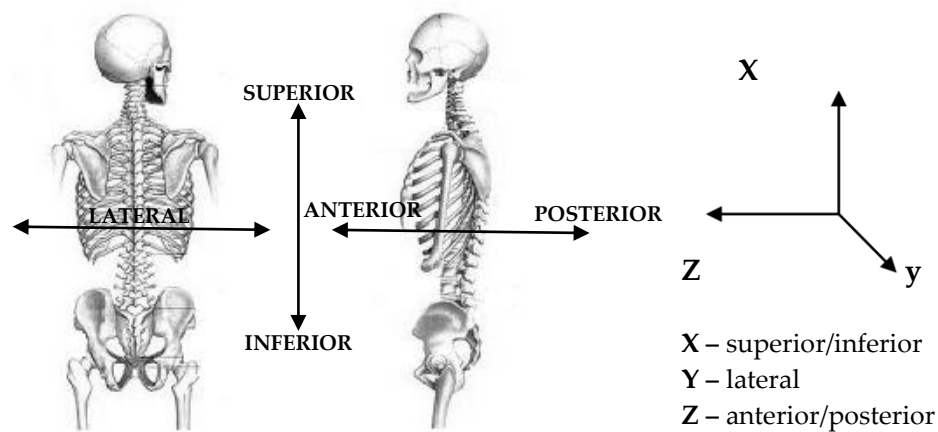


Figure 2.1 The layout of motion direction of the thorax and internal organs, and related Cartesian coordinate system.

2.1.1 Tumour motion – range

Cancerous tumour displacements inside the lungs volume have patient specific pattern. However, research on lung motion and cancer tissues behaviour has enabled researchers to identify typical characteristics. Such information has been exploited to design a device such as the MAESTRO phantom to assess motion management techniques in radiotherapy.

Many tests carried out were notably different. The range of tumour motion identified by Land (2009) was: superior-inferior (SI) direction equals to 31.9[mm], anterior-posterior (AP) equals 28.4[mm] and lateral (LR) direction equals 24.6[mm]. The average and observed period of respiratory cycle was 3.5[s].

These findings were based on a review of respiratory motion and research carried out mainly by Shirato et al. (2006) and Shimizu et al. (2001). Both studies used internal fiducial markers and fluoroscopy technique for tracking displacement and measuring velocity of lung tumour motion on 21 patient samples. Based on these

investigations, it was assumed that tumour displacements in SI direction of respiratory motion cause the most significant movement with amplitude up to 32[mm]. The other directions displacement, were in general lower than max SI, and for the AP the maximum distance was 28.4[mm], and the LR tumour dislocation was respectively up to 24.6[mm]. It is worthy to notice, that some cancerous tumours can have changes even 5[mm] between cycles, which depends on hysteresis inspiration and expiration trajectories (Shirato et al., 2006).

These displacements were rounded up such that superior-inferior, anterior-posterior and lateral directions became 32[mm], 29[mm] and 25[mm] respectively.

In Land (2009), the minimal significant displacement Δ was identified to be not lower than ± 1.8 [mm] to allow an adaptive system to track and deliver an effective treatment. This condition was formulated by the International Electrotechnical Commission (IEC) definition for dose variation at the edge of a field, and the International Commission on Radiation Units and Measurements (ICRU) specifications for the dose variation across a target.

2.1.2 Tumour motion – speed

Respiratory speed depends on age and many other determinants such as breathing by nose or by mouth, weight, physical condition, type of work, nervousness, cough etc. Typical respiratory rates classified by age, are for newborns, 44 breaths per minute (bpm); infants: 40-60 bpm; preschool children: 20–30 bpm; older children: 16–25 bpm; adults: 12–20 bpm; adults during strenuous exercise 35–45 bpm; athletes' peak 60–70 bpm. Note that patients receiving treatments are normally lying down; hence their respiration rate is normally lower than 20 bpm.

Data review of the patient respiratory motion and analysis of the findings with respect to time has identified that typical tumour velocity is 8.7 millimetres per second with maximum speed of 36.4 [mm/s].

Shirato et al. (2006) have reached similar conclusions for a series of 21 patients with median respiratory speed equals to 9.9 ± 5.4 [mm/s] with a minimum speed of 6.6 ± 3.6 [mm/s] and a maximum speed of 21.1 ± 18.9 [mm/s].

According to Benchetrit (2000), breathing speed was determined to be in the range 6 to 31 respiration cycles per minute. Skworcow (2006) computation by use Fourier analysis, based on 350 lung tumour trajectories, achieved following results for breathing period, where mean 4.4 ± 2.8 second ($13.3 \text{ bpm} \pm 21 \text{ bpm}$), median 3.8

second (15 bpm), minimum 2.6 second and maximum 8.5 second. Shirato et al. (2006) reported that the average of the median speed was 9.9 ± 5.4 [mm/s], while the minimal speed was 6.6 ± 3.6 [mm/s], and the average maximal noticed speed was 21.1 ± 18.9 [mm/s]. The period of the breathing cycles was around 3.5 sec meaning that the respiration frequency was approximately 0.28 Hertz.

2.1.3 Tumour motion – simulation patterns

The first type of signal used for motion simulation can be a patient respiratory data collected in the column of a text or spreadsheet e.g. excel file. The trajectory replicated by the MAESTRO phantom were mostly taken from the experimental data collected by George et al., (2006) and analysed in Skworcow (2006).

Currently, the most widely used test signal is based on the Lujan et al. (1999) sinusoidal model with flat bottoms.

The general mathematical equation describing respiratory pattern by sinusoidal wave is:

$$y(t) = A_0 * \sin\left(\frac{\pi * t}{\tau} - \varphi\right) + A_{offset}$$

Equation 2.1 Sinusoidal waveform.

Where A_0 is the amplitude in mm, t is the time in second, τ is the period in second, φ is the starting phase angle in degree and A_{offset} is the offset in mm. Sinusoidal patterns of motion are similar to patient breathing motion. Moreover, it is helpful to have such fluent, symmetric and periodic motion for the phantom testing and development, and it provides good benchmarks for research observations.

However, respiratory motion is not symmetrical. Therefore, Lujan et al. (1999) implemented more adequate pattern modelling lung tumour motion by a mathematical expression including a power term:

$$y(t) = A_0 \cos^{2n}\left(\frac{\pi * t}{\tau} - \varphi\right) + A_{offset}$$

Equation 2.2 Lujan breathing pattern.

where A_{offset} is the offset in mm, A_0 is the amplitude in mm, t is the time in second, τ is the period in second, φ is the starting phase angle in degree, n is a coefficient of breath in/out ratio and an integer parameter $n \in \mathbb{N}$. The crucial advantage, compared

to a sinusoidal signal, is the ability to control of the inhalation-exhalation ratio by n and achieving a pause while exhalation. Typically the n parameter can be between 1 and 3 with an average value of 2 for patients' respiratory motion. Lujan model can be used to simulated realistic rib-cage movement of calm patient with regular breathing.

Because there is a large amount of patients with irregular respiratory pattern, the Lujan formula was modified, to replicate this motion. Thus the breathing pattern was modified according to Equation 2.3,

$$y(t) = (A_0 * \vartheta) * \cos^{2n\rho} \left(\frac{\pi * t}{\tau * \mu} - \varphi \right) + A_{offset}$$

Equation 2.3 Irregular respiratory pattern.

where: ϑ, ρ, μ are randomly chosen variables $\in \mathbb{R}$ from 0 to 1 for each cycle, A_{offset} is offset in mm, A_0 is amplitude in mm, t is the time in second, τ is the period in second, φ is the starting phase angle in degree, n is a coefficient of breath in/out ratio and an integer parameter $n \in \mathbb{N}$.

Taking into account irregularities in the breathing cycles can improve the realism of the trajectory produced. To evaluate the ability of Lujan model to replicate measured motion, the following trajectory from Shirato et al. (2006), see Figure 2.2, was adopted.

This item has been removed due to third party copyright. The unabridged version of this thesis can be viewed at the Lanchester library, Coventry University.

Figure 2.2 The breathing measurement from Shirato real patient data.

The estimation of the best parameters that would match the model given by Equation 2.2 was computed and outcomes were plotted below.

This item has been removed due to third party copyright. The unabridged version of this thesis can be viewed at the Lanchester library, Coventry University.

Figure 2.3 First 4 cycles of breathing measurement from Shirato (2006) data and estimated Lujan wave.

The Figure 2.3 shows fitting of the average model over 4 cycles using Lujan respiration model. The criterion used to identify the model was the minimum of the sum of the absolute values of the error. The error computed was the difference between real patient data and simulated Lujan waveform.

The method adopted to find the model parameters was a form of exhaustive search where each parameter was changed in small step increment and the solution corresponding to the best (according to the absolute value of the error) set of parameter was selected.

The parameters found for the Lujan model were: amplitude $A_0 = 12.1$ [mm], coefficient $n = 2$, and cycle period $\tau = 6.4$ [s]. These parameters are specific to these four cycles and identifying models for other cycles would result in different model parameters. In this work, one of the aims was to obtain a single average model. The typical average and representative pattern of lung tumour movement, based on the Lujan model, was obtained and found to be: amplitude $A_0 = 10$ [mm], coefficient $n = 2$, and cycle period $\tau = 4$ [s].

These parameters, describing the breathing model, were used to control the quality assurance device for radiotherapy treatment which is the MAESTRO thorax phantom, described in the next chapter.

In summary, based mainly on average patient data, the following parameters were used for the thorax phantom control:

- Respiratory cycle 3.5 [s].
- Range of the movement through SI, AP, and LR direction are the maximal obtained values, and equals to 31.9 [mm], 28.4 [mm] and 24.6 [mm] respectively.

The phantom is aimed to be used as a reference device to evaluate a method of radiation dose delivery or to adjust X-ray treatment equipment. Motion accuracy is therefore one of the most important criteria. It is strongly recommended that motion needs to be repeatable, highly precise and similar to real patient breathing. Ideally a phantom should replicate typical motion along superior-inferior direction (SI) – the largest motion generated by diaphragm, anterior-posterior (AP) and lateral (see Figure 2.1).

Notice that in reality no one general breathing motion pattern should be adopted as a particular patient breathing pattern prior to making suitable observations. All patients have unique tumour motion characteristics in terms of displacement, direction and phase.

2.2 Review of phantoms for RT

The MAESTRO phantom described in the next section is only one of many existing phantoms aimed to evaluate lung cancer treatment in the presence of motion. This section reviews the advantage and limitations of current research and commercial phantoms.

2.2.1 Review of existing phantoms for lung cancer treatment.

Phantoms have long been used in medical physics to evaluate the effect of radiation and compare the dose delivered to that calculated by various software systems. Phantoms have two main roles; the most important is that of quality assurance and control to ensure that the machine delivering treatment is working as expected and within tolerances. These phantoms are normally non anthropomorphic designed to be easy to handle and provide a straightforward means to evaluate the equipment dosimetric as well as mechanical errors.

The second type of phantoms is aimed at research. These are generally more complex and aimed to push equipment to their limits as well as provide realistic clinical conditions without endangering patients.

Many current commercial and research phantom can simulate motion in only one direction (see Table 2.2) and do not contain any anatomical body parts. Platform based phantom apply the motion to the whole phantom body instead of separating the tumour motion to that of the rest of the body. Some phantoms that can simulate lung tumour motion have already been developed but they still have some limitations such as restriction to sinusoidal or periodic motion with limited amplitude and period, while patient's breathing is mainly irregular. The review presented below consists of the relative merits of the existing phantoms.

Designed by Duan et al. (2003), the platform's phantom model has respiratory motion along 1 DOF – a superior-inferior direction. That system generates a sinusoidal motion with a changeable frequency from 0 up to 1.6 cycles per second and an adjustable amplitude range of 0 – 2.5 [cm]. The phantom could be placed onto platform for dosimetric tests.

The phantom built by Dietrich et al. (2003) comprised a moving platform onto which a lung phantom was placed. The motion was replicated by platform able to simulate various periodic movements along one direction.

Similarly, Jiang et al. (2003) have created a motor-driven platform that simulates tumour motion along the SI direction. The motion was limited to sinusoidal traction with a peak-to-peak amplitude of 2 centimetres and a period of 4 seconds.

This item has been removed due to third party copyright. The unabridged version of this thesis can be viewed at the Lanchester library, Coventry University.

Figure 2.4 Phantom built up by Jiang et al. (2003).

The phantom constructed by Alasti et al. (2006) was also platform driven and was able to move periodically in one direction. Its amplitude range was limited from 1 to 3 cm with a period of 3 to 8 seconds.

Keall et al. (2004) placed a thorax phantom onto a moving platform that moved with sinusoidal action toward SI direction.

Schaefer et al. (2004) developed a phantom where the moving platform simulates respiratory motion toward SI direction with a cylindrical phantom mounted onto the platform. This was used to investigate the influence of breathing motion in step-and-shot IMRT.

The phantom developed by Fitzpatrick et al. (2005) was a moving platform able to simulate motion along superior-inferior direction. The displacement range was up to 5[cm]. Depending on the needs, the phantom could be placed on the platform driven using a stepper motor controller. Most types of respiratory motion could be simulated, including patient respiratory data.

This item has been removed due to third party copyright. The unabridged version of this thesis can be viewed at the Lanchester library, Coventry University.

Figure 2.5 The movable irregular breathing platform. Phantom developed by Fitzpatrick et al. (2005).

Hugo et al. (2002) developed phantom placed onto a 2D drive system with high precision stepper motors. A complex motion function could be used to drive the motion of the stages. The phantom was a water-filled acrylic cylinder with Teflon spheres' markers of radius 1 cm mounted on acrylic posts.

This item has been removed due to third party copyright.
The unabridged version of this thesis can be viewed at the
Lanchester library, Coventry University.

Figure 2.6 In-house quality assurance phantom by Hugo et al. (2002).

A 3D motion simulator was developed by Zhou et al. (2004). The device consists of two platforms that can be programmed independently and simulate the motion of skin and an internal tumour in three directions. The simulator was designed to test the effect of internal-external motion relationship. The system was able to simulate sinusoidal motion or reproduce human respiratory skin and tumour motion with precision better than ± 0.1 [mm].

This item has been removed due to third party copyright. The unabridged version of
this thesis can be viewed at the Lanchester library, Coventry University.

Figure 2.7 The phantom expanded by Zhou et al. (2004).

Recently Nioutsikou et al. (2006) developed an anthropomorphic, tissue-equivalent breathing phantom with deforming lungs. A tumour with the lung can be driven on any arbitrary 3D trajectory. The maximum speed of the drive system was limited so that the cycle duration of the simulated motion is larger than commonly found for patient's breathing. For example, during their experiments an experimental cycle of 20 seconds simulated a real cycle of 5 seconds.

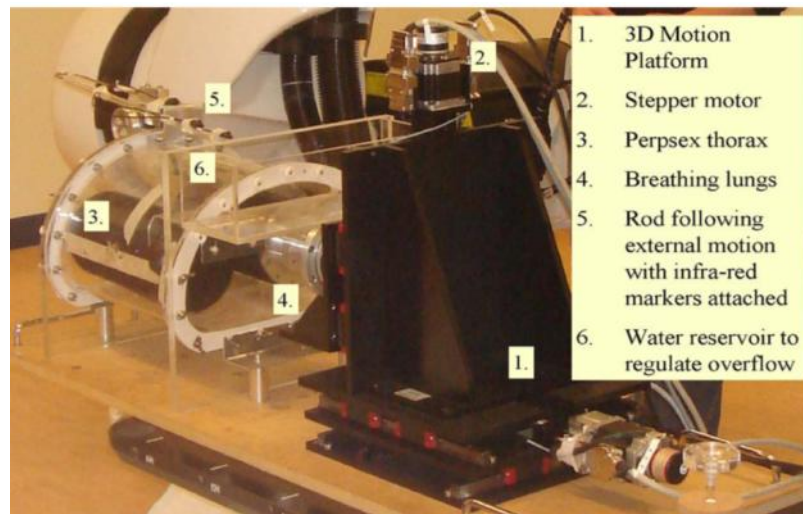
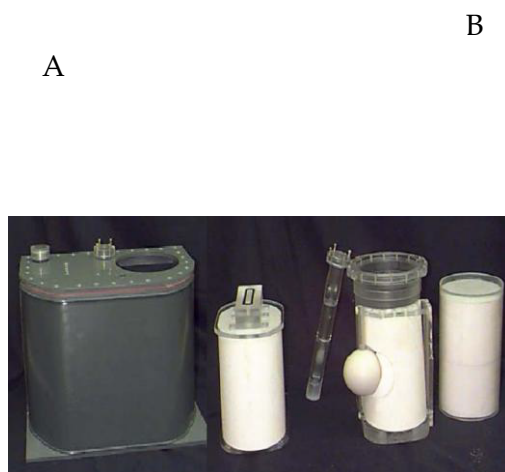


Figure 2.8 *The breathing phantom, PULMONE. Treatment setup.*

The Radiological Physics Centre's (RPC) developed a thoracic phantom (Radiological Physics Center, 2010) used in dose distribution measurement (Figure 2.9). The motion range was up to 15cm maximum, with the range of respiratory motions typically 0-2 cm. The reciprocal motion is superior-inferior (SI) direction. The RPC thoracic phantom has an ellipsoidal tumour insertion inside the left lung where Thermo-Luminescent Dosimetry (TLD) and film can be inserted for dose measurement. The phantom is filled with water when scanned or treated, to simulate surrounding tissue. The Figure 2.9.B) shows the 4D CT imaging setup.



This item has been removed due to third party copyright. The unabridged version of this thesis can be viewed at the Lanchester library, Coventry University.

Figure 2.9 *A) The RPC thorax phantom with insertions includes the lungs, heart, and spinal cord, B) example of experimental set up made by researcher of the University of Texas Southwestern Medical Center at Dallas.*

Other examples may be given by commercial phantoms which are usually more advanced and complex or alternatively designed to be simple and easy to use. The dynamic thorax phantom developed by Computerized Imaging Reference Systems Inc. (CIRS, 2010) was used for simulating lung tumour motion (Figure 2.10). Tumours of various size and shape can be positioned within the thorax. This model was manufactured from tissue equivalent materials and looks like a simplified human thorax.

This item has been removed due to third party copyright. The unabridged version of this thesis can be viewed at the Lanchester library, Coventry University.

Figure 2.10 The IMRT dynamic thorax phantom built by CIRS - Model 008 .

Various shapes of tumours can be positioned inside the thorax phantom. It can move along three-dimensions with sinusoidal and other complex motions (based on piecewise linear motion), with sub-millimetre accuracy. The ranges of motion were limited up to 40mm in superior-inferior direction, up to 7mm in anterior-posterior direction and up to 7mm in lateral direction with a period of 4 to 7 seconds. The CIRS Model 008 phantom disadvantage is that it is very expensive, with a price in the order of \$30000.

The next commercial phantom is a thorax model by Modus Medical Devices Inc. (2009), which developed a respiratory motion phantom called "Quasar", see Figure 2.11.

This item has been removed due to third party copyright. The unabridged version of this thesis can be viewed at the Lanchester library, Coventry University.

Figure 2.11 A) *The respiratory motion phantom QUASAR*, B) *optional insert with film and marker*(Modus Medical Devices Inc., 2009).

The phantom consist a body shaped part in which a moving cylindrical insert with a diameter of 2cm can be placed. Respiratory motion can be simulated in the superior-inferior direction with variable speed, variable amplitude and 4 to 50 respirations per minute with a sinusoidal motion profile with approximately 20kg weight.

The dynamic breathing torso phantom was made by the The Radiology Support Device Inc. (2008). The RSD based on the Alderson Radiation Therapy phantom. The phantom construction is anthropomorphic including lungs, ribcage bones, skin and sub-dermis, and an independently movable tumour within one of the lung volume.

This item has been removed due to third party copyright. The unabridged version of this thesis can be viewed at the Lanchester library, Coventry University.

Figure 2.12 The RPC thoracic phantom (The Radiology Support Device Inc., 2008).

The programmed application is increasing and decreasing air pressure, so the phantom lungs fill and empty air to replicate humanoid lung function. Chest movement of one centimetre or more can be programmed, and controlled by several sinusoidal signals with respiratory intensity 5-20 breath/min. The obvious

disadvantage is cost of the torso model which is \$29500 and more if optional components are used. For the price \$30000 customers will receive the phantom model, external control hardware and control software that are based on industry standard LabVIEW™ software.

The properties of the existing phantoms reviewed are summarised in the Table 2.2.

Phantom name / Authors	DOF	Chest & Tumour Independent Motion	Bone/Tissue equivalent/ Skeletal structure	Motion Pattern	Motion Range SI/AP/LH [mm]	Respiratory Frequency	Comments
Assumption data (see section 2.1)	3-D	yes	Yes/yes/yes	sinusoidal, Lujan, from patient data	32/29/25	0-4Hz	Average parameters base on research of patients respiratory motion
MAESTRO (2009) A) thorax B) tumour	3-D 2-D	yes	Yes/yes/yes	Sinusoidal, Lujan, Irregular, patient data	20/35/5 40/40/30	breathing frequency from 0 to 4 Hz	
Saracen (2005)	3-D	no	Yes/yes/yes	-	-	-	
Varchena et al. (2010)	3-D	no	Yes/yes/no	-	-	-	
Duan et al. (2003)	1-D	no	Yes/yes/yes	-	25	0 to 1.6 Hz	
Dietrich et al. (2003)	1-D	no	-	-	-	-	
Jiang et al. (2003)	1-D	no	-	Sinusoidal	20	0.25 Hz	
Alasti (2006)	1-D	no	-	-	30	-	
Schaefer et al. (2004)	1-D	No	-	-	-	-	Able to investigate the influence of breathing motion in step-and-shot IMRT

Table 2.1.a) Review of phantom for IMRT research.

Phantom name / Authors	DOF	Chest & Tumour Independent Motion	Bone/Tissue equivalent/ Skeletal structure	Motion Pattern	Motion Range SI/AP/LH [mm]	Respiratory Frequency	Comments
Keall et al. (2004)	1-D	no	-	sinusoidal	-	-	
Fitzpatrick et al. (2005)	1-D	no	no/yes/no	sinusoidal, patient data	50	developed a moving platform	Cylindrical phantom placed on platform
Hugo et al. (2002)	2-D	no	no/yes/no	no	-	-	No pattern; active breathing control
Zhou et al. (2004)	3-D	yes	No/no/no	sinusoidal, patient data	170	0,2 Hz	Respiratory motion simulator; accuracy better than $\pm 0,1$
Nioutsikou et al. (2006)	3-D	no	no/yes/yes	sinusoidal	-	5 Hz	motion precision better than $\pm 0.1\text{mm}$
RPC (2010)	3-D	no	Yes/yes/no	sinusoidal, irregular	150		
CIRS Inc. (2010)	3-D	-	Yes/yes/no	sinusoidal, irregular	40/7/7	0,14-0,25 Hz	Commercial-cost \$28500
Modus Medical Devices Inc. (2009)	1-D	no	Yes/yes/no	sinusoidal	-	0,07-0,84 Hz	QUASAR SI movement direction
RSD Inc. (2008)	3-D	yes	Yes/yes/yes	sinusoidal	-	0,083-0,33 Hz	Commercial-cost \$30000 LabVIEW software

Table 2.2.b) Review of phantom for IMRT research

2.2.2 Limitations of the existing phantoms

At the start of the MAESTRO project many of the existing phantoms did not cover all the expectations associated with a representative phantom for ART.

Most of the existing phantoms can simulate motion in only one direction, and mostly within SI. However, AP and/or LR direction of the tumour movement has been observed and should therefore be implemented as it influences ART treatments. Ideally 3D tumour motion should be able to be programmed into a phantom's ribcage.

Most phantoms are static and make use of a moving platform to generate motion. This means that the whole torso is moved instead of the tumour. Ribs motion are traditionally ignored when planning and delivering treatment. This can however significantly impact dose distribution if proton therapy is used. At the start of the MAESTRO work, most phantoms were only able to simulate sinusoidal or periodic motion with limited amplitude and period, whereas patient breathing pattern is mostly irregular. Nowadays, however, many phantoms are able to follow similar trajectories like real measured motion of the patient or cancerous tumour.

In relation to the needs of expanding ART techniques it was decided to create a new thorax phantom as a part of the MAESTRO project. The new dynamic thorax phantom was supposed to:

- a) be similar to real human body so its parts should to be heterogeneous, anthropomorphic and tissue equivalent,
- b) be easy to manufacture and assemble with low productions costs,
- c) have precise motion control of the tumour along 3D and ribcage wall motion separately,
- d) have a motion control which use various patterns of movement: regular (like sinusoidal or Lujan) and irregular (modified Lujan or real patient respiratory measurements),
- e) be easy to use in clinical practice.

The next Section reviews the MAESTRO phantom at the start of this project and summarises the issues addressed by this work.

2.3 The MAESTRO phantom

This following Section summarises the required features of a phantom to be used for ART. Afterward, it illustrates the development of dynamic thorax phantom and describes the thorax phantom built for the MAESTRO project. The phantom design, operating principle and finally material characteristics are now summarised.

2.3.1 Desirable attributes for and ART phantom

An ART phantom should replicate realistic treatment conditions, and therefore move similarly to human body. The most important criteria for the phantom are repeatable, dynamic and highly accurate motion. Ideally a phantom should replicate typical motion along three dimensions. The superior–inferior (SI) displacement should to be the largest motion and is mainly caused by the diaphragm. The anterior–posterior (AP) and a lesser extent lateral (LR) motion also should to be included. Phantoms could to be used as a reference to quality assurance of RT machine, to adjust RT equipment or evaluate methods of dose delivery. To evaluate realistic treatment plans it is beneficial for a phantom to be manufactured with heterogeneous body parts and be of an anthropomorphic nature. Ideally, the creation of the phantom components and parts should be easy to manufacture. Moreover, the overall phantom design should be easy to exploit in a clinical practice.

2.3.2 The RT thorax phantom design of the MAESTRO project

The thorax phantom was mainly developed by the PhD student Imke Land together with technicians at the University Hospitals Coventry and Warwickshire, as part of work package No.1 (WP1) of the MAESTRO project, which was coordinated by Dr O. Haas. This Section is based on Imke Land's PhD (Land, 2009). The entire phantom was created from tissue equivalent materials. Its internal structures were modelled to be heterogeneous and anthropomorphic, including spine, lungs, ribs, see Figure 2.13.

The thorax phantom comprises two main parts: an x-ray sensitive sensor fixed to a 3D drive system and a ribcage. Both parts are able to mimic motion separately

or together. The simulated tumour is replaced by an X-ray sensor which is inserted into the lungs volume of the ribcage.

The phantom's ribcage was assembled from precisely formed static spine, positioned between two separately modelled stationary lungs. This unit was then placed into a rib-cage construction, where ribs were able to move along two directions: SI and AP above immobile lungs. The expansion along the LR direction for the ribcage was not implemented originally due to the limited amount of motion observed in reality. Such motion could however be implemented, see section [5.1](#) which describes the author's proposal.

This item has been removed due to third party copyright. The unabridged version of this thesis can be viewed at the Lanchester library, Coventry University.

Figure 2.13 The anthropomorphic MAESTRO thorax phantom and major parts (Land, 2009).

In relation to the phantom dynamic motion, the ribs motion were synchronised, but each rib motion was adjusted using mechanical means to mimic the motion of the different ribs. The skin was adjusted onto the ribs. To make the phantom lighter during transport, it was decided to use water as a tissue equivalent material. The space between skin and lungs was therefore filled in with water.

All the parts, soft tissues and hard bones, were moulded from casts taken from representative body structures. Different types of bones were designed to have similar atomic structure as well as material composition to actual bones resulting in equivalent mass density as well as Hounsfield units. The substitute materials were

a mixture of epoxy resin and calcium carbonate (CaCO_3) based on the work of Bolton (1974) and Schneider et al. (1996) resulting in the material presented in Land (2009) and reproduced here.

This item has been removed due to third party copyright. The unabridged version of this thesis can be viewed at the Lanchester library, Coventry University.

Table 2.3 *The listing of the parameters of substitute materials for specified body parts (Land, 2009).*

For more details on the phantom construction please refer to Land (2009).

The most important part of the thorax phantom from a dosimetric assessment of the dose delivered is the three dimensional (3D) motion drive unit. It is able to carry at the end of a set of rods a target that can be inserted into the lungs. Sensors and devices of various size and shape can be fixed onto the rod to evaluate the dose delivered or visualise the motion. The rods can be moved within either lung. In this work X-ray film e.g. Gafchromic film were inserted into a cylindrical disk holder to measure the dose irradiation using a circular field in the presence of motion.

The tumour motion along three dimensions was realised by using three stepper motors capable of doing 200 steps per turn (see Appendix 3). This allows generating high precision motion with 0.9° per step together with the required torque. The stepper motor characteristics together with the motion requirements were used to derive gearbox ratio in view to achieve both the required velocity and movement patterns (Section 2.1.3), see Table 2.4.

3D Tumour And 2D Rib-Cage		Stepper Motor		Gear- box Ratio	Ribs Ratio	Screw		
		Type	Number Of Steps Per Turn			Screw Pitch	Max Screw Length	Used Screw Length
		SN	[steps/turn]					
Tumour	X Axis	23HSX-102	200	40:12	---	1	105	30
	Y Axis	23HSX-102	200	1:1	---	1	70	10
	Z Axis	23HSX-102	200	36:12	---	1	80	5
RIB CAGE		23HSX-306	200	1:1	35:11	2	12	10

Table 2.4 Mechanical properties of thorax phantom movement.

The gearboxes ensure that the appropriate torque can be delivered for the required resolution and accuracy. The Table 2.4 contains the screws parameters, which are important for motion programming. The ‘screw pitch’ converts rotational into linear displacement. The ‘maximal screw length’ is used as boundary conditions, and the ‘used screw length’ describes the typical range employed during testing.

2.3.3 Thorax phantom operating principles

One of the major MAESTRO phantom’s aims was to support the MAESTRO project which focused on image guided radiotherapy (IGRT) development with the aim to increase the cancer treatment efficiency. One of the other thorax phantom purposes was to be a quality control tool of the X-ray machines used at the hospitals for radiotherapy.

This Section briefly describes the part of MAESTRO project, which was aimed at increasing the X-ray beam targeting accuracy during radiotherapy.

There exist several companies that produce treatment systems for RT such as Elekta, Siemens, Varian or Philips. Most of these RT treatment machines were routinely used to deliver treatment using fixed gantry position. The X-ray particles emitted by RT **Linear accelerator** (Linac) are focused onto patients and their cancerous cell. Regularly treated patient have to be positioned on a couch and set under high energy X-ray beam (typically from 6 [MeV] to 20 [MeV]). Considering

lung cancer treatment, it is known, that the lungs motion due to breathing significantly affect the tumour location during the treatment. Methods to overcome this problem include increasing treatment margin, holding respiration and stopping the beam if the target is outside a predefined location. The Figure 2.14 visualises tumour displacement, caused by lungs movement during respiratory phases, and X-ray radiation margin of affected normal tissue.

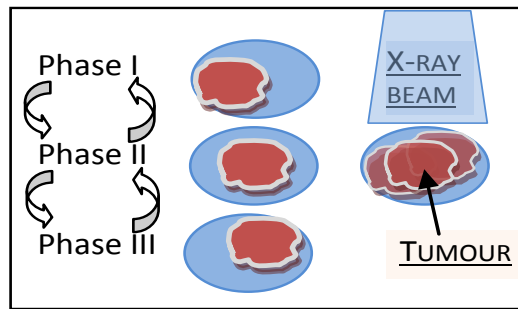


Figure 2.14 Tumour movement phases during RT treatment without displacement's compensation by patient support system (PSS).

Another solution was initiated to shorten therapy time without holding breathing. It involves compensation of the tumour, lungs and/or chest motion by PSS reposition in real time. To achieve such treatment, the PSS positioning system was automated and extended by a tracking system, a motion predictor as well as a motion controller. The overall idea of motion compensation using a PSS was to track two external markers, located on the thorax phantom (alternatively patient's chest). The first marker, which served as a reference, was usually placed on the PSS table while the second was either fixed to the rib with the largest displacement or to the moving arm holding the lung insert target. All the motion measurements were made using a camera video tracking system, using a FOculus FO124TB CCD digital industrial camera with IEEE 1394 interface (see Appendix 9) and where programmed using the NI LabVIEW software environment, see Figure 2.15 and Figure 2.16.

The measured positions were sent to the predictor module in real time. The predictor applied was a Kalman filter (KF) algorithm, which is an optimal estimator dedicated for linear signals. Next, the data of predicted trajectory were sent to a model predictive controller (MPC).

The controller collected information from the PSS sensors about the actual PSS location and the distance between two markers placed on the phantom model measured by the camera video tracking system. The controller calculates on-line the

optimal control action using current as well as predicted positions. It results in compensation of the PSS motion in the opposite direction to the measured target displacement at the same time. These cancelling most of the observed delays in the position video tracking, the control loop, the dynamics of PSS to move the PSS table and to compensate its movement for the measured location at the right time. The Figure 2.15 and Figure 2.16 illustrate the set-up used during motion compensation experiments. This approach was found to be able to cancel most of the observable delays resulting in significantly reduced observable target motion with respect to the treatment beam.

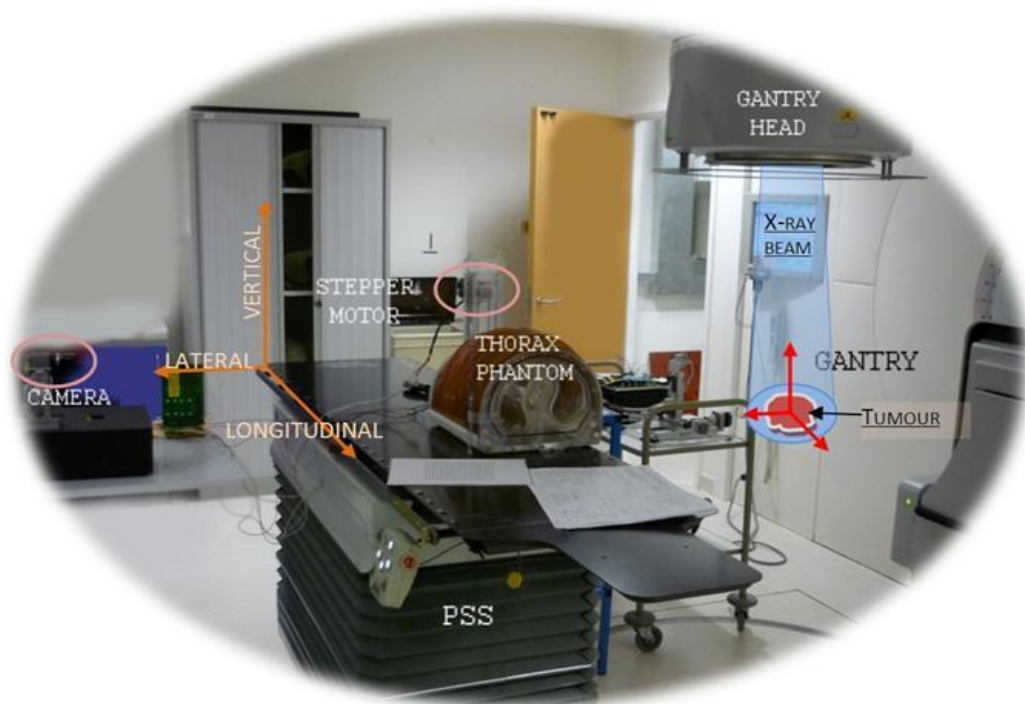


Figure 2.15 Experimental set-up illustration. The machine for radiotherapy treatment and PSS, phantom, camera video tracking and used coordinate system.

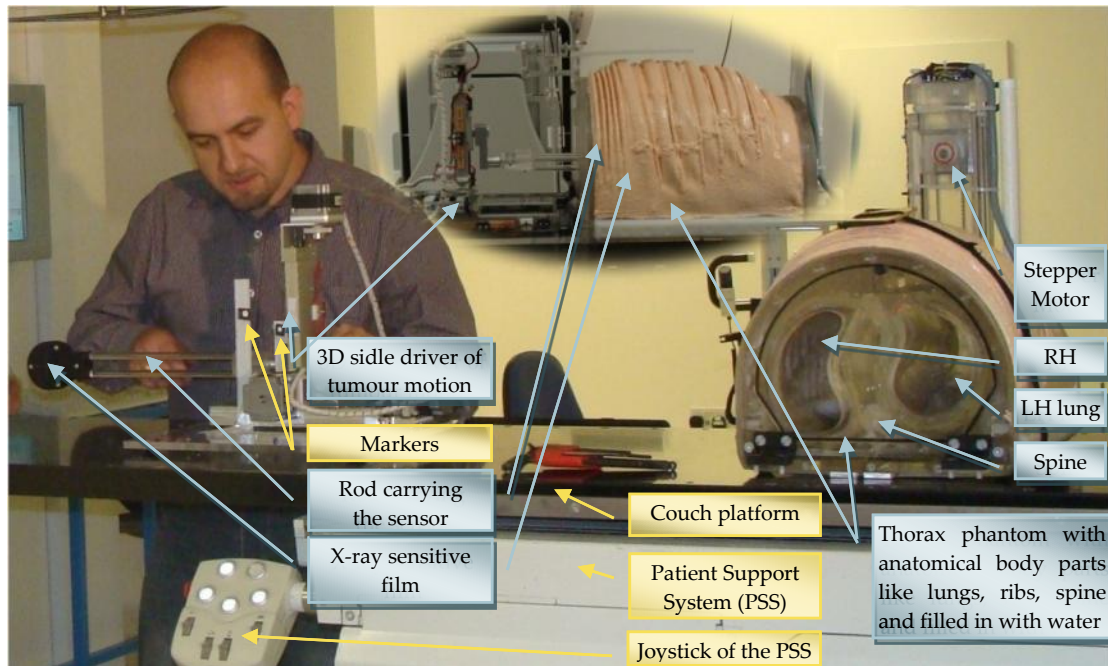


Figure 2.16 Set up of the thorax phantom model placed on the PSS couch. Preparation to the tests of the complex compensation system.

The new MAESTRO thorax phantom replaces a real patient affected by lung cancer with an anthropomorphic robotic patient with adequate bone structure, (see Section 2.3.2) and relevant respiratory action. The MAESTRO phantom can reproduce motion trajectory along SI, AP and LR direction and replicate several different tumour patterns of movement, presented by Figure 2.17 and specified by the user control panel.

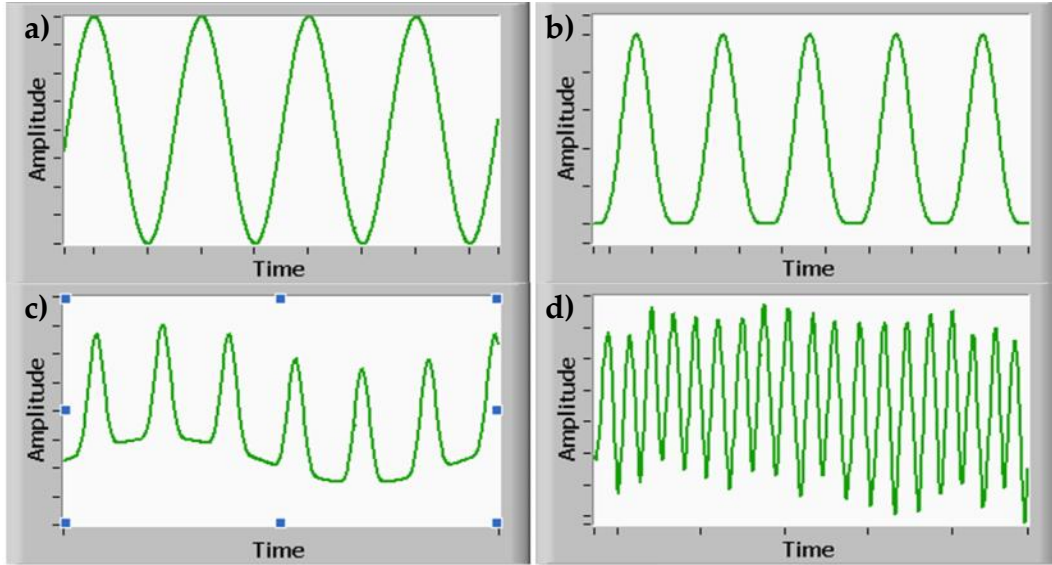


Figure 2.17 *Patterns of phantom respiratory motion simulated alternatively by: a) Sinusoidal wave, b) Lujan model, c) Irregular model, d) Data from patients measurements.*

As mentioned, the thorax phantom prototype of MAESTRO project, can simulate real patient respiratory data (see (d) of Figure 2.17) previously saved in excel or text file. Patterns described by mathematical formula such as sinusoidal, Lujan or irregular motion's model (Figure 2.17 (a), (b), (c)) can also be generated. However, more signals could be produced. The phantom motion control could also be adapted to any periodic or irregular pattern of simulation. The only limits are maximum range of the displacement and maximum speed, which are specified by the hardware.

2.3.4 Limitations

The common side-effects during designing any prototype are compromises. The development of the MAESTRO thorax phantom exhibits the following limitations.

There are only two degrees of freedom for the phantom's rib-cage motion (not 3D). The rib-cage expansion along the third-lateral direction would be beneficial for ART treatment and more adequate while simulating treatment. However, such motion previously was not included as it is not essential and because of fairly small movement amplitude (about 5 [mm] with peaks up to 10 [mm] during coughing).

The second restriction is the use of static lungs fixed inside the phantom. Therefore simulated respiratory motion have no influence on lungs expansion. This

phantom structure can limit in some cases dose measurements. However, the compromise was caused by the need for the lungs to have an easily accessible opened structure to insert X-ray sensor fixed to the external motion drive.

Finally, the thorax phantom restraint is not representative of body dimensions for all range of patients' anatomy. The rib-cage is based on an average torso build. Thus the phantom is not appropriate to simulate the treatment of 'small' or 'large' patients.

2.4 Conclusions

The review of all above information provides a better understanding of cancer treatment issues. There are a number of radiotherapy cancer treatment methods, however no one is effective to cure all patients. It is therefore necessary to take action against cancer, and improve existing treatment by refining them as well as exploring new methods of cancer treatment methodology. Adaptive radiotherapy is one of such new methods which require new quality assurance and new treatment validation procedures.

The brief review of the organ motion and existing thorax phantoms has highlighted advantages as well as limitations associated with the current phantom including the MAESTRO thorax phantom prototype. The dynamic MAESTRO thorax phantom has been described with a level of detail sufficient to prepare the reader for the programming work involved in controlling the phantom. The phantom has the ability to realise 3D (longitudinal, lateral, vertical) tumour motion within the lungs volume at the same time as 2D (longitudinal, vertical) rib-cage motion. The tumour is represented by X-ray sensor is an observed target fixed to a 3D linear slider unit. The motion control is separated for each part: the tumour is moved by a 3D linear motion drive and the rib-cage with a single stepper motor. The phantom motion control can be simulated by varied patterns based on results of measurements or described by mathematical formula. The representatives and used motion patterns were: sinusoidal, Lujan, irregular wave or real patients breathing observation and measurements, which reproduces breathing amplitude and frequency. The motion control is very precise with the use of a stepper motor capable of 200 steps per turn and a gear transmission.

The construction of the phantom was made using anthropomorphic 'body parts'. All parts were made with tissue and bone equivalent materials with a substitute material capable to absorb, scatter and ionise the X-ray radiation, and where their density was identical to human body structures.

The phantom can be used with X-ray radiation to compensate the tumour displacement effect within a lung while simulating patient breathing. This was one of the aims of the MAESTRO project, which required a phantom for the evaluation of the PSS compensation system of the RT cancer treatment machine.

Moreover, the hospital that exploits RT treatment machine for lungs cancer treatment can take advantage of the developed thorax phantom. By phantom connection to the respiratory compensation system of the RT machine it is possible to check the treatment quality and help calibrate RT machine. It needs to be highlighted, that the thorax phantom can also be used for ART evaluation.

The phantom design has separated tumour and rib-cage motion. This enables phantom usage with various methods of adaptive delivery system. External markers affixed onto the ribs can be used to simulate the chest expansion during inhalation. The relationships of the external chest movement and the internal target displacement can also be tested.

Some of the 'imperfection' could be considered and improved in future work and several suggestions will be presented in the following chapters. However, the present phantom model is a practical and usable tool for researchers in motion management in cancer treatment by radiotherapy. The developed dynamic thorax phantom is one of the most advanced and multifunctional tool and therefore is very helpful and fully functional instrument for ART treatment development.

Chapter 3

LabVIEW Motion Control of Radiation Therapy Phantom

The motion control of the phantom depends on materials and assembly. Thus hardware has a crucial influence on programming, irrespective of the software used. In this project NI LabVIEW software versions 8.6 and 2009 were used to control the thorax phantom.

The chapter starts with a description of the hardware involved in the Motion Controller implementation for the MAESTRO Phantom. It starts with a brief explanation of motion control using step sequences and then by frequency together with the hardware used. Each method of control is then expanded in separate Sections to include the LabVIEW implementation and the demonstration of its operation. The chapter concludes with a discussion on the relative advantages and disadvantages of the proposed control methods.

3.1 Resources for stepper motor control – electrical design and LabVIEW implementation

The motion generation and control of the MAESTRO thorax phantom was realised through the systems presented in Figure 3.1. The implementation adopted for the hospital trials of the phantom was based on sequence control.

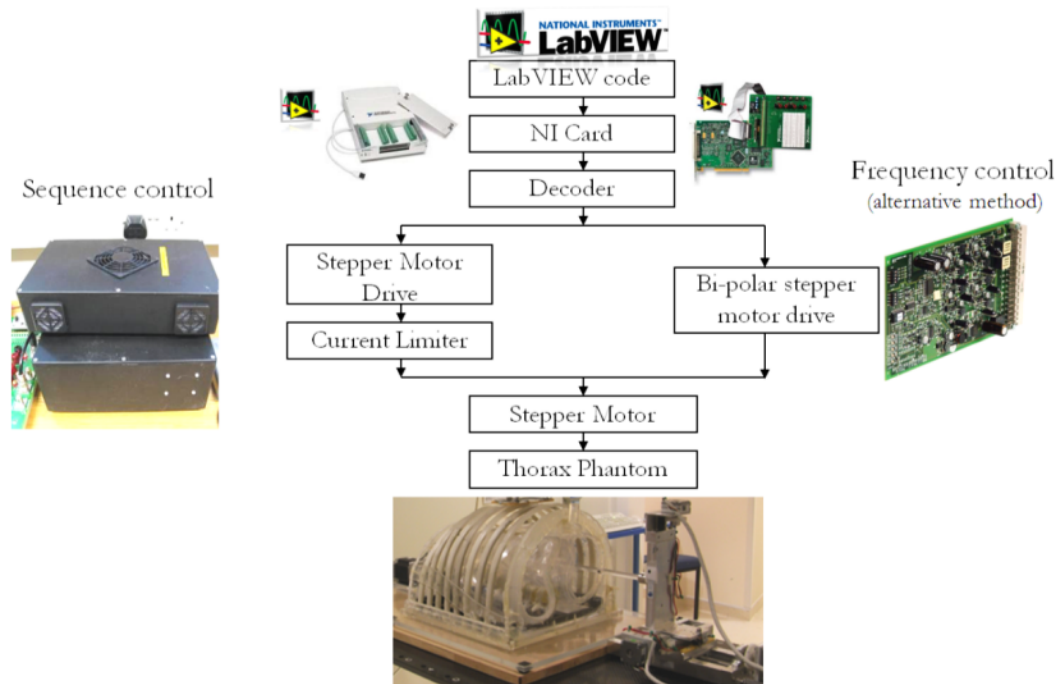


Figure 3.1 *Diagram of electrical motion systems: sequence motion control and motion control by frequency modulation.*

Figure 3.1 presents an overview of the approaches adopted within this work to control the phantom stepper motors. The control software is common to both approaches. It enables communication with the hardware via different types of NI cards and electronic interfaces. The signals are sent to a coder/decoder within the electronic interface built at the University Hospital, Coventry. Depending on the motor drives adopted the phantom motion can be controlled using either sequence motion control (Stepper Motor Drive and a Current Limiter units) or secondly motion control by frequency modulation (Bi-polar Stepper Motor Drive). The signals from the motor drives are then sent to the phantom's stepper motors.

3.1.1 LabVIEW software environment

The National Instrument LabVIEW software environment was used to program the MAESTRO phantom. Laboratory Virtual Instrumentation Engineering Workbench (LabVIEW) software was developed by National Instruments and introduced in 1986 (National Instruments, 2011). According to NI, the LabVIEW platform is highly advanced, graphical 'G' programming language, developed for engineers, students and researchers as many advantages like clear understanding about programming, program structure and data flow are especially helpful. National

Instruments software is aimed to create code that works with any sophisticated measurement, test, and control system by drawing a diagram using intuitive graphical icons and wires that are resembles a flowchart. The LabVIEW software can realise almost any task and control of any one real device or system, e.g. nuclear power plant by use one of the dozens of external or internal cards and sensors (National Instruments Corporation, 2011).

LabVIEW provides high-level functions to make the program more flexible and easy to understand. Because of that high-level language, it is easy and simple for researchers or students, to acquire or send data from computer to other objects. Low-level functions can be used especially when efficient code is required. The latter, however requires more experience from the programmer. In this work both high level and low level programming methods were employed e.g. DAQ assistant vs. DAQmx.

It is worth noting that the LabVIEW code for the same stepper motor can be completely different because of the software capabilities. NI argues that the graphical representation of the program gives the user a good understanding about its structure and data flow.

Based on experience, it was observed, that the graphical structure of the code is helpful for non- programmers. However, LabVIEW can become complicated when the code size increases and advanced constructs are employed. The data flow becomes difficult to track and understand when local variables are used. Good structured programming should employ subVI, however it is the experience of the writer that a large number of subVI may make it harder to track the various code functionalities.

Two different versions of LabVIEW were used, however the VI developed were available on both versions and thus no issues arose from the upgrading from 8.6 to LabVIEW 2009.

3.1.2 Data acquisition hardware

The communication between LabVIEW programs and the controlled device was realised initially with NI I/O card – SC-2075 (Appendix 8) and computer supported by PCI-6024E Data Acquisition board,

Figure 3.2. The laptop used either the NI DAQ Card 6024E for PCMCIA (see Appendix 7) or the NI USB-6229 DAQ module (see Appendix 5).

This item has been removed due to third party copyright. The unabridged version of this thesis can be viewed at the Lanchester library, Coventry University.

Figure 3.2 I/O card: NI PCI-6024E and NI SC-2075 data acquisition module (National Instruments Corporation, 2011).

At the beginning this card was found to provide sufficient capabilities for a relatively low cost system. The card included 8 DIO, however 16 DIO were required to control 4 stepper motors using sequence control. To resolve this problem, technicians at the University Hospitals Coventry and Warwickshire, realised a signal coder / decoder. The coding was realised programmatically using LabVIEW and the decoding of the sequences was executed by an electronic circuit. The diagram of the decoder representation is shown in Figure 3.3.

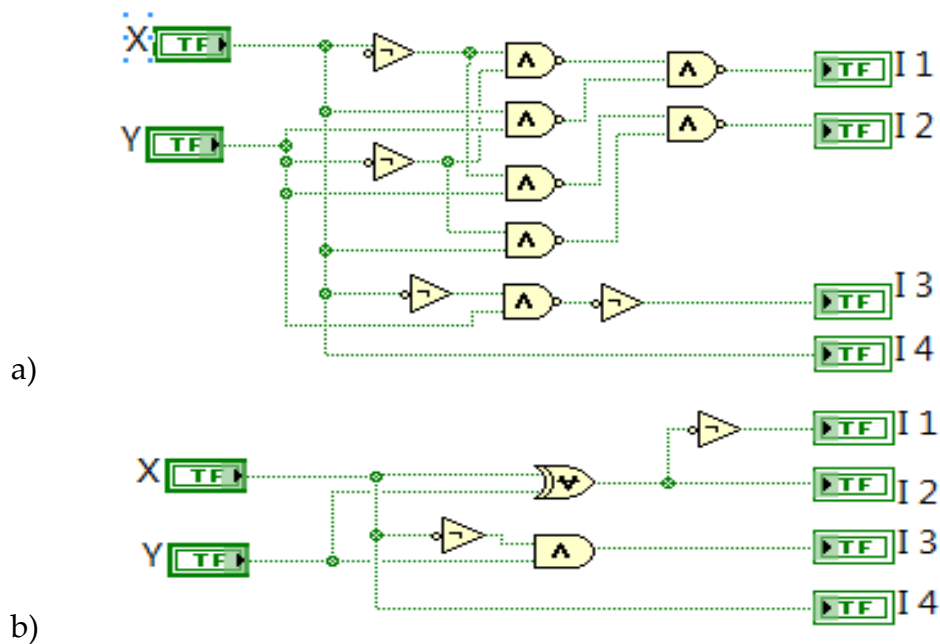


Figure 3.3 Decoder of the control signal for full stepper sequence: a) with NAND and NOT gates, b) alternative decoder based on EX-OR, NOT and AND gates.

The Table 3.1 below summarises the logic implemented using the LabVIEW code shown in **Error! Reference source not found.**Figure 3.3.

Card DO		Stepper Motor Sequences			
x	y	I 1	I 2	I 3	I 4
0	0	1	0	0	0
1	0	0	1	0	1
0	1	0	1	1	0
1	1	1	0	0	1
Realised function $f(x,y)$		$I1 = \bar{x}\bar{y} + xy$	$I2 = x\bar{y} + \bar{x}y$	$I3 = \bar{x}y$	$I4 = x$

Table 3.1 Table of logical states to reduce number of the digital outputs (DO).

The coding unit was combined with a current limiter box for the power supply module. The University Hospital interface used an NI SC-68 interface unit to control stepper motor drive instead of the SC 2075 which was used for development.

To prevent damages to the phantom and motor drives, safety 'end switches' indicating the range of possible motion for each axes were implemented. An additional switch per axis was added to indicate the centre or 'zero' position. Such increase in the number of digital inputs together with the need for an independent clock signal to time the motor sequence did require new hardware to drive the phantom. This led to the use of the NI USB-6229 DAQ module, see Figure 3.4. This M series USB unit comprises 32 inputs and works with 250kS/s, and has multifunction I/O data acquisition with 48 digital I/O channels with clock rate 1MHz frequency (see Appendix 5). This unit was used in the latest tests using the phantom.

This item has been removed due to third party copyright. The unabridged version of this thesis can be viewed at the Lanchester library, Coventry University.

Figure 3.4 I/O card: NI USB-6229 data acquisition module (National Instruments Corporation, 2011).

During the testing phase a desktop computer equipped with the NI DAQ PCI-6229 data acquisition board (Appendix 6) combined with NI I/O interface cards such as SC-2075 (Appendix 8), NI BNC-2111 or NI SCC-68 was also used.

3.1.3 Stepper motor drives

The stepper motors were selected by the technicians at the University Hospital, Coventry. Their selection was guided by the need for high torque with sufficient power to move the phantom mechanisms, together with small motor dimensions. To provide drive motion with sufficient accuracy, stepper motors with a resolution of 200 steps per turn were combined with gear box to drive either a linear drive or a belt drive.

One stepper motor model 23HSX-306, by (McLennan Servo Suppliers Ltd, 2009) (see Appendix 3) with high holding torque of 1630 [mNm] was used to move the phantoms ribs, and three stepper motors model 23HSX-102, with sufficient holding torque 470 [mNm] were used to move the tumour along 3 directions on the linear slider. The step resolution gives angle of $1.8 [^\circ/\text{step}]$ and consequently 1 turn equals to 200 steps in full step mode or 400 steps in half step drive mode. The Figure 3.5 presents the electrical connection of the motor.

This item has been removed due to third party copyright.
The unabridged version of this thesis can be viewed at the
Lanchester library, Coventry University.

Figure 3.5 Electrical cable connection (McLennan Servo Suppliers Ltd, 2009).

The torque characterising the stepper motors is shown on Figure 3.6. The initial slope increase is caused by static friction. Then the torque decreases with the rotational velocity. This means that to make sure that steps are not missed due to a torque demand higher than possible; the velocity of the motor should be kept below an upper limit.

This item has been removed due to third party copyright. The unabridged version of this thesis can be viewed at the Lanchester library, Coventry University.

Figure 3.6 Typical performance – torque in function of angular speed (McLennan Servo Suppliers Ltd, 2009).

Both stepper motors have 4 phases and are supplied with $U=5[V]$ DC voltage and current $I=1[A]$ if in unipolar mode, or $1.4[A]$ if phase parallel and bi-polar operation. Note that the four phases of the stepper motor need a control signal from the stepper motor driver. In full step mode 4 sequences were used while in half step mode there were 8 sequences in use to move the motor. Half step mode exploits 8 steps combination of power supply switching between stepper motor solenoids, where every second step the energy is supplied into two adjacent coils.

3.1.4 Sequence control

The step sequences order required to make the motor turn in clockwise direction is given in Table 3.2.

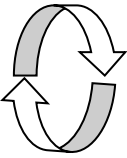
Lead identity	1	1'2'	23	3'4'		
Phase No.	"1"	"2"	"3"	"4"	Step No.	Direction
FULL-STEP	1	0	1	0	step 1	
	0	1	1	0	step 2	
	0	1	0	1	step 3	
	1	0	0	1	step 4	
HALF-STEP	1	0	0	0	½ step	
	1	0	1	0	1 step	
	0	0	1	0	1½ step	
	0	1	1	0	2 step	
	0	1	0	0	2½ step	
	0	1	0	1	3 step	
	0	0	0	1	3½ step	
	1	0	0	1	4 step	

Table 3.2 Table of stepper motor sequences.

To turn the stepper motor shaft in the reverse direction the sequences are required to be sent in opposite order, from the current step to the previous one and so on (e.g. step 3, step 2, step 1 then step 4, and again step3 (for full-step). Any inappropriately usage will cause problematic start of the motor, it overheating, motor buzzing, low torque value or not working mode.

Note, that the limitation of the initial I/O card to 8 digital inputs/outputs meant that it was not possible to use the half step mode. The optimal coding of the half step sequences would result in 3 digital outputs to represent 8 different sequences. However, there were only 2 DI/O so the sequence control was limited to full-step mode. Table 3.1 and Table 3.2 present the coded/non coded sequences order. Having selected the step sequence method of control, the next activity was to design gear boxes to provide sufficient velocity assuming full step mode.

Table 3.3 contains the mechanical characteristic of the phantom which is required to be considered whilst programming its motion. Note that if half steps were used, then the velocity would only be half of that required. This means that the gear box would have to be redesigned to provide sufficient accuracy.

3D Tumour And 2D Rib-Cage (Direction)		Stepper Motor		Gear-box Ratio	Ribs Ratio	Screw			Real Possible Displacement
		Type	Resolution			Screw Pitch	Max Screw Length	Used Screw Length	
		Serial No	[steps/turn]			[mm]	[mm]	[mm]	
Tumour	X Axis (SI)	23HSX-306	200	40:12	---	1	105	105	100
	Y Axis (LR)	23HSX-102	200	1:1	---	1	70	70	70
	Z Axis (AP)	23HSX-102	200	36:12	---	1	80	80	80
RIB CAGE (SI+AP)		23HSX-102	200	1:1	35:11	2	12	10	25

Table 3.3 Mechanical properties of the thorax phantom design.

3.1.5 Bi-polar stepper motor control

An alternative to the sequence control was the use of the bi-polar stepper motor drive model MSE570 Evo2, see Figure 3.7.

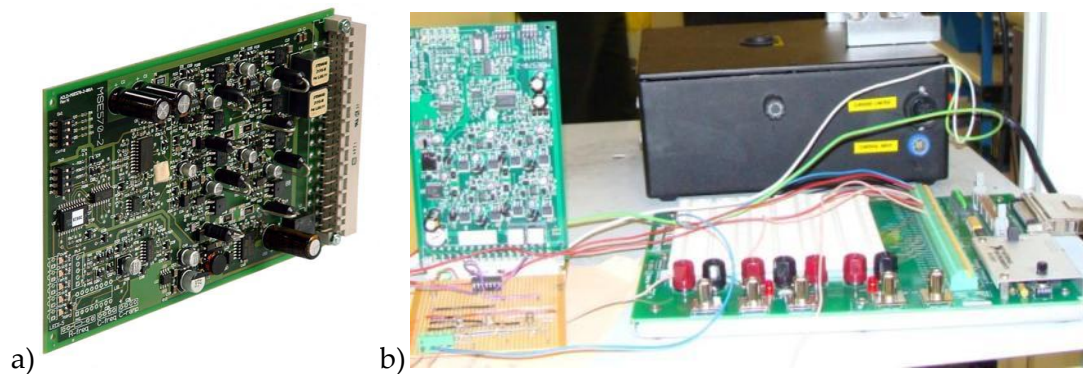


Figure 3.7 MSE570 Evo2 bi-polar stepper motor drive: a) card, b) experimental set-up during tests.

The MSE570 Evo 2 card is a bi-polar drive, with pre-set drive currents up to 3.5 Amps per phase with an operating voltage up to 48 [V]. This card was selected by the technicians at the University Hospital to fulfil the requirement for the phantom operation. It is capable of half-step drive option for improved damping, it does not require heat sink has an increased efficiency and operates from external clock and direction signals. This low cost drive unit of £142 (RS Components Ltd., 2011) is smaller than the previously mentioned unit. Other advantages are described in the technical specification (see Appendix 4).

As can be observed on Figure 3.1, the motor control was implemented in two ways. The hardware most widely used was a ‘Stepper Motor Drive’ combined with the ‘Current Limiter’. The alternative approach making use of the ‘Amp Bi-polar stepper motor drive’ was investigated to reduce the weight and volume of the electronic associated with the current limiter and drive system. This bi-polar drive was recommended by stepper motor manufacturer. Each set of the hardware components required different control software. The software developed for this purpose is described in Section 3.2 and Section 3.3.

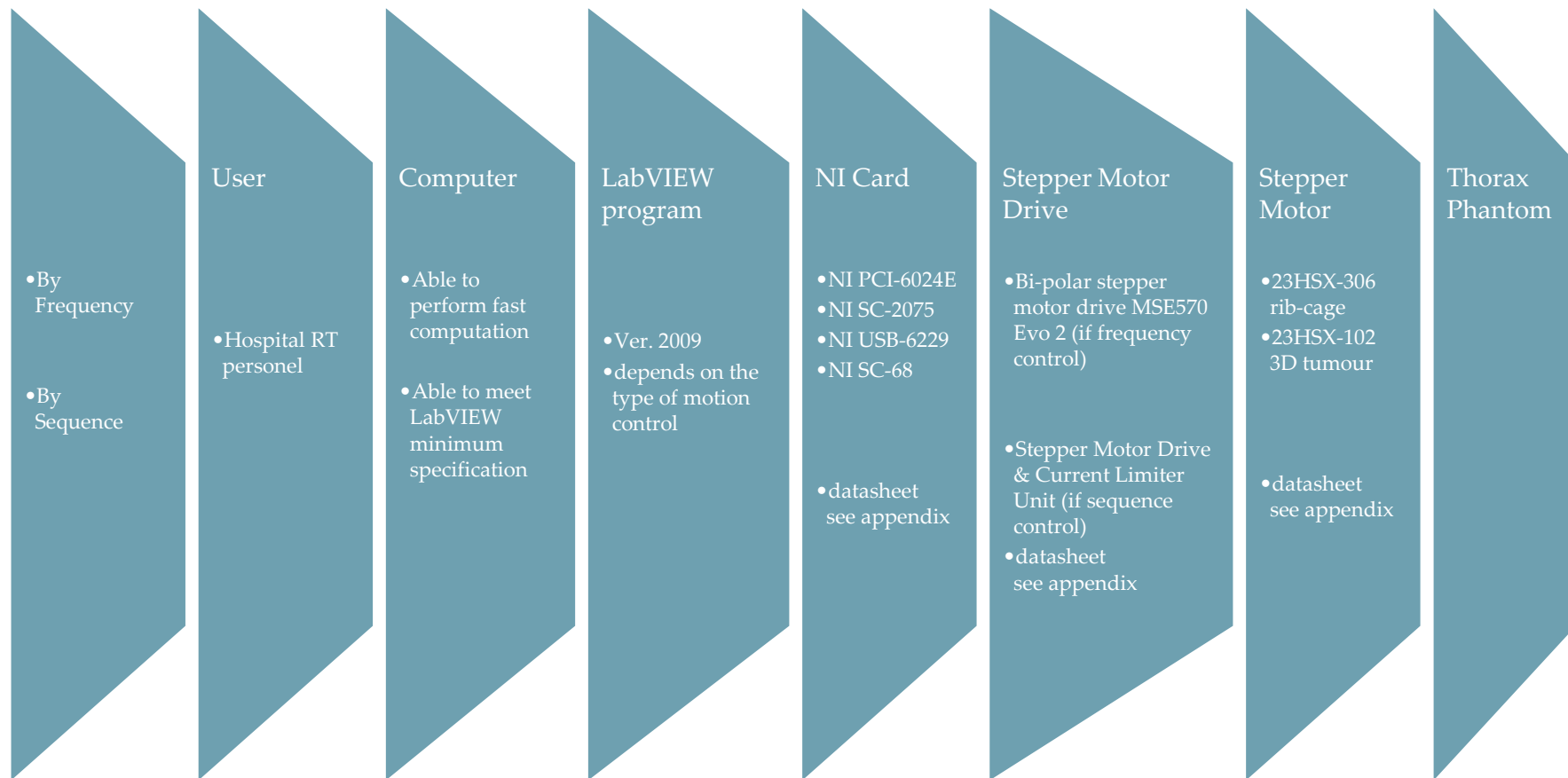


Table 3.4 Organisation of the thorax phantom control as a function of the type of control and hardware used.

3.2 Sequence motion control

3.2.1 Hardware components

The Stepper Motor Drive unit was used to realise the de-coding of stepper motors sequences according to Table 3.1 and Table 3.2. The motion control of the thorax phantom uses the Stepper Motor Drive Unit combined with Current Limiter, shown on Figure 3.8.



Figure 3.8 Set of the Current Limiter unit (upper) with Stepper Motor Drive (below).

The hardware built for the digital inputs/ outputs motors interface was realised at the University Hospital to accommodate the high power motor requirements. It included the DIO decoding from two to four digital signals implemented using the combination of TTL *nand* gates (UCY 7400) with *not* logical gates (UCY7404) shown by *Figure 3.3***Error! Reference source not found..**

3.2.2 Program description – diagram, explanation of program

In this project, the part of my work was aimed to modernise the existing code for motion control by sequences signal, which was initially created by PhD student Imke Land. The reason was to investigate the drift observed in the phantom mechanism caused by some limitations of the existing program.

Analysis of the code and also time spent on improvements, it led to the decision to create an entirely new program with a new code structure. The program should be able to realise the following:

- A. Generate control signal for 4 stepper motors and assure smooth motion.
- B. Generate Sinusoidal/ Lujan/ Irregular wave to replicate breathing pattern.
- C. Tune wave parameters such as amplitude, frequency, offset or phase for every single motor separately and n parameter of the mathematical representation of the Lujan or Irregular pattern.
- D. Read real data measurements to mimic patient's respiratory motion.

Additionally the planned improvements included improvements such as:

- E. Speed up and simplification of the motion start; reduce the number of operations.
- F. Enable to calibrate the phantom's position.
- G. Assume the same start/ stop position to avoid necessary calibration.
- H. Work interactively to enable the user to make changes while the program is running like tune the motion model or turn ON/OFF specified stepper motor.
- I. Improve the user interface to make it more user "friendly".

3.2.2.1 Existing motion control program

The code, written by Imke Land (2009) had advantages and limitations. It was the most advanced working program from the existing and therefore was used for the thorax phantom motion control. Figure 3.9 presents the user interface. The user interface presents eight tabs. First the *GENERATE ARRAY* tab shows the controllers with a choice of mathematically generated motion models such as Sinusoidal/ Lujan/ Irregular Model, as well as a choice of Amplitude, Offset, Phase for individual stepper motor and respiratory frequency. The generated signal was saved into an array as a set of sequences. Usually, the first operation during the phantom motion generation is to either generate or load a previously calculated data set such as an expected respiratory pattern. The *OPEN ARRAY* tab is the second step of the process, when it opens and then loads to the memory the array containing the motion as a global variable. Once these two operations have been selected the step 3 is: *SAVE ARRAY* where sequences are saved into file or *GENERATE MOTION*. Because saving array was normally used with the first Generate Array tab, the third Tab is a repetition and not a necessary function. The

motion generation by the forth tab allows to turn ON/ OFF each motor separately. These first four tabs allow to control the thorax phantom.

This item has been removed due to third party copyright. The unabridged version of this thesis can be viewed at the Lanchester library, Coventry University.

Figure 3.9 Front panel of the existing program designed by PHD student (Land, 2009).

It is the view of the author that the operations of the software and its GUI are not sufficiently intuitive and need re-ordering. The last tab was *HOME POSITION*. It is taking too long to realise the initialisation of the phantom as it requires the phantom to move to each of the end switches of the slide. The initialisation could not be fully tested with the card used at the University Hospital due to the lack of digital I/O. The 3rd tab and tabs from 5th to 7th are normally not necessary during regular test procedure and are only used to move the phantom manually to a given position using forward and reverse motion of the stepper motors. Despite the author's reservation, such interface provided the required functionality and was used throughout the MAESTRO project to be replaced afterwards by another interface and software based on the DAQmx approach implemented by the author. The decision to realise a new program for the phantom motion was caused by the last four assumptions described in Section 3.2.2.

The major undertaking of this work was to realise a routine to enable calibrating of the phantom 'home' position and provide the means to change the trajectory on-line, by contrast to pre-calculating the whole trajectory and then sending it to the motors. The ability to modify the trajectory on-line would enable the use of signals from patient's motion measurements e.g. by combining phantom with spirometer, or other device.

Writing the program was not a trivial task. The challenge was to accommodate the required increase in complexity and the issues with phantom availability. The LabVIEW programming became increasingly challenging and difficulties as the code became more complex. The work on the phantom motion took up several months due to the limited phantom availability. Some of the problematic issues were not solved so the code was not fully working when the testing were made with the thorax phantom. The final program (see Appendix 2) meets almost all the specified statement with the exception, however, of obtaining a fluent motion generated for chosen patterns. Pattern motion generation or stepper motor control by linear loop incrementing works properly. The detailed code description is presented in the following sub-sections (see section 3.2.2.3).

3.2.2.2 Front panel and operating principle

The user interface presented by Figure 3.10 visualises the code functionality. On the upper left quadrant, a knob control is used to select the breathing frequency (*a*) and a slider controls the motion amplitudes (*b*) for each X, Y, Z and rib stepper motor of the tumour drive, where X represents superior-inferior (SI), Y – lateral(LR) and Z – the anterior-posterior (AP) motion direction. The breathing frequency knob (*a*) can be tuned between 0.1[Hz] to 4[Hz] based on the range of breathing frequencies identified in the literature review. Note that these limits could be easily adapted if required e.g. to replicate breathing with higher frequency. The waveform reproduced represents real patient data with typical breathing action combining regular patterns together with irregular motion showing a significant baseline drift at the start. The slider controllers represent the global position where “0” means home position. The sliders (*b*) are scaled in millimetres, adequately bounded to accommodate for possible phantom displacements, see Table 3.3. The “0” value indicates that the program has to set up the initial/home position of the real device, calibrated previously. The phantom has fixed rulers so its displacement can be easily checked. Switchable between four tabs (*c*), the controllers allow the user to select different patterns of motion and modify their motion characteristic e.g. amplitude. It is possible to use pattern of Sine, Lujan, Irregular or Data of the Patient (read from Excel file). The segment (*d*) below the Amplitude slider controls consists of a set of constant parameters used to calculate the phantom’s displacement. The parameters are based on the phantom design such as screw length, screw pitch,

ratio of the gear-box transmission. Some of the constants were specified to correspond to breathing frequency for patient data collection (sampling), or sampling info of the main sine wave.

The constant parameters used by the program which relate to the mechanical properties of the design and to the real phantom parts where typically:

- SP Screw Pitch equals 1[mm] for all: X, Y, Z (tumour) axis and for R (ribcage) axis as well,
- GB Gear-Box Ratio, corresponding to the X, Y, Z and R axis, where equal to GBX=0.3, GBY=1, GBZ=0.33(3), GBR=1 respectively,
- RDF Real Data Frequency of the patient respiratory measurements saved into file equals 30 [Hz],
- NoSPT Number of Steps Per 1 Turn of The Stepper Motor Sequences Table, computed for all axes and related to one turn where for X=60, Y=200, Z=67 and R=62 respectively.

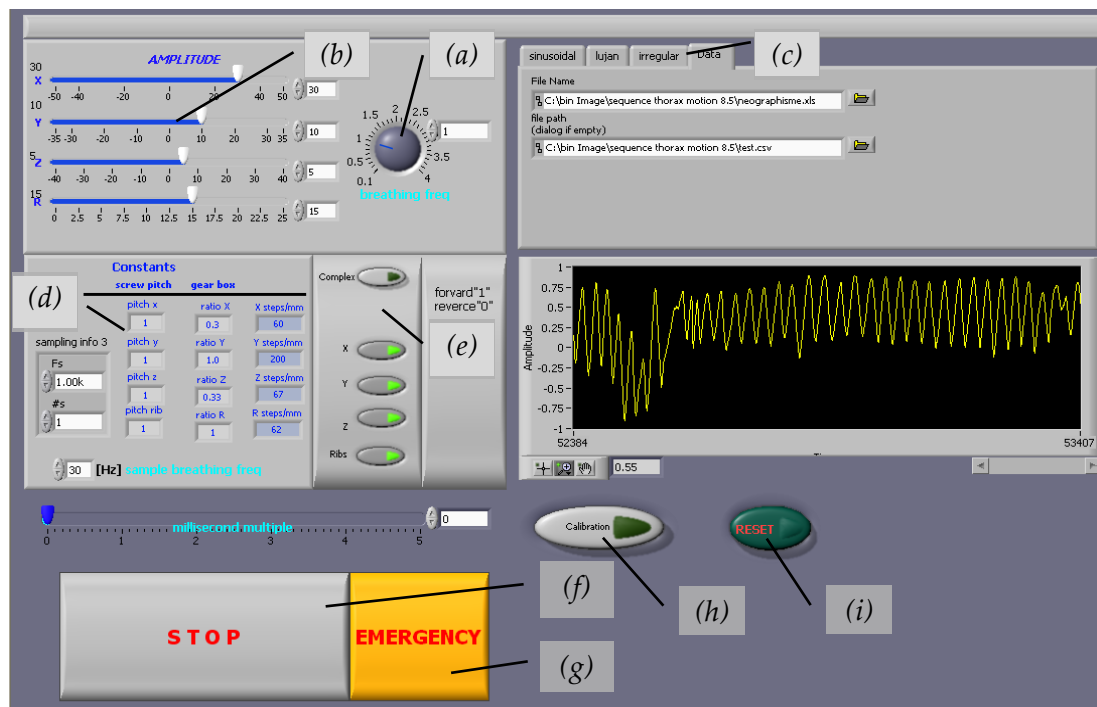


Figure 3.10 Front panel of the in real time working program.

To reflect that depending on the use of the phantom not all the motion are required, the section contains 5 vertically positioned switches which allow turning on/off selected stepper motors. The *Complex* (e) button enables to turn on all axis of the phantom motion.

Once the program is running, a user can stop it using two options namely by pressing the *STOP* (f) or the *EMERGENCY* (g) button. The use *STOP* switch will stop the running code when the phantom is back to its 'home' position. With this solution, the phantom will remain at its home or initial position and will be ready to restart. The second '*EMERGENCY*' button will stop the program immediately.

The program allows calibrating the phantom and setting it to its initial position automatically by pressing the *Calibrate* (h) button. The phantom position and direction are saved to file when it stops. Therefore restart should keep movement in the correct range of work unless there was observed discrepancy or the phantom sliders were moved manually.

Switch *Reset* (i) causes the reset of the data file which contains the saved position (steps number) and save zeros into it. It needs to be noticed that this button should be used carefully and only if necessary as it changes the zero position.

3.2.2.3 Block diagram

The overall idea of the control method is, for each axis of motion (or stepper motor), to code stepper motors sequences into two binary values then to send them to the stepper motor drive module and afterward through the "Current limiter" module to the stepper motors.

This method of motion control involved using relatively large and complicated electronic units such as the "Stepper Motor Drive" and the "Current limiter" . The existing code written for controlling the motion of the thorax phantom was extensive thus difficult to understand and modernise for other programmers. The bulky construction of the existing code contains very developed case structure with dozens of case loops and many high and low-level functions and local variables.

To overcome the issues associated with the code complexity and the excessive use of local variable an alternative code for the thorax phantom motion controller, was developed and is illustrated in Figure 3.11.

The block diagram of the program could be illustrated by the LabVIEW block diagram itself as the LabVIEW graphical interface shows the program structurally. However understanding of LabVIEW programs requires training, hence the choice to illustrate it using a simplified block diagram.

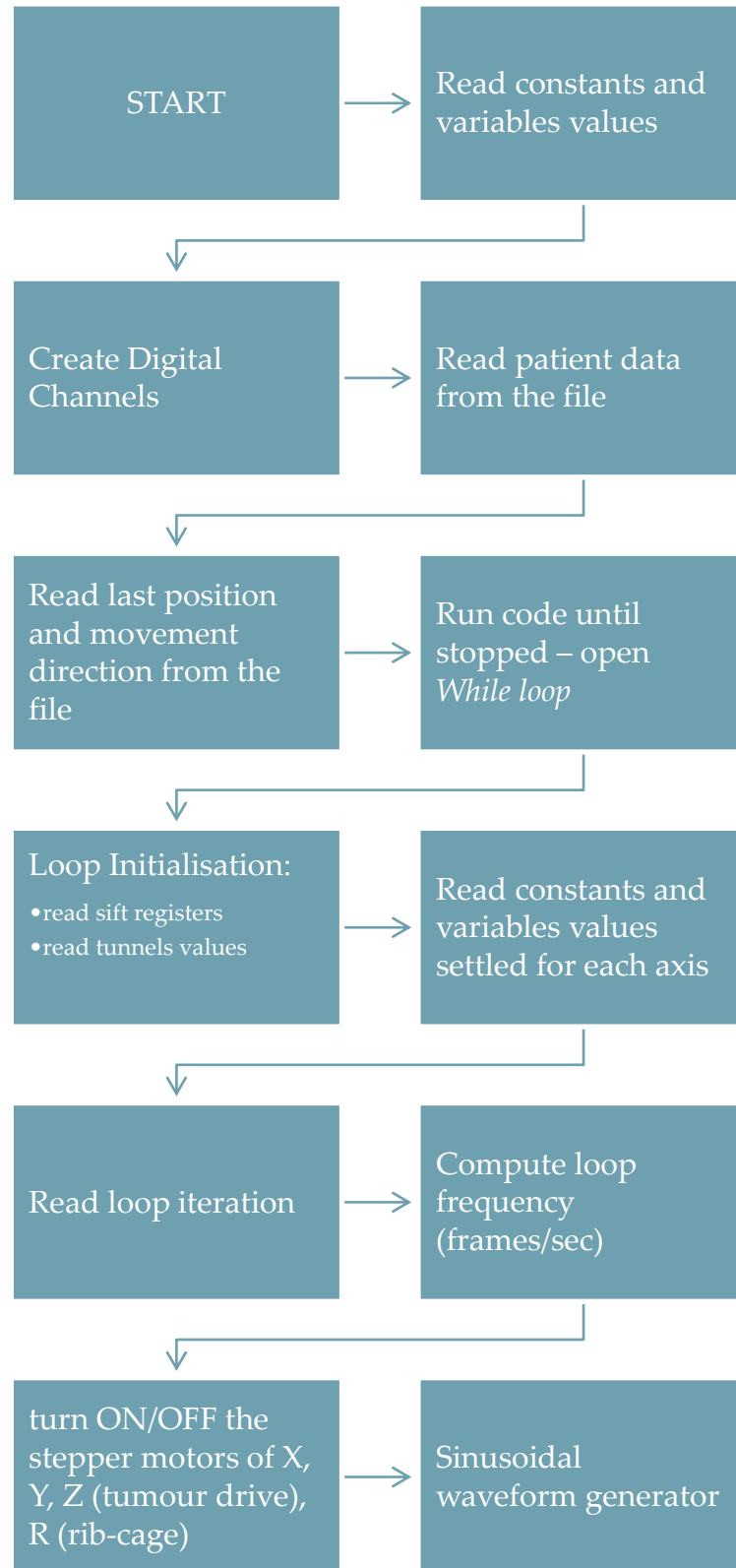


Figure 3.11.a) Sequence motion control code – diagram.

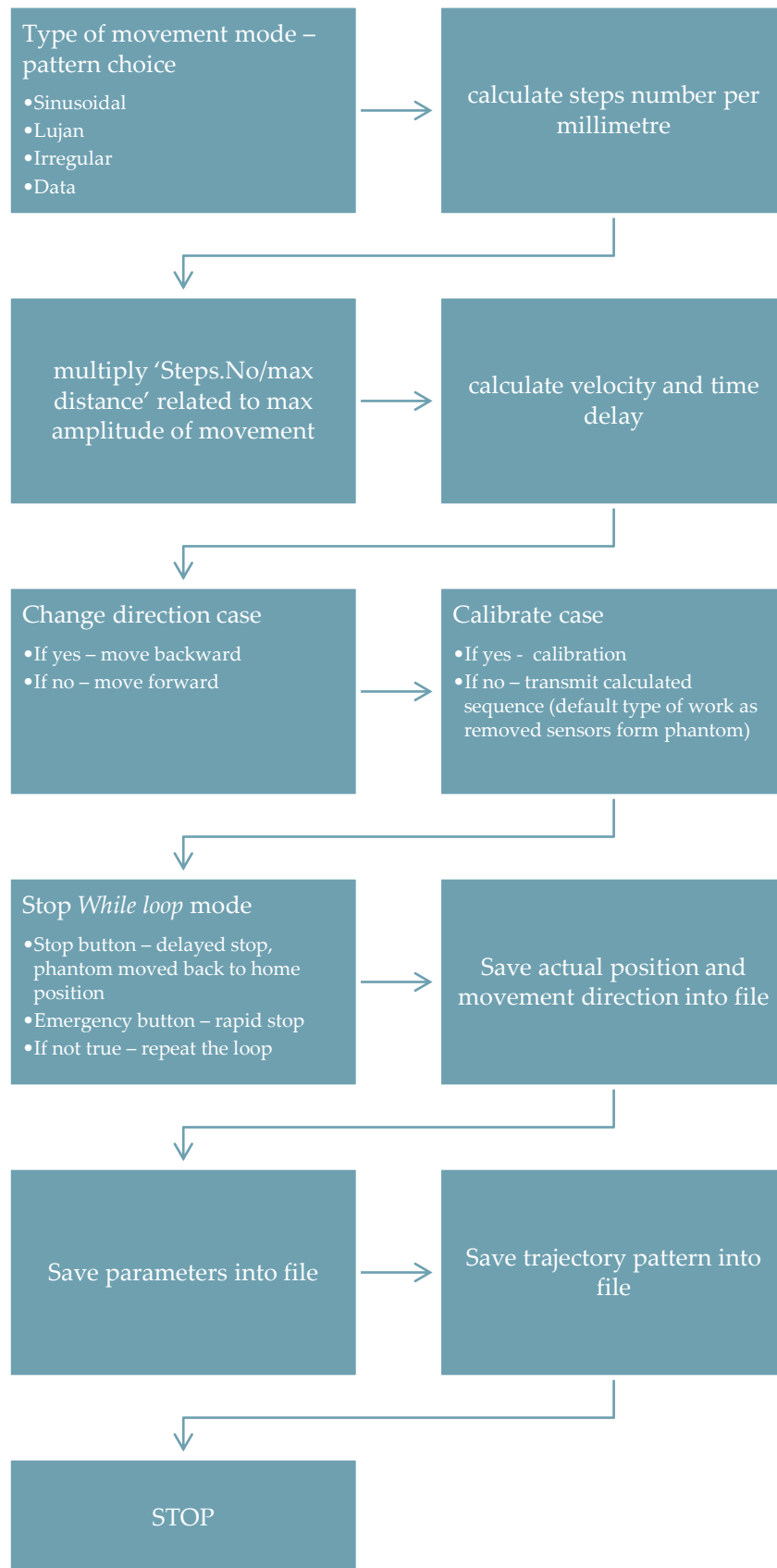


Figure 3.11.b) Sequence motion control code – diagram.

The diagram functions description:

- Start

Start LabVIEW program using the 'Run' button or combination of the 'Ctrl' + 'R' keys.

- Read constants and variables values

Read all parameters of the constants and controls, outside the *While loop*. Usually all commands and parameters are executed in order from the left to the right hand site of the code.

- Create Digital Channels

Create Digital Channels to send the sequence of the stepper motors step. To ensure more stability to the program work and high frequency of the code execution, low-level DAQmx functions were used. The program needs to control 4 stepper motors with resolution 200 steps per turn, therefore the minimal number of channels required is 8 (2 channels for 1 stepper motor).

This solution required to use coded signal, where 2 channels provide 4 combinations of the digital signal sequence.

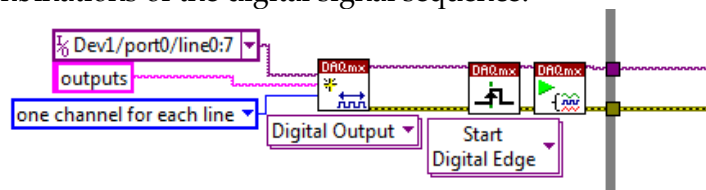


Figure 3.12 The 8 channels DO task creation with low-level functions use. Block diagram.

The channels were constructed from low-level DAQmx functions that comprise:

DAQmx Create Channel – set to Digital Output (DO) Pulse Frequency;

DAQmx Timing – set to Continuous Samples

DAQmx Start Task

- Read patient data from the file

The file used for respiratory motion replication can contain the real patient breathing measurements or cumulates individually prepared movement pattern. In this case, all data should be saved in column vertically and contain double precision real values. The 'Read From Spreadsheet File' function, illustrated by Figure 3.13, can open and read file with *.xls extension (excel file).

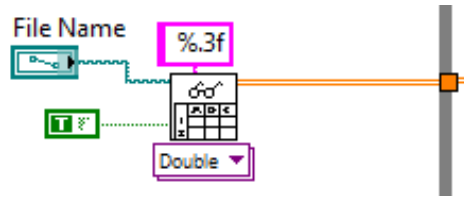


Figure 3.13 Spreadsheet file use to read motion pattern data. Block diagram.

- Read last position and movement direction from the file

The parameters that describe position and direction of the thorax phantom motion, saved previously after program was stopped, were restored from the spreadsheet file. The file was formatted to *.csv extension and can be reset if needed.

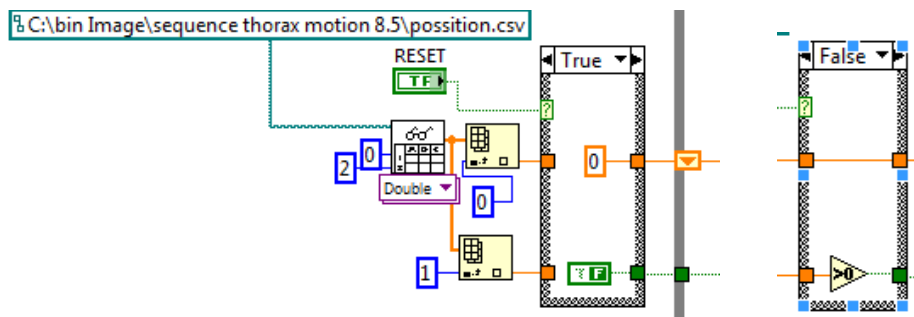


Figure 3.14 Restoring parameters of last one position. Block diagram.

- Run code until stopped – open *While loop*

The assurance of the on-line motion control requires to run the code continuously, where sub VIs inside are repeated until the stopping condition becomes 'true'. Thus a '*While loop*' was used. This function allows the continuous operation of the phantom where all operations are executed periodically with high frequency.

- Loop Initialisation:
 - read sift registers
 - read tunnels values

Previously computed parameters obtained from outside of the loop, they become the initial values for the tunnels and shift register inputs. All parameters have to be collected from shift registers and tunnels values.

- Read constants and variables values for each axis

The task realised by this part of the program was the collection of all values required (see Figure 3.15) to compute stepper motors needed steps number per cycle and then used for the future frequency computation and sequence sending. Notice that all the code functions are executed, in order, from the left to the right hand side.

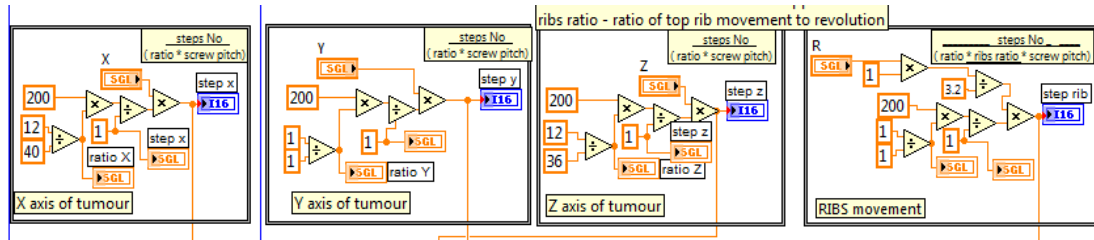


Figure 3.15 Set of constants and controllers for all stepper motors. Block diagram.

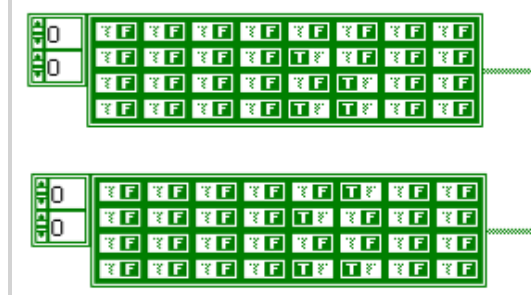


Figure 3.16 Arrays of coded sequences for Z-axis (other axes were set as zero); the lower array represents reverse rotation.

The Figure 3.16 presents the sequences table for Z-axis only which is reflected by 5th and 6th column. The others were set as *false* (F).

- Read loop iteration
- Compute loop frequency (frames/sec)

The loop frequency computation was very important parameter during the experimental work. The algorithm was shown on Figure 3.17 and includes a combination of the low-level functions.

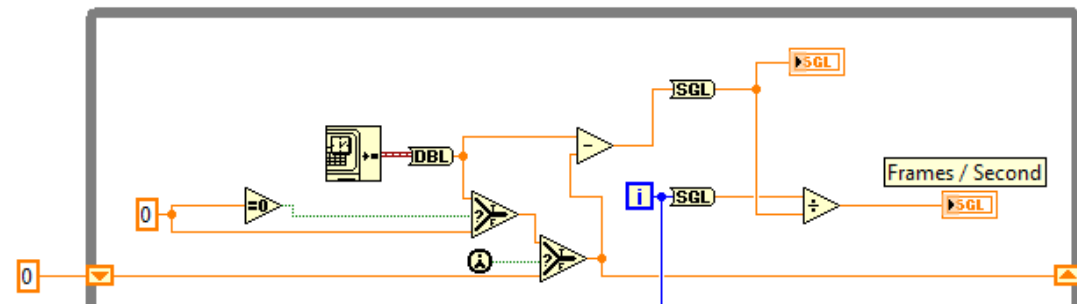


Figure 3.17 Frequency of the LabVIEW code execution. Block diagram.

The VI used does not significantly affect the rest of the code and was used to calculate the frequency parameter. The function 'get time' returns the global time in seconds. By comparing the current time obtained during code execution with the time from the initial iteration, and then dividing the loop iteration by the computed time of the code execution, it was possible to calculate the elapsed time.

- Turn ON/OFF the stepper motors of X, Y, Z (tumour drive), R (rib-cage)

Program was equipped with complex stepper motors activation switches. see Figure 3.18 .These switches were found to be beneficial in the research work as they enable to activate the stepper motors and thorax phantom movement direction separately or use a 'Complex' switch for quick start.

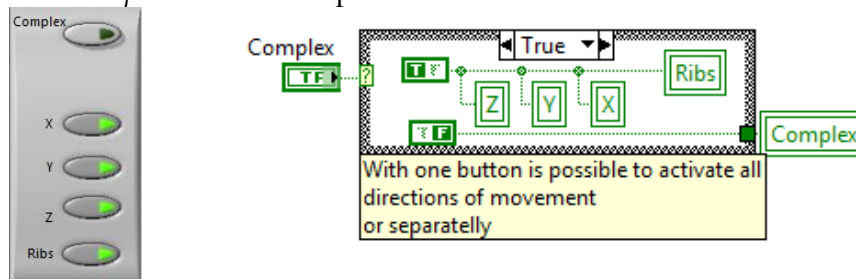


Figure 3.18 Turning ON/OFF of the stepper motors function. The users interface (LH) and block diagram (RH).

- Sinusoidal waveform generator

The basic function of sine waveform generator (Figure 3.19) was used for the computation and simulation of motion patterns. The only changeable parameter was patient breathing frequency from 0.1 to 4 Hz (the range can be easily extended). The maximum amplitude was set to unity value and phase and offset were set to zeros as this waveform was used as a pattern for mathematical representation of the first three breathing trajectories listed below.

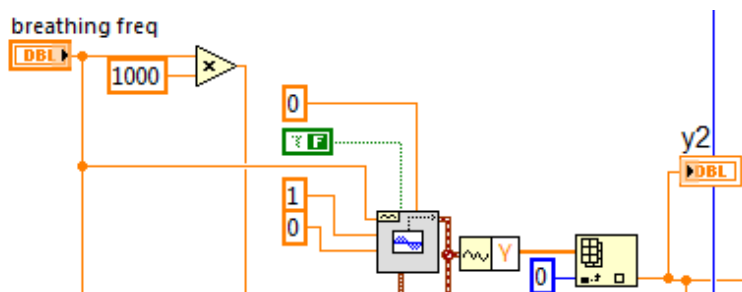


Figure 3.19 The sine waveform generator; block diagram.

- Type of movement mode – pattern choice
 - Sinusoidal
 - Lujan
 - Irregular
 - Data

The pattern choice, as was described before, serves three simulated movement modes and a patient respiratory motion acquire from data file.

- Calculate steps number per millimetre

The steps number per millimetre was shown on Figure 3.15. The mathematical representation for the rib-cage shows Equation 3.1 and for the stepper motors of tumour drive shows Equation 3.2:

$$\text{StepsNo_conversion} = \frac{\text{steps No}}{\text{ratio} * \text{ribs ratio} * \text{screw pitch}}$$

Equation 3.1 Computation of the rib-cage steps number per millimetre.

$$\text{StepsNo_conversion} = \frac{\text{steps No}}{\text{ratio} * \text{screw pitch}}$$

Equation 3.2 Steps number per millimetre computation for tumour X, Y, Z axis.

- Multiply 'Steps.No./max distance' related to max amplitude of movement

This task returns the number of steps for adequate stepper motor in relation to distance set by the amplitude slider on the front panel.

- Calculate velocity and time delay

The maximum of steps number per distance computed before, it represents the phantom movement amplitude. Because some of the stepper motors use more steps per breathing cycle, there is a need to perform some synchronising. Next there were calculated synchronising motors ratios of max steps number to actual and needed steps number. Afterward the loop iteration divided by the achieved ratio returned the number of step used for sending the required sequences of motion.

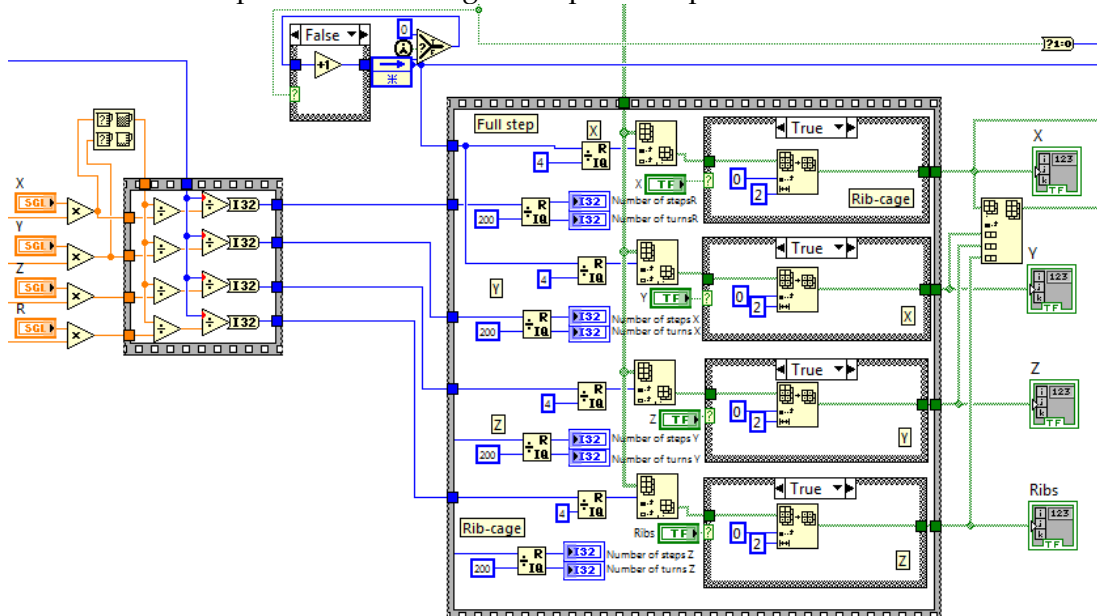


Figure 3.20 Steps synchronisation and sequence sending to DO.

Above part of the code and synchronisation with velocity computation needs to be improved. Currently this program allows to generate movement linearly only with loop increment and is not able to follow generated motion pattern thus is not fully working. Instead of loop executions number, an obtained pattern signal or real patient measurements data should be present. However, even with linear movement replication some shacking was noticed and the motion was not fluent. It is not known what was the cause of this phenomena but it was observed that some of the calculations were executed several times for one stepper motor while other computations were performed only once.

- Change direction case
 - If yes – move backward
 - If no – move forward
- Calibrate position case
 - If yes - calibration
 - If no – transmit calculated sequence (default type of work as removed sensors form phantom)

The positioning of the home position was completed as the construction of the phantom was modified and safety switches removed. Instead of these the initialisation was done by saving the latest position and direction into a file. The counter of the steps (shift register) was added to set up the home position indirectly when it equals zero.

- Stop *While loop* mode
 - Stop button – delayed stop, phantom moved back to home position
 - Emergency button – rapid stop
 - If not true – repeat the loop

Normally the phantom stops when it reaches the home position (stop button + counter set to logical '0'). The emergency button stops the code immediately and should be used if any incident happened.

- Save actual position and movement direction into file. Saves the required code parameters and trajectory pattern into file.

When the end of while loop has been reached then code saves all required parameters into file.

- STOP

3.3 Frequency motion control

3.3.1 Used hardware

Depends on hardware or software used and also reliant on programmer, there are numerous solutions for stepper motors motion control. One of them is motion control by frequency modulation with use of a bi-polar stepper motor drive.

The search for alternative control solutions and motor control improvements led to the use of a dedicated driver to stepper motor named Amp Bi-polar stepper motor drive MSE570 Evo2. The key aim of using this new card was to simplify the electrical design and to test a new way of stepper motor control by controlling the frequency.



Figure 3.21 Comparison sizes proportion of two drivers: set of the Current limiter (upper) with Stepper motor drive to the new Card MSE570 Evo 2.

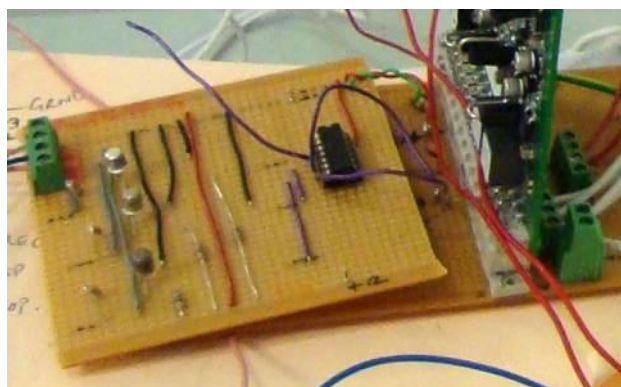


Figure 3.22 Laboratory version of extending electronic board for bi-polar card.

The MSE570 Evo2 bi-polar drive unit provided the means to remove and considerably reduce a quantity of electrical devices. In addition the program done for motion control system was much smaller and as a result, much easier to understand.

3.3.2 Program description - diagram, explanation of the program

3.3.2.1 Front panel and operating principle

Several programs for motion control of the MAESTRO thorax phantom have been created using LabVIEW. Whilst the same hardware was used, each programmer implemented his own flavour of the required functionalities and associated graphical user interface. The examples in Figure 3.23 and 3.24 present two different front panels of the codes for motion control by frequency modulation. The user interface implemented in Figure 3.23 was created by my colleague and internship student Armel Tassot. Figure 3.24 shows the author's implementation.

This item has been removed due to third party copyright. The unabridged version of this thesis can be viewed at the Lanchester library, Coventry University.

Figure 3.23 Front panel of the program used to generate phantom motion (Tassot A.).

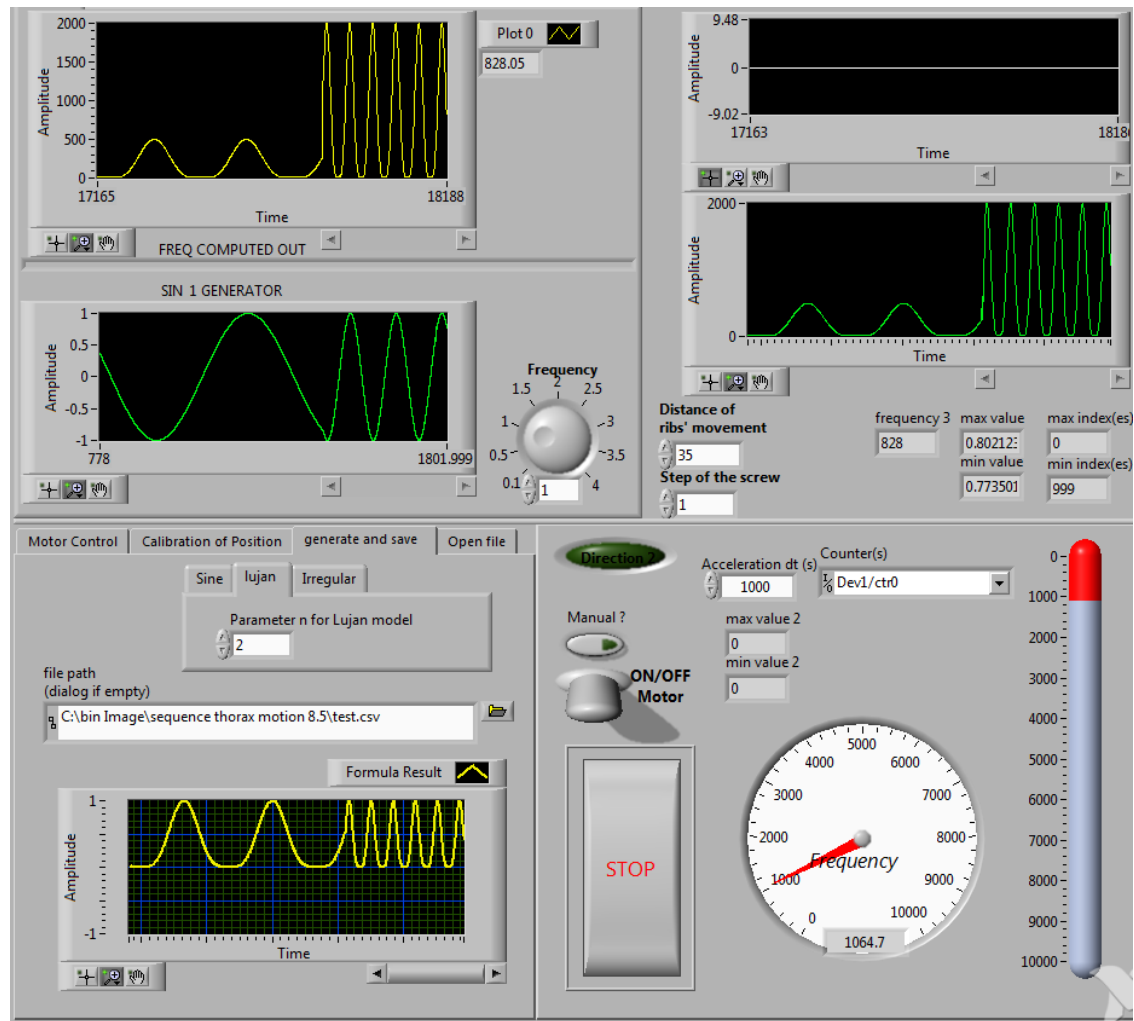


Figure 3.24 Front panel of the program used to generate phantom motion.

The first code presented on Figure 3.23 has a menu based interface structure. This presents a small amount of information to the user at any one time. The drawback is that it requires the user to switch between different tabs of the program to observe or have access to different functionalities. The first tab graphically describes the process to follow from the code initialisation and set up before running the program. The user should follow the arrows to first select the counter to use to provide the frequency control to the interface device, the time of simulation, and lastly to decide to check the simulation of the motion or save it to file for subsequent use. The breathing frequency can be adjusted if it was found not to be acceptable during the visualisation of the results in simulation.

The second front panel, shown on Figure 3.24, was designed to have easier access to control functions instead of using an ordered configuration. In this case the

user has to know the order and number of steps to follow to be able to use the program.

Choosing one of the tabs, on the left lower part of the interface screen, will generate a specific motion mode. It is suggested by the author to perform the calibration the first time the program is run (available through the *Calibration of Position* tab). Once the calibration is done the programs switches off. It is then possible to restart the program and select the required motion pattern.. Note that all the controls have default parameter values to generate an average motion. Whilst the phantom is operating through the program, it is possible to alter its motion type and its characteristic. The phantom and program stops when the *STOP* button is pushed. Such approach was adopted to save time during the experimentation when the software is used by qualified personnel and researchers where a direct access to the programs functionality is advantageous.

Note that before the program can start, it is required to select the counter to use in the upper right corner of the interface illustrated in Figure 3.24. That is the only condition to run the code. Such selection can be saved as a default parameter and requires to be changed only if a different device is used. The other parameters can be changed and tuned during the selection of the signal to send to the motor on-line.

The overall functionality is almost the same as the code designed by A. Tassot. The motion control for the sine pattern gives fluent and expected movement of the rib-cage. In addition Lujan/ Irregular/ Patient Data File patterns and position calibration of the phantom functionalities were added to the code. Base on the tab/case function only one of the types for motion control had been implemented by A Tassot. In this work four tabs have the following functionalities:

Tab No	Type of movement	Movement Type/Pattern	Description
1	Motion Control	Manual/ Linear	Manual motion control whilst within the range of possible motion limited by the emergency switches. Used mainly during research and tests. Can be used also to produce random movement pattern. Tuneable parameters are: the pulse train frequency(speed) and duty cycle, direction and motion acceleration
2	Calibration of Position	Auto/ Linear	Function to set up a home position before normal movement initialisation. Program works until it reaches the home initial position. Then the program is stopped automatically.
3	Generate And Save	Auto/ Sine; Lujan; Irregular;	Simulated mode with selectable and mathematically described movement pattern. Tuneable parameters are: The program works within the range of motion until the 'STOP' button is pushed. When stopped, the program saves the motion pattern into a spreadsheet file.
4	Open File	Auto/ Real Patient Data	The motion pattern is read from a spreadsheet file. The file can contain real patient measurements or other data prepared for motion control. The program works within the range of motion until the data file is read or the 'STOP' button is pressed. When stopped, the code saves the motion pattern into a spreadsheet file

Table 3.5 *Movement types of the program for frequency motion control.*

In contrast to the GUI illustrated in Figure 3.23 , the GUI from Figure 3.24 enables the user to identify the allowable frequency range using the control knobs and associated indicators can be recognized. The program uses frequency with range up to 10 [kHz] for motor control. By implementing data file (real patient breathing measurements) or Sine/Lujan/Irregular waveform, the code is able to generate respiratory motion automatically.

The software implemented takes into account the limitations associated with the hardware selected. The MSE 570 Evo2 bi-polar driver card required the creation of a new program. It is the opinion of the author that this new software is easier to

operate compared to the motion control by sequence. The frequency control implementation required a smaller amount of code that makes it easier to understand. From a hardware perspective the use of bi-polar drive reduces the volume of electronic associated with the drive system which is a significant advantage when considering travelling with the phantom.

3.3.3 Evaluation of motor drive implementations

In order to decide on the solution to adopt a number of tests have been carried out in CTAC as well as at the hospital on the phantom and individual motors connected to the bi-polar drive. In addition to these tests other aspect involving the robustness of existing solutions and practical aspects such that the presence of existing code that had been shown to work were considered.

The process followed to evaluate an approach was to initially develop the code without connecting it to the hardware but instead writing the code and signals to file. Once the information written to file was correct, the solutions were deployed and the actual stepper motors were used. In CTAC a test stepper motor and slider were used together with smaller stepper motors.

One contribution of this work was the adaption of programs realised for research to the classroom environments. These programs are currently used for m09mse laboratory on LabVIEW stepper motor control.

The program currently used to control the thorax phantom is based on sequence control. The bipolar control was only applied to a single motor (Figure 3.9). This choice was based on the fact that the current software was acceptable for the purpose and whilst not ideal provided the required functionalities. As was shown on the front panel (Figure 3.9) of its LabVIEW code, the GUI can make a user feel a bit confused and its block diagram is complicated with its case in the case looped structure.

The program with frequency motion control (Appendix 1) has potential if the overheating observed can be resolved. The overheating was caused by the large currents sent from the Bi-polar drive to the stepper motor. As a consequence, the stepper motor became very hot and exhibited some vibration when operating at high frequency and in some occasion during changes of direction. Provided that a solution to these problems can be found then there is scope for frequency control to be used in the future.

3.3.3.1 Block diagram

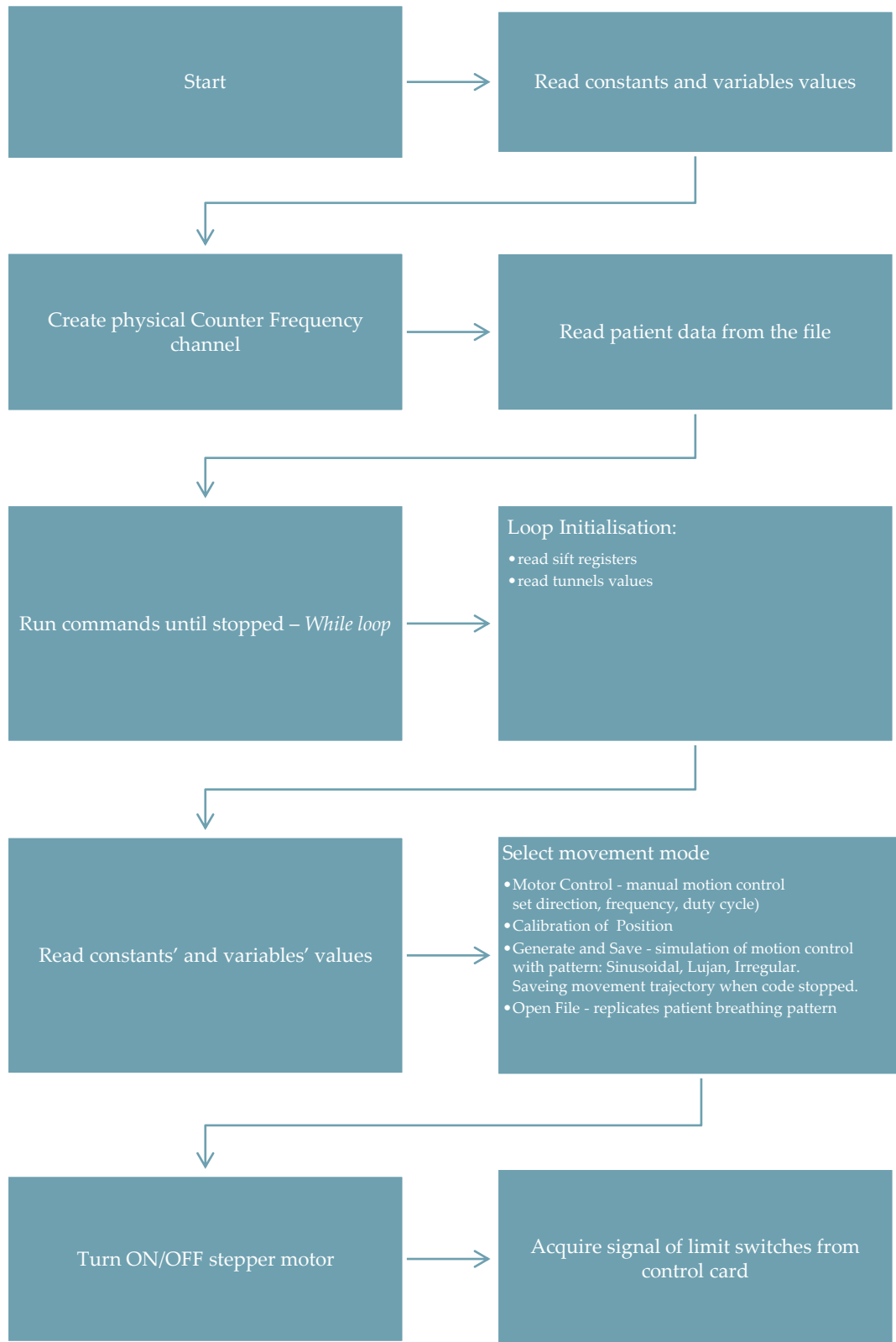


Figure 3.25.a) Frequency motion control of the phantom – diagram.

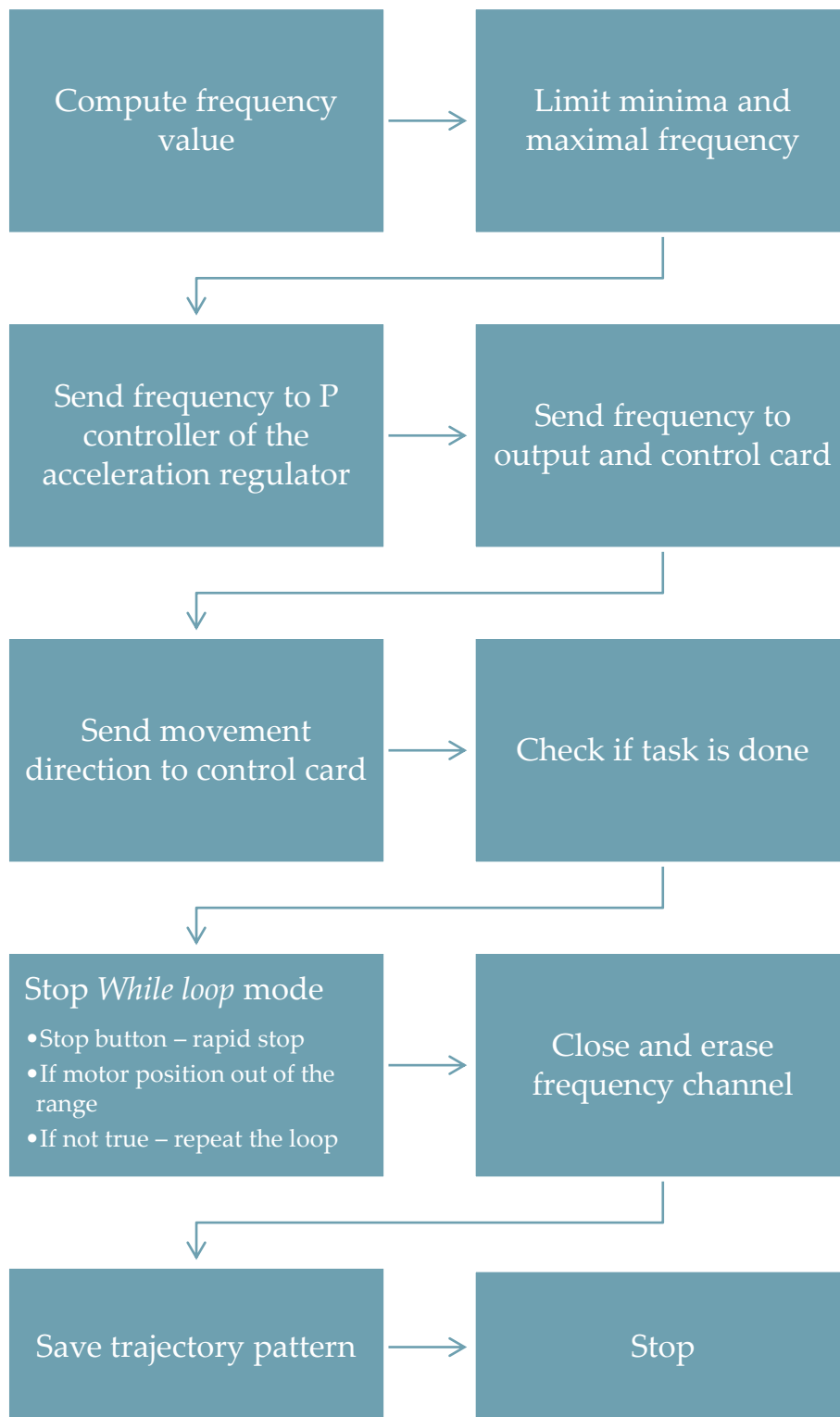


Figure 3.25.b) Frequency motion control of the phantom – diagram.

The diagram functions description:

Note that this programs uses a counter to ensure that appropriate timing can be generated. The user should check the presence of a counter on the hardware used. LabVIEW In this work the default value set was device Dev1 counter 0.

- Start

Run the LabVIEW program by pressing the 'Run' button or the 'Ctrl' + 'R' key combination.

- Read constants and variables values

Read all parameters of the constants and controls, outside and on the left of the *While loop* as commands and parameters are executed by LabVIEW by following the wires connecting the VI normally from the left to the right hand site of the code.

- Create physical Counter Frequency channel

The Counter Output (CO) was created and provided with the frequency value, to control stepper motor via bi-polar stepper motor drive MSE Evo2. To ensure more stability to the program work and high frequency of the code execution, low-level DAQmx VIs were used for the physical channels creation. The bi-polar drive unit required much higher frequency than the control by step sequence 10 [kHz] by contrast to 1 kHz.

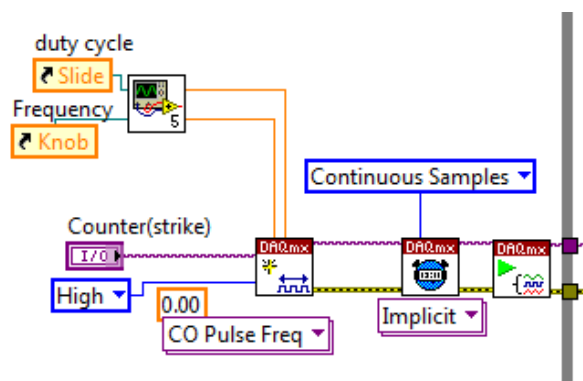


Figure 3.26 The Counter Output creation with low-level functions use.

The CO channel was constructed from low-level DAQmx functions and consists:

- DAQmx Create Channel* – set as Counter Output (CO) Pulse Frequency;
- DAQmx Timing* – set to Continuous Samples
- DAQmx Start Task*

- Read patient data from the file

The program reads the file saved e.g. real patient respiratory measurements or individually prepared data for motion generation in research use. In this case, all data should be saved in column vertically and contain double precision real values. The 'Read From Spreadsheet File' VI, illustrated by Figure 3.13, can open and read file with *.xls extension (excel file).

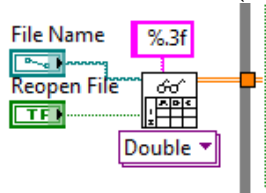


Figure 3.27 Spreadsheet file used to read motion pattern data. Block diagram.

- Run commands until stopped – *While loop*

This function assures the continuous code execution until stopping condition becomes 'true'. Program works periodically. Loop frames are iterated with high frequency which value depends on period of the sub VIs realisation inside the 'While loop'.

- Loop Initialisation:
 - read sift registers
 - read tunnels values

The parameters obtained from outside of the loop, they become the initial values for the tunnels and shift register inputs of *while loop*. All parameters need to be collected from shift registers and tunnels values.

- Read constants' and variables' values

The parameters were generally acquired from the left to the right hand side of the code. Most of the constants representing physical parameters such as dimensions or gear-box ratio (Figure 3.28) were boxed into subVI in the main code (see Appendix 1).

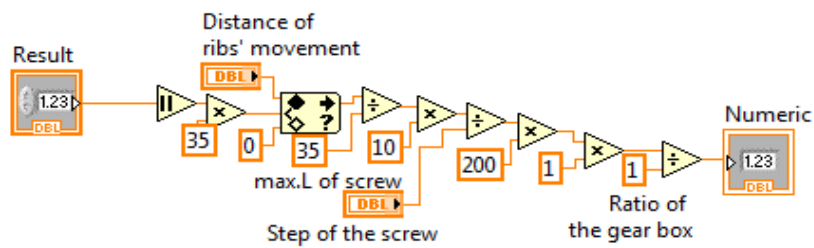


Figure 3.28 Set of constants and controllers for all stepper motors. Block diagram.

- Select movement mode

The movement mode is selectable by a tab on the front panel. It allows the selection of one pattern at the time.

There are 4 available possibilities:

- (1) 'Motor Control' - manual motion control (set direction, frequency, duty cycle)
- (2) 'Calibration of Position' (adjustable frequency)
- (3) 'Generate and Save' - simulation of motion control with one of the following mathematical function:
 - 'Sinusoidal'
 - 'Lujan'
 - 'Irregular'
- (4) 'Open File' - replicates patient breathing pattern

The generated signal waveforms were collected using parameters such as: amplitude (represents distance of the movement), frequency (state speed of motion), and time sample if amplitude = 0 (used for direction change).

- Turn ON/OFF stepper motor

This switch replaced the physical switch of the bi-polar card in an attempt to reduce the heat generated by the stepper motor. The power supply of the stepper motor can be turned on/off using LabVIEW.

- Acquire signal of limit switches from control card

There are three switches on each axis, two of them limit the range of motion and the 3rd indicates the middle position.

- Compute frequency value

The motion is obtained by frequency modulation. The higher frequency, the faster turns the motor. The frequency f is sent out to stepper motor drive thru counter frequency output of the NI card and is calculated by using *Equation 3.3*:

$$f = f_b * y_p * \frac{LS * S_n}{G_{BR} * R_r * PS}$$

Equation 3.3 *The frequency computation.*

where: f_b is the breathing frequency [Hz]; y_p the amplitude value of the sample taken from generated pattern (variable, in millimetres); LS the length of the screw; S_n the number of steps per revolution i.e. 200 [steps/revolution] for full step and 400 [steps/revolution] for half step; G_{BR} is the gearbox ratio for two of the axes of the 3D slide system, R_r is the ribs ratio, relating the largest rib movement to the maximum screw displacement and PS is the pitch step of the screw.

The selected pattern of the motion gives a shaped waveform with a maximum amplitude equals 1. This allows normalising any pattern where the maximum amplitude, which represents the distance of the movement, can be equal to 100% of that distance.

Such pattern of the movement is sampled with the loop iteration and gives an amplitude value, which is multiplied by the breathing frequency and then by a set of constant parameters that depends on the phantom design. The constant parameters LS, S_n , G_{BR} , R_r , PS are given in Table 3.3 where i.e. for the ribcage are equal to 10[mm], 200[steps/rev], 1, 3.2 (which is relation of 35:11) and 2[mm] relatively.

- Limit minimal and maximal frequency

For safety reasons limits are imposed to checking if the signal is in range.

- Send frequency to P controller of the acceleration regulator

A PID controller working as a proportional (P) controller was used. The idea was to slow down the acceleration of the stepper motor by setting $dt(s)$ input.

- Send frequency to output and control card

The computed and bounded frequency previously calculated was sent to the counter output and then to the NI interface card.

- Send movement direction to control card

Direction uses a Boolean signal to switch between forward/ reverse movement.

- Check if task is done

This is a quality assurance task to avoid missing data. It checks if the signal was sent to the created counter channel. If an error occurs then a warning is displayed on the screen.

- Stop *While loop* mode

(1) If not true – repeat the loop

(2) Stop button – rapidly stops the loop execution

(3) Stop - If motor position out of the range

- Close and erase frequency channel

Clear memory: erase physical channel.

- Save trajectory pattern

Pattern of the movement can be saved into file (*.csv) where whole movement trajectory written.

- Stop

3.4 Video tracking of the thorax phantom motion

In addition to the thorax phantom and its motion control, a part of the author's practical work was the camera video tracking system development. Existing code was analysed and tuned, to achieve the best performance during the experimental work.

3.4.1 Used hardware

Different types of camera have been used in this work such as industrial cameras by FOculus model FO323TB and FO124TB, professional video camcorder by Canon model XL2, universal internet camera by Logitech.

The best available camera was FO124TB which was therefore used for the final set-up and tests of the video tracking system see Figure 3.29.

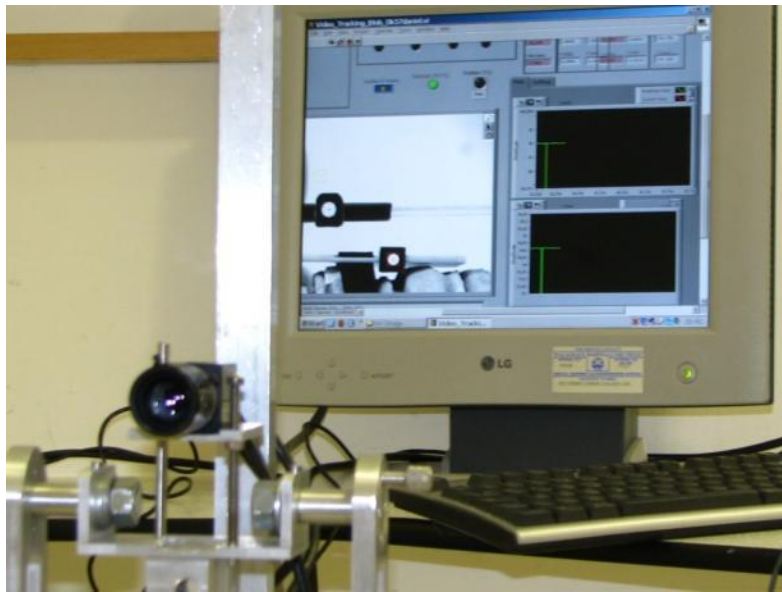


Figure 3.29 The IEEE1394 camera and software for video tracking two targets.

The FOculus with model FO124TB offered has a fire-wire IEEE1394a interface, a monochrome image sensor and is capable of acquiring images with frequency up to 60 frames per second and with maximal resolution 659(H) \times 494(V) of effective pixels. The focal distance was $f=50\text{mm}$.

The data transfer of the measurements to external computer was realised via two analogue outputs (AO) of the LabVIEW cards: I/O card: NI PCI-6024E and NI SC-2075 data acquisition module Figure 3.2 (initially), and on Figure 3.4 the I/O card: NI USB-6229 data acquisition module (finally). Both were presented in Section 3.1.2.

Different camera calibration grids have been used. One of the grids had dots with a diameter $d=2.5[\text{mm}]$ and distance of $6.4 \times 6.4 [\text{mm}]$ between the dots. This grid was used mainly for a short distance (1 metre and lower) between observed object and a camera. Another grid had dots of diameter $d=4[\text{mm}]$ and were separated by $12.7 \times 12.7[\text{mm}]$. During the experimental work the distance between camera and the markers tracked was about 2 metres. The grid that offered the best compromise

between the detection of the dots and the grid resolution for the distortion correction is presented overleaf (see Figure 3.30) with black dot diameter of 4[mm] separated by distance 9.5×9.5 [mm]. The image calibration was done automatically within the LabVIEW software, see Section 3.4.2 for details on the VI used to perform the calibration and then transform the target coordinates from pixels to mm.

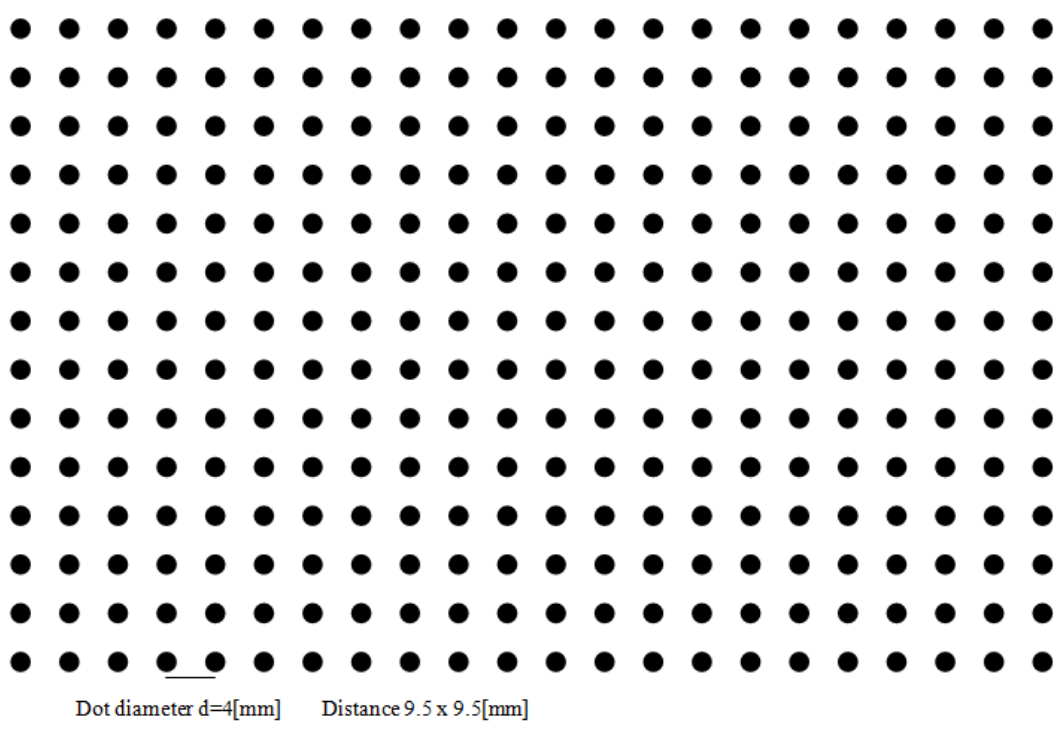


Figure 3.30 The calibration grid for the video tracking system with dot diameter equals 4[mm] and distance =9.5[mm] between.

The imaging set up was used in different environments with various lighting conditions impacting on the brightness or grey level of the markers being tracked. Markers of different sizes and grey level were investigated, see Figure 3.31. It was found that the first three rows were acceptable and perform similarly. To extract two targets from the background circular elements were bounded by a square of : 8[mm] diameter for a reference and 6[mm] diameter for the moving marker.

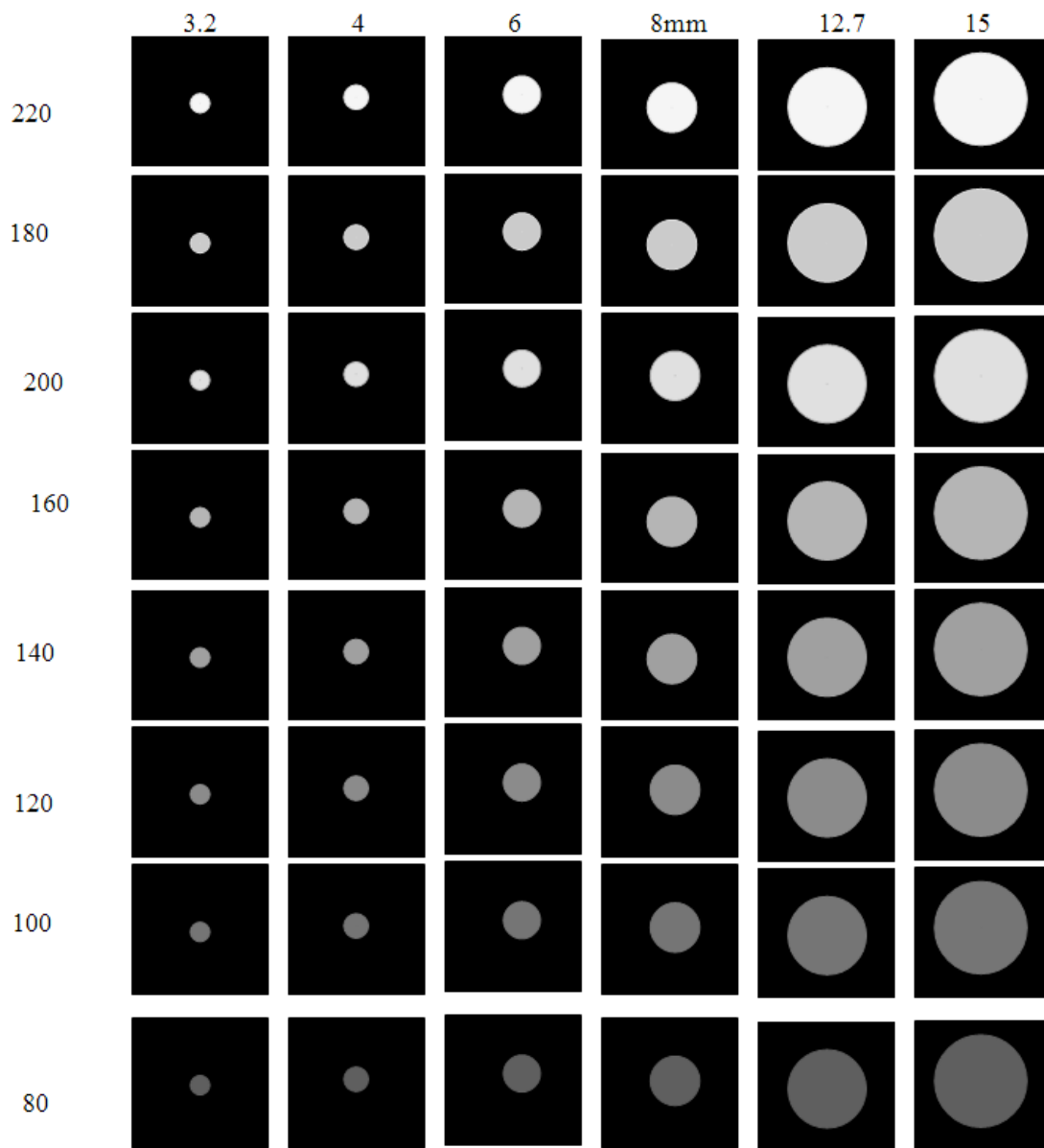


Figure 3.31 Marker samples of different size and contrast threshold.

To evaluate the video tracking system a small stepper motor was used and the position of a rotating arm was tracked together with that of a reference marker located in the corner of the frame, see Figure 3.33.

3.4.2 The program description.

The idea of the program was to track two markers with high accuracy and with frequency of 30 [Hz] or higher. The markers displacement was analysed from the

images and then measured, where lastly the result could be sent to the motion compensation system controlled by other computer.

3.4.2.1 General operating principle on the image

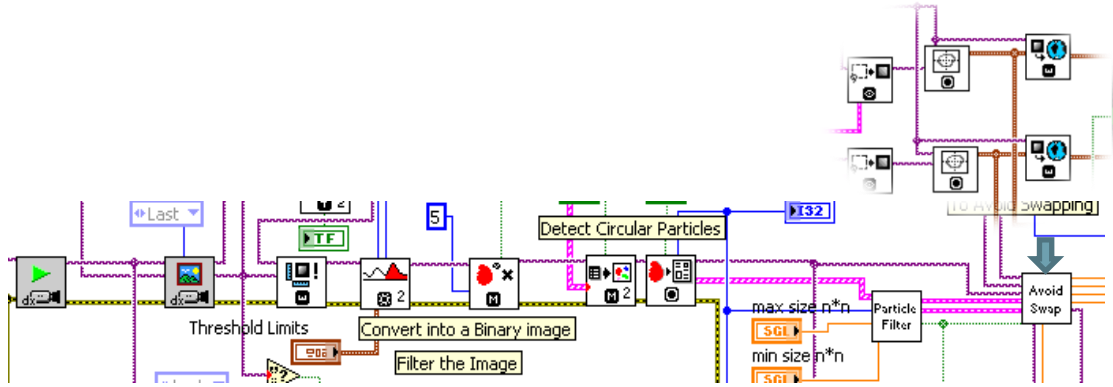



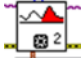



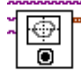



Figure 3.32 Block diagram of the image tacking code.

The video tracking code can be generally described by block diagram shown on the Figure 3.32, where functions in the serial line shows the main operations made on the acquired images.

Initially, the created video channel starts  and the last acquired image is collected by get image block  configured to grey-scale image acquisition. The image is then calibrated . Next, program computes the optimal threshold value with AutoBThreshold2  function. Then, it applies this value for binary image conversion. This conversion means that pixels are changed to "0" dark object or "1" if bright object. The bright objects' clustering method was used, because targets are normally white on a black background. It is worth to notice, that the grey-scale range is from 0 (black) to 255 (white). Markers with different level of contrast with respect to the background were investigated, see Figure 3.31. IMAQ Remove Particle  VI removes small particles with number of erosion set to x5. Furthermore, the other particle filter  was used to keep only circular elements meeting specified criteria such as measurements model of Heywood Circularity. If an insufficient number of circular shapes are removed, the IMAQ Particle Analysis Report  returns the number of particles detected in a binary image and reports common

characteristic such as: Area, Centre of Mass, Bounding Rectangle, Orientation and Dimensions of each particle. The centre of the bounding rectangle surrounding the detected element was used. Ideally there should be two detected particles representing moving and not moving target. It was observed that the bounding box

was not centrally positioned therefore *IMAQ Centroid*  VI was used to improve the accuracy of the centroid measurements. All these operations were made on the acquired image before converting the parameters from pixels to Real

Word . Lastly, all the parameters obtained were used mainly for distance calculation between markers or position moving target computation in relation to (0,0) image corner (left, upper).

The above VI form the core of the target tracing. Other VI was added to calculate distance, reduce the influence of the environment (bright sun light, fluorescent light, shadows, and light reflections), the number of lost target or the detection of too many detected targets.

3.4.2.2 Modifications

A number of changes were implemented by the author to increase the efficiency of the program. The main aims of the practical work on a video tracking system was to reduce vents such as 'lost target' or 'too many targets', and speed up the code. These modifications came about from being in charge of the system operation during tests at the hospital.

Depending on the light condition, the program could lose target or acquired too many targets from the background (see for example on Figure 3.33 the straight line at amplitude 0 corresponding to loss of tracking at the start of the procedure). This error was indicated by LEDs.

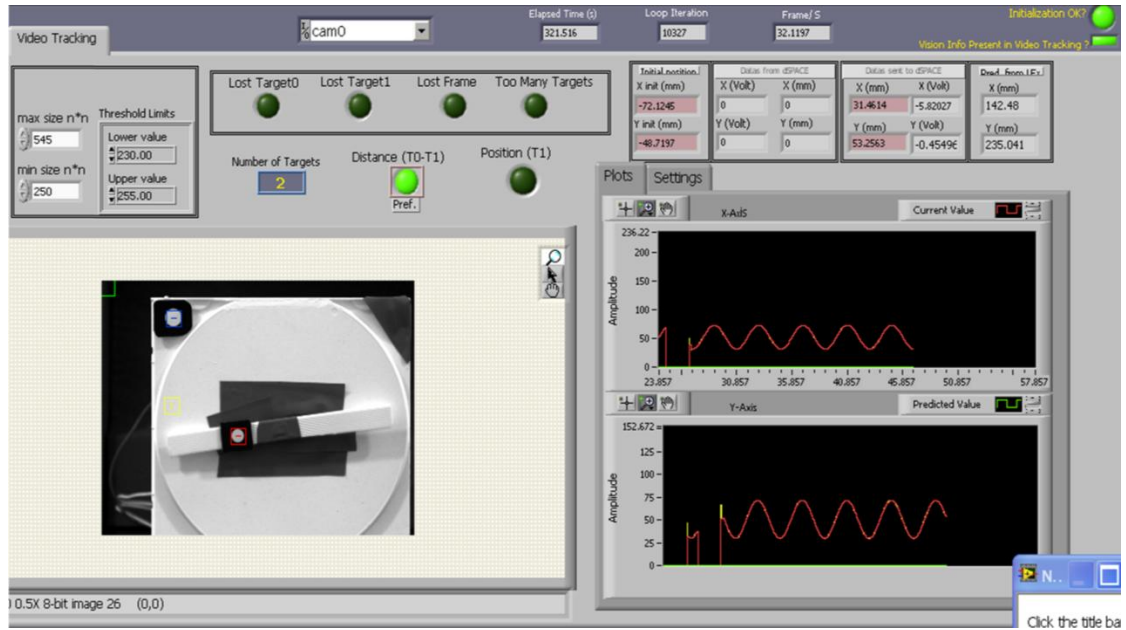


Figure 3.33 User interface of the video tracking. Lost target visualisation.

The user interface (see Figure 3.33) comprises a set of controls in the upper left corner. The controls are limits for the targets detection. The template area and threshold for the brightness/contrast can be manually adjusted.

To reduce the number of targets detected by the particle filter, the minimal and maximal sizes of the targets detected can be manually adjusted (see upper left corner of the Figure 3.33). The markers area depends on marker diameter, lighting and distance to the camera. In this work, considering markers of 6[mm] and 8[mm] diameter 2 m from the camera, the maximum and minimum areas were set to 550 pixels and 330 pixels respectively.

The threshold controls the grey value of the pixels that will be considered as the target (here between 230 and 255 - white). A number of indicators were implemented to facilitate the software operation and simplify the experimental set-up. The view from the camera is displayed on the bottom left of the screen with the moving markers indicated by coloured squares. In this case the markers were fixed to the DC motor. The reference marker is fixed to the frame of the motor unit and the moving marker to the moving arm. The relative motion, along the X and Y coordinates and between the two markers are two sinewaves which frequency changes depending on the speed of the motor. The distance measured in pixel is converted to mm and displayed in the upper right corner of the screen. The constants used to perform the calibration and conversion from mm to Volt is displayed on the right top of the screen. Note that a signal in volt is sent to the PSS

which then perform the conversion from Volt to mm using the same scale. In the upper middle part of the screen, four boxed indicators visualize error occurrences: 'Lost Target 0' is on when the reference marker is lost, 'Lost Target 1' is on when the moving target is lost, 'Lost Frame' indicate that an image frame has not been detected resulting in the loss of both targets. A scalar indicates the 'number of targets' detected. The mode of measurements 'Distance' or 'Position'. 'Distance' is the default mode during the experimental set up as it gives the relative horizontal and vertical distance between the two markers. The 'Position' gives a position relative to the origin of the image which is the upper left corner of the image.

It was observed that in some cases it was beneficial to set camera lens to provide a slightly blurred image. This reduced the effect of reflections and speed up the code (quicker particles filtering). Given that the code calculates the centre of mass, blurring the image should have a minimal impact on measurement errors. However, these improvements did not eliminate totally the above errors. The last modification was to send that last valid measurement in case where the target found is different than two.

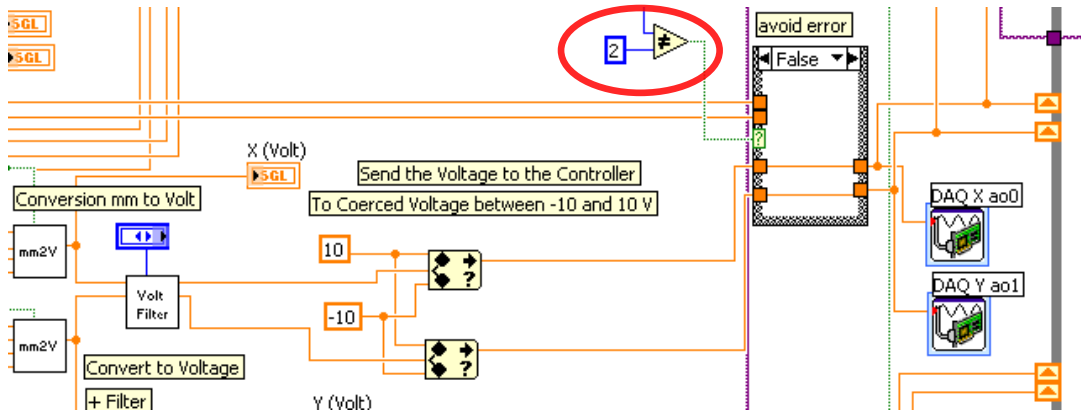


Figure 3.34 Elimination of the targets error. If false – send actual measurements, if true – send previous data. Block diagram.

The other aim was to obtain faster loop iteration during tests with different environmental conditions. To increase the frequency of the code iteration, the first step was to reduce unnecessary VI such as graph plotting or motion control of a small stepper motor included in the main program. In addition converters (mostly to the *Single Precisions* numbers) to unify parameters representation were used resulting in a further increase of the tracking frequency. It was found that the image processing functions consumed most of the time used for code execution and specially the *IMAQ AutoBThreshold2* function. Thus this command was analysed in

detail. Having investigated different marker sizes and contrasts (Figure 3.31) and different light conditions, the contrast range was manually limited level of the contrast from 180 to 255.

The improvements to the code increased its average operating frequency to 32 [Hz].

3.5 Difficulties associated with LabVIEW programming

LabVIEW is a graphical language with a large amount of useful tools and is easy to understand compared to other programming language with similar possibilities. However, this software requires appropriate drivers to communicate with the hardware. Drivers from previous LabVIEW version are not always compatible. The disadvantage of this software is also the incompatibility of the *.vi programs from previous version and lack of compatibility between different versions even if the same VI are used. To make the software compatible it is necessary to save it 'for previous version'. This means that several version of the same code have to be kept to accommodate for version changes.

Cost of the LabVIEW is important £4000 for 4 seats research licences. NI DAQ Devices and cables are also expensive. Note that alternative suppliers can also be used which offer driver supports for NI LabVIEW.

During my research work with LabVIEW the pseudo real time data acquisition implemented using windows was not a trivial task and required NI training and support, as information within the help was not sufficient.

This software performance depends on the computers used and the windows version. The same code tested on one computer returns code frequency execution of 5000 frames/sec while on the other frequency was over 32000 frames/ second. Such differences impacted significantly on the accuracy of the timing of the sequence sent to the motors.

Another difficulty was associated with the flow of information and data execution in LabVIEW. To investigate these errors, 'highlight execution' tool was used.

To solve some of the issues, it was necessary use additional multimeters and oscilloscopes.

3.6 Conclusions

This phantom has been successfully used for many hours over 3 years during the testing of the patient support control system at the university hospital. The thorax phantom mechanical, electronic and software design has continuously evolved over the course of its use within the MAESTRO project. It can still be improved using software or hardware solutions. For example, further code simplification can be carried out and its accuracy can be improved by using real time hardware as opposed to windows based solutions.

Through applying the MSE 570 Evo2 bi-polar drive unit, it was possible to remove and considerably reduce a quantity of electrical devices. In addition the program done for its motion control system became also much smaller and consequently easier to understand.

The main disadvantage was overheating of the stepper motor caused by large current sent from the bi-polar drive unit. This was the main reason for the staff at the University Hospital to reject the idea of motion control by frequency modulated signal and keep the existing sequence control approach.

Apart from this fact, it is the belief of the author that frequency control has potential through the use of bi-polar motion drives. Indeed the stepper motor motion was in most cases found to be reliable and accurate. Similarly to the sequence control approach, the addition of a current limiter seems to be warranted. Additionally in the MSE 570 driver specification, there were found possibility current reduction from 0.5[A] to 3.5[A].

As a second possibility, the phantom motion could be obtained by control sequence signal sent to the driver. The initial code had been created by PhD student I Land (2009). The program contained some limitations such as missing calibration mode or position drifting. The existing code was analysed, however improvements of the existing programme was found to be a challenging task due to the complexity of the code. Several trials have been undertaken to evaluate the proposed motion control sequence. However, not all the issues encountered could be resolved in the time allocated to this work.

Having established that sequence control was the most convenient approach, the next Section presents the experimental evaluation of the code and the evaluation of motion compensation using the phantom.

Chapter 4

Experimental evaluation

The work presented in this chapter was carried out at the Control Theory and Application Centre (CTAC) of Coventry University and also at the University Hospital Coventry and Warwickshire, NHS Trust (UHCW), Coventry.

Several experiments were made in preparation of the testing of the software on the thorax phantom.

The initial tests were carried out at CTAC of Coventry University. The programs were initially evaluated on simulation and then using test set up involving a single stepper motor fixed to a slider and supplied with the same power supply and current limiter units than the phantom, see Figure 4.1.



Figure 4.1 The stepper motor with current limiter and power supply units.

Due to the limited access to the phantom or bi-polar motor drive and because there were no model of the phantom the required testing was performed using multimetres, oscilloscope and other data acquisition devices. This equipment was used to evaluate the timing of the signals sent to the stepper motors and diagnose issues, and analyse the results. The Figure 4.2 shows oscilloscope during one of the pulse frequency test used for motion control by frequency modulation. This test aimed to identify if the correct frequency was sent and if noise was an issue.

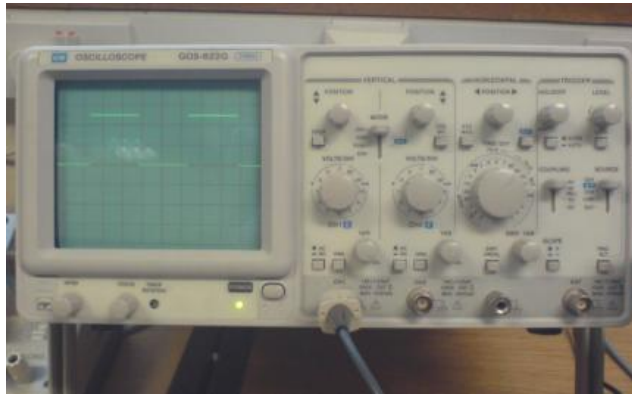


Figure 4.2 Testing of the frequency motion control code with GW oscilloscope use.

Some of the errors to be observed, they required high frequency digital oscilloscope. The example below (Figure 4.3) presents print screen of the control signal of the pulse waveform in blue, together with shifting direction wave in orange. In this particular case the observation of 'direction' waveform (in yellow), it allows to highlight the noise on the edge periodically generated by stepper motor, and its shaking behaviour. The square waveform (in blue) exhibited some transient behaviour resulting in the addition of a bias to the square wave of amplitude (+/-1 [V]).



Figure 4.3 The error identification with Tektronix oscilloscope use.

Having carried out the initial testing of the code in CTAC the new and modernised code was then tested with the real thorax phantom at the University Hospital Coventry and Warwickshire, where the phantom was normally kept. Thus the most important tests were prepared at the hospital.

Most of the testing done at the UHCW was aimed at evaluating the software and methods developed to control the PSS. The author supported most of the test carried out during the last year of the MAESTRO project on the clinical Elekta Synergy machine. In addition to operating the phantom program the author also operated the motion tracking software that he contributed to develop and evaluate.

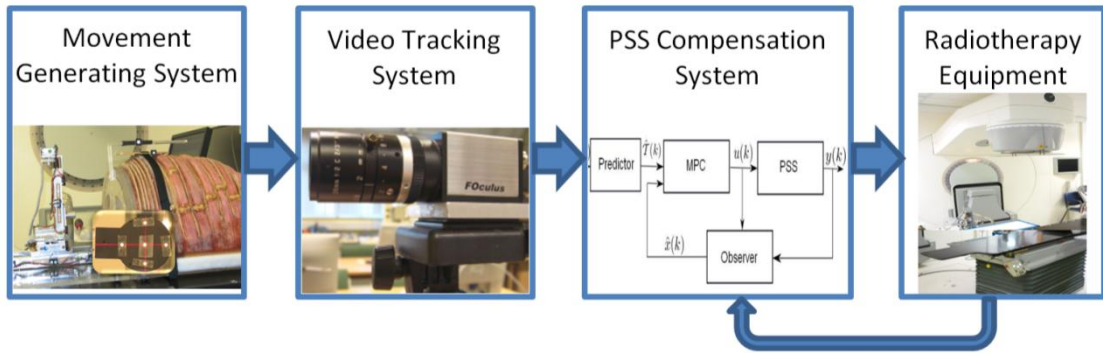


Figure 4.4 Structure of the overall control system including the phantom with markers positioned onto it being tracked by a camera. A motion predictor anticipates the motion of the markers and is used by a controller to move the PSS.

The flowchart (see *Figure 4.4*) briefly visualise the combination of four systems. The first is a *motion generating system* which operates in open loop as the phantom does not use position feedback to adjust its motion. The camera is detecting the marker position at a frequency between 20 and 30 Hz. The *patient support compensation system* acquires input signals from camera tracking software to provide on-line target displacements and used the feedback signal from the PSS sensors to predict and compensates that measured motion.

An illustration of the real experimental set-up at UHCW is presented in *Figure 4.5*.

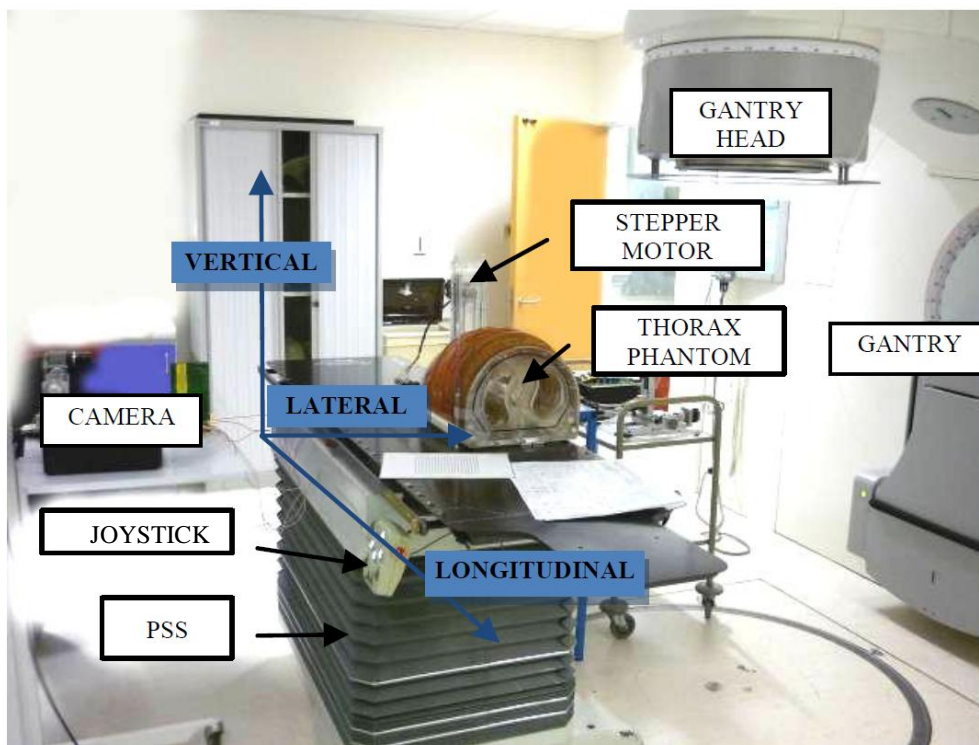


Figure 4.5 Typical set-up for thorax phantom prototype tests.

The whole system contains: the RT treatment machine (clinical Elekta Synergy machine in this case) and its associated movable PSS, the thorax phantom model, an IEEE1394 camera and associated video tracking system as well as the PSS control system implemented in dSPACE software (dSPACE, 2011).

The idea of this set up was to predict and compensate the patient breathing during radiotherapy and to assure that the beam remained focused on the target irrespective of the target motion simulated using either the 3D sliders or the ribs. The PSS control system was designed to move the PSS in the opposite direction to the motion of the phantom.

The thorax phantom generates motion with selected patterns of movement (see Figure 2.17). Two markers were fixed to the phantom surface and tracked by the camera. The measured distance between the markers was sent to the PC controlling the PSS. Afterward the tracked position was predicted to compensate for measurement delays and systems latency and finally a control signal calculated and sent to the PSS to move it with appropriate distance and velocity in opposite direction to the phantom movement.

Most of the testing was carried out without the use of radiation but solely with the use of an independent camera or the actual camera used for tracking.

One of the last series of tests performed involved the use of radiation. The x-ray beam was focused onto a radiation sensitive film which was held by the 3D slide part of the phantom. The result shown in Figure 4.6 are the results of the following experiments (from the left) film was irradiated when phantom and PSS were stopped, the second was irradiated while the phantom moved with Lujan pattern but PSS was stopped. The last film on the right hand side visualises the effect of irradiation when the thorax phantom movement was compensated by the PSS system.

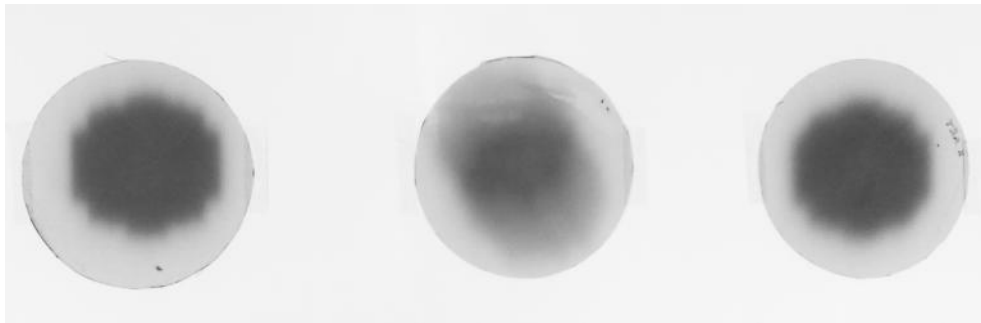


Figure 4.6 Outcome of phantom and PSS controller tests.

These results were very satisfying. It shows that the irradiation of normal tissues surrounding the tumour almost was not affected by the target motion. Additionally, the phantom can be used to support the research of the other areas of the MAESTRO project, e.g. to develop work on video tracking system and feedback control system as well.

It should be mentioned, that besides the thorax phantom and its motion control, a part of my practical work was also the camera video tracking system development. Previously created code was analysed and tuned. Several modifications of the code were also made. The main achievement was to accomplish the required frequency of program work in windows 'real time', and eliminated errors due to lost targets.

Since the end of MAESTRO the phantom has been used by Dr Haas in collaboration with Brussels University Hospital and BrainLab to evaluate the VERO tracking system and the use of fiducial markers with a realistic phantom, see Figure 4.7. A new version of the program was used based on the work of the author and in particular the use of DAQmx low level VI.



Figure 4.7 VERO experimental set-up.

Chapter 5

Propositions to the thorax phantom development

Most of my research work was focused on practical issues. Some of them were focused on the MAESTRO thorax phantom and its design improvement. There were six modernisations proposed to the phantom construction.

The first one was to generate a third (lateral) direction of the movement for the phantom's ribcage. Three proposals were designed and sketched. The second idea was to add a clutch for the phantom's ribcage motor for safety reasons. The third idea was to re-design the rod for the x-ray sensor to avoid bending and re-design the IEEE 1394 camera holder to use it on a standard camcorder tripod. Fourth, the video camera holder was adapted to allow usage a universal camcorder's tripod and consequently made the modernisation of the base plate for tripod holder. The use of a laser pointer to speed up the calibration and set up the camera video tracking was proposed. Finally it was suggested to implement a "hard" switch for the power supply of the logical card and controlled by LabVIEW to avoid overheating of the stepper motor if frequency or sequence motion control were used.

5.1 Propositions of rib-cage lateral movement

A few alternatives to implement the rib-cage lateral movement were proposed.

It should be noticed, that solutions should respects several conditions described below:

- 1) The lateral motion should use the existing thorax phantom components or should not involve significant redesigns.

- 2) The amplitude displacement of the ribs is changing from the lowest rib (the smallest movement) to the highest rib (amplitude is the biggest). The value of the maximal amplitude of lung displacement is not more than 9.8[mm] when coughing therefore the considered displacement could be specified up to 10[mm].

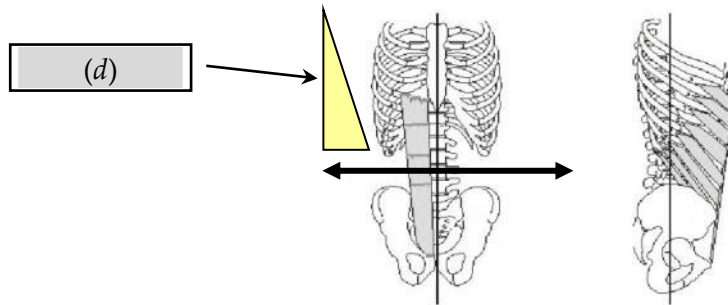


Figure 5.1 The rib-cage lateral expansion visualisation.

- 3) To keep lungs volumes without other additional elements that could affect X-ray beam trajectories and interfere with the target insert.
- 4) Do not to use additional electrical/electronic devices i.e. motors. Focus on mechanical modification where pattern of movement could be modelled by shaped insertion like cam.

The thorax phantom shown in Figure 5.2 represents the view from the back of the phantom with the spine visible under a transparent Perspex plate. The pulley of the stepper motor which drives the screw that moves the ribs through the opaque plastic component is on the left hand side. The idea was to transmit the rotary movement to linear motion by nut on the screw, fixed to white board with a trapezoidal cut out.

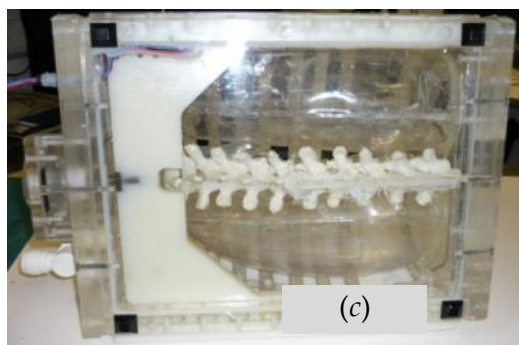


Figure 5.2 The thorax phantom model – bottom view.

A few proposals for lateral movement with using the existing thorax phantom were briefly described below:

Solution 1:

The first idea bases on taking the advantage of existing moving board observed on Figure 5.2 and uses an additional beam shaped with teethes. With this design would be possible to set different character of movement for each separate rib by using different teeth shape for each rib (see Figure 5.3).

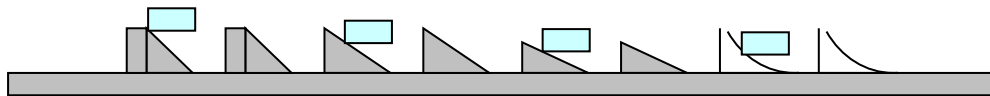


Figure 5.3 Possible types of the pattern movement regulated by shaped slope.

The proposal is to locate saw-tooth beam over the moving board but with very close distance about 5[mm], and on the internal side of ribs shown on Figure 5.5. In addition, instead of the existing screws is to use a mandrel or screw with longer pivot part. This allows to push easily the ribs outside and to achieve the third direction of the rib-cage motion at the same time see Figure 5.4.

Polyamide (PA) or polytetrafluoroethylene (PTFE) known as a Teflon or other synthetic material, inter alia with low friction, low hygroscopic molecule's structure or even hydrophobic polymer could be used.

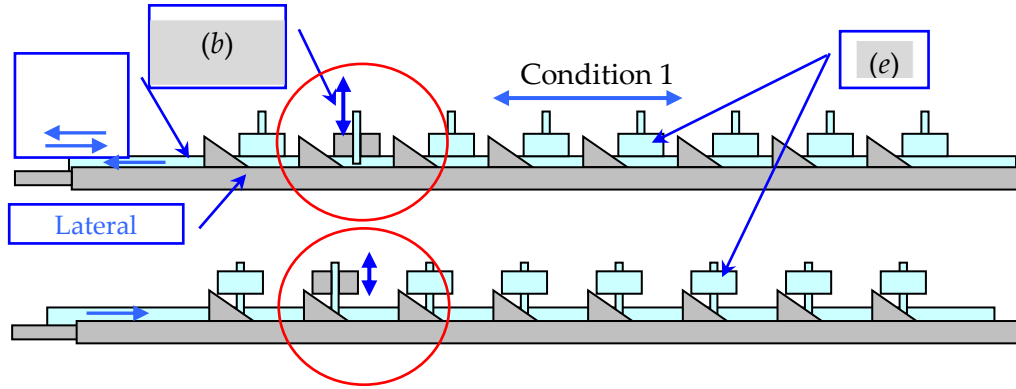


Figure 5.4 The illustration of the mechanism operating principle.

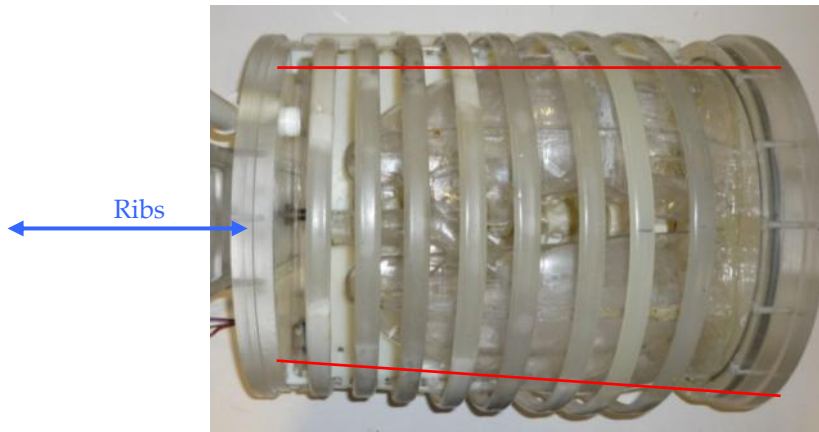


Figure 5.5 Top view of the rib-cage and marked by red lines the saw-tooth beam position.

Solution 2:

The second solution assumes the use of bars/beams that are pushing out the upper part of the ribs marked with red colour circle on Figure 5.6. The idea is to fix one side of these static previously beams to the orange beam (see Figure 5.7), and push it outside by rotation of green cam. The cam shape is reflecting the pattern of motion and can be formed at the user discretion, i.e. to obtain sinusoidal movement. We can easily change the amplitude of that movement and its character through the cam shape. The angle of that rotation " α " would have approximately 60 degree so there is a need to use a gear transmission with proper ratio. The ratio depends on rib-cage gear and the proportion would be about 36:1, if hypothetically the drive has a maximum of 6 rotations. Moreover it is proposed to place the wheel of a gearbox with a slightly bigger diameter $d_2 \approx 10\%$ and symmetrically with the 'red cross' position of the Figure 5.6. It allows generating movement for the both side of the walls in parallel.

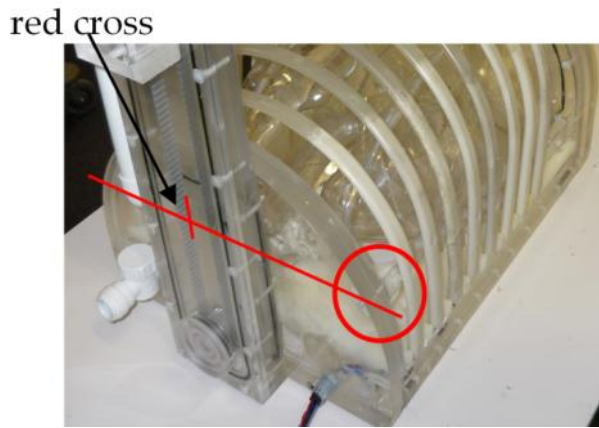


Figure 5.6 The illustration of strategic change points location.

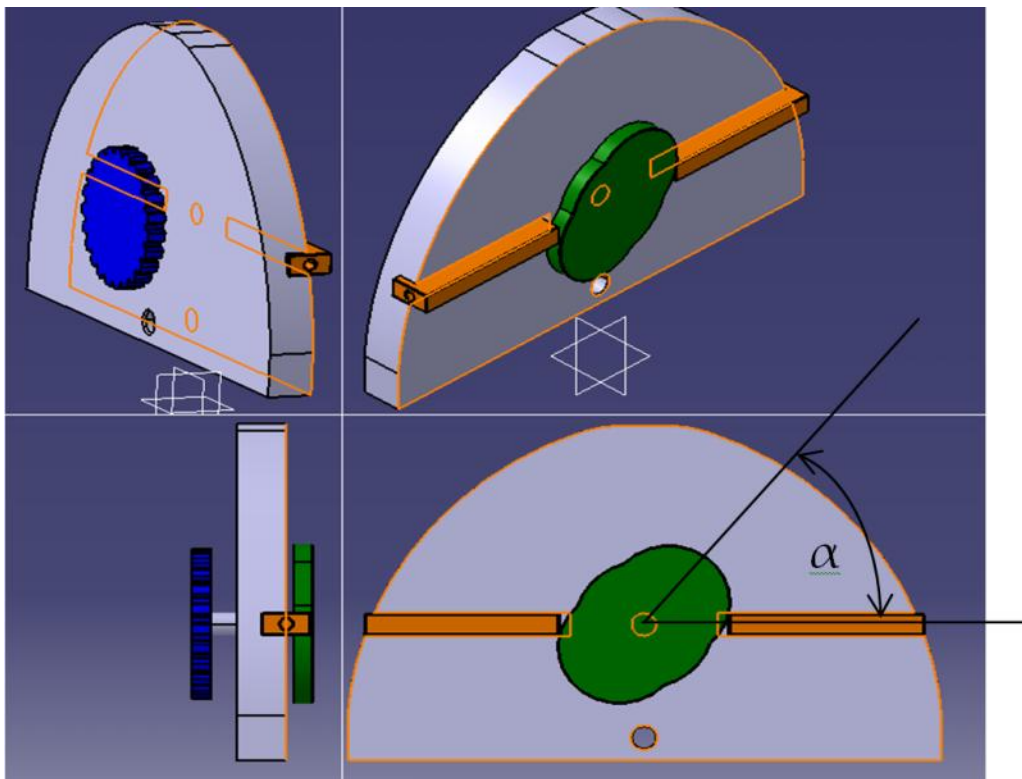


Figure 5.7 The rib-cage side wall model.

Considering the example presented on the Figure 5.7 above, if there is set angle $\alpha=90^\circ$, and the gear wheel (navy colour) have got the same size like a lower transmission wheel fixed in a hole below, and we know that the lower gear wheel is giving maximum 6 turns per cycle, then as a result from proportions we can found that ratio for gearbox should be equal 1:24.

Solution 3:

This solution is similar to the previous one. It assumes that the same two horizontal beams (RH and LH) are used and fixed to the top and not moving beam of the phantom (red circle on Figure 5.6).

However, the idea of the motion transmission is different: instead of pushing out the orange beams, they can be pulled. Therefore, inside the pocked could be placed a spring or elastic material that would normally push the beam (ribs) outside. A tape or steel ring can be fixed to the end of the orange beam and rolled onto a shaft. A shaft replaces the green element connected with the sprocket drive (in blue). The ratio of motion would be changed by the diameter of the shaft, where with bigger diameter would increase the lateral amplitude of motion.

5.2 Improvement of mechanical phantom's protection

There were a number of discussions and suggestions to modify the design of the phantom to increase the phantom's safety and efficiency.

Because the phantom was used during numerous tests there were possible situations where electrical or programme failure could not stop the motor rotation when required. For example, if a motor drive does not change direction in time and reaches the mechanical limit of the motion, then any further efforts from the motor to move the slider could result in motor damage or worse breaking the phantom shell, resulting in significant water leaks.

Therefore, the idea was to improve the thorax phantom safety by attaching a clutch for the new ribcage stepper motor. A shaft mounted clutch Type FO/FL or Type SO, made by HUCO and supplied by RS website were suggested. The important thing is to choose and attach the clutch with a lower torque than the stepper motor and sufficiently high to move the ribcage mechanism but not break the phantom.

The Unipolar Hybrid Stepper Motor Type No. 23HSX-306 with Holding Torque 1630mNm and manufactured by McLennan Servo Supplies can have attached clutch suited for 8mm shaft diameter. The suggestion could be Shaft Mounted Clutch model FO15 by HUCO (see attached link) that have proper diameter and is characterised by 1.13 Nm of torque, so lower than 1.63 Nm produced by the stepper motor and enough high to drive the phantom's rib-cage.

The above proposal is one of the many other and existing options. On the market, there are many clutches available, so particular choice can be modified.

However, the main idea to insert clutch between the stepper motor and the ribcage of the phantom is reasonable and therefore is strongly recommended.

5.3 Suggestion of the rod redesigning and X-ray sensor's shaking reduction.

One of the suggestions was re-designing the rod to hold the X-ray sensor attached to mimic the tumour.

The previous element had a diameter of 10 mm which was too small for the tube. As a consequence the rod was bending by over 7mm, after attaching the X-ray sensor and heavy holder. Moving such rod resulted in 5mm amplitude oscillation of the target during normal motion. These unwanted oscillation had to be reduced.



Figure 5.8 Initially designed rod and X-ray sensor's holder.

Two solutions were proposed to resolve this issue. Firstly, it was proposed to replace the rod with 'I' shape beam. There were prepared several simulations with RDM Le Mans software and then with HyperWorks. It was found, that beam with 'I' shape 10[mm] x 10[mm], assured the highest stiffness with the lowest dimensions and weight at the same time and had a nearly 50% lower bending.

However, for aesthetic reason it would be beneficial to have a rod with circular section. Thus, the second idea was to increase diameter of the tube from 10[mm] to 15[mm], as there was not necessary to keep such low rod diameter. It is

worth to note that the rod material was chosen to be Plexiglas as it needs to be manufactured with isotropic, homogeneous and transparent matter for X-ray radiation.

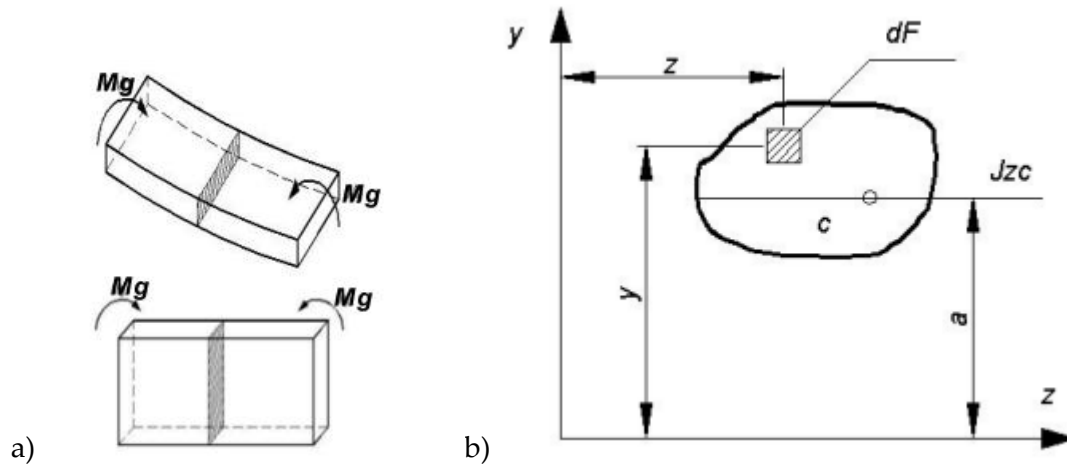


Figure 5.9 The moment of inertia J_z determination: a) general beam model; b) the beam section.

Considering the Figure 5.9 can be determined the moment of bending J_z :

$$J_z = \int_F y^2 dF$$

Equation 5.1 Moment of bending

Base on the figure above and the Equation 5.1, can be calculated the moment of inertia shown in table below:

Section	J_{zc}
	$\frac{b * h^3}{12}$

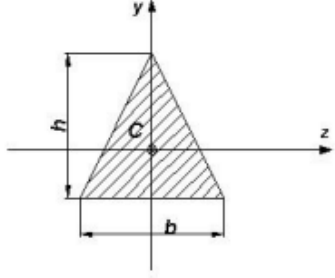
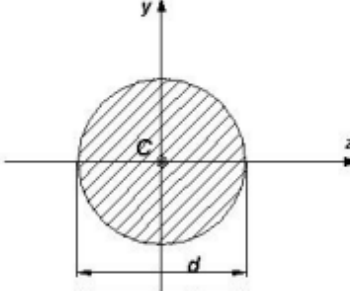
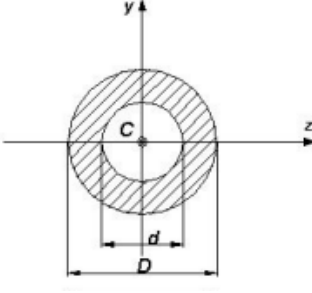
	$\frac{b * h^3}{36}$
	$\frac{\pi * d^4}{64}$
	$\frac{\pi * (D^4 - d^4)}{64}$

Table 5.1 The moment of inertia equation examples in relation to shape of the section.

Base only on Table 5.1 it is visible that the section's shape influence the moment of inertia, and in general the bending of the rod or beam. The presented equations were shown with the intention to explain the beam shape dependence on the stiffness. The other parameters such as Young module, material density or existing tensions were omitted as the material choice was imposed.

All of the above show how significant is the influence of the rod diameter on the bending. Thus it would be recommended to increase the beam section size to improve its stiffness of the element.

However, instead of above and to avoid bending, another prototype was implemented using two rods instead of one, see Figure 5.10, contain two ϕ 10[mm] rods instead of a single rod.



Figure 5.10 *Changed and actual sensor holder of the tumour drive unit.*

5.4 Proposal of the unification stand for CCD camera

The fourth recommendation was to adapt the video camera stand holder. The existing and previously used stand, presented in Figure 5.11, had several disadvantages. It was bulky and heavy as well as difficult to operate and set-up. It was not required as the IEEE1394a CCD camera was very light and small size.

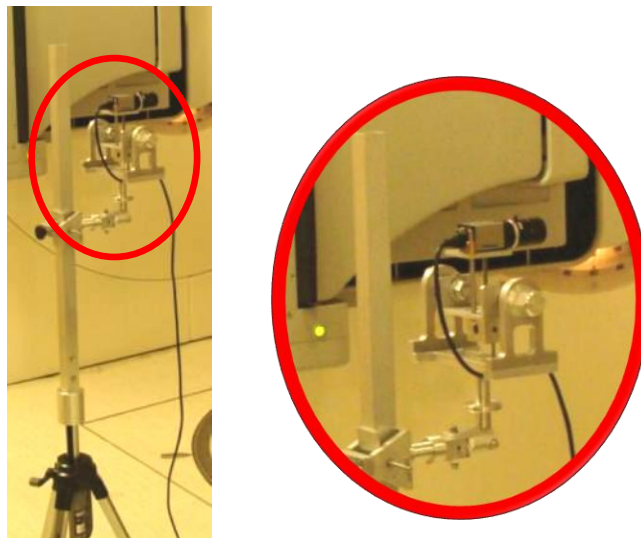


Figure 5.11 *Previously used tripod for CCD camera holding.*

Instead of using the described adaptor, a universal tripod for camera or camcorder stand was considered and lastly used during several tests. Notice that the camera body size is: 29 (W) x 29 (H) x 39(D) [mm], and its weight approximately 63 gram so almost every tripod is accurate to carry the camera used. It was beneficial as with cranks, screws and quick locks combinations it was very easy to

set-up in any place, and reposition in the hospital room during experiments. The example of the stand and some of its properties are presented by Figure 5.12.

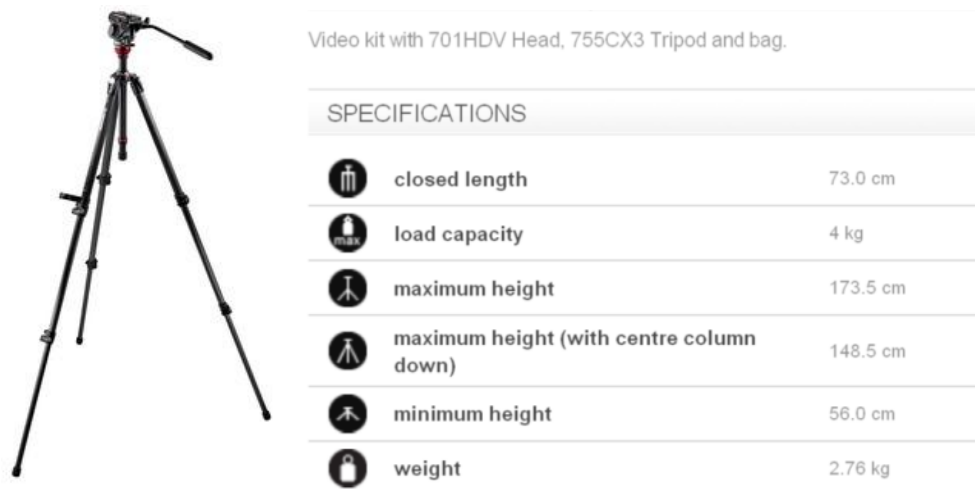


Figure 5.12 The example of the camera stand manufactured by Manfrotto (36).

This proposal required a plate redesign; with a unified thread 1/4" used for all current camera devices (older camera devices have a standard 3/8" thread).

A new camera base plate was modelled and manufactured from aluminium. Both, the FOculus camera and holder plate assembled, see Figure 5.13, weight not more than 0.2[kg] while tripod load weight is usually over 2.5[kg].

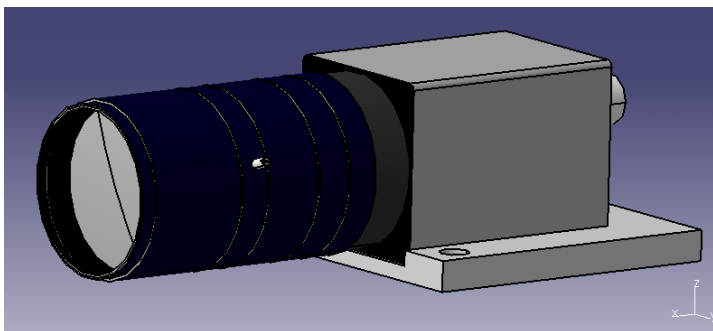


Figure 5.13 The CCD camera mounted to base plate.

Redesigned the FOculus CCD camera's plate for the use with a standard camcorder's tripod was successfully implemented and used during the course of this research.

5.5 Facility calibration of the camera for video tracking system

One of the ideas to simplify the set-up of the camera and video tracking system was use the laser pointer.

The laser pointer could be fixed onto the camera's holder and as close to the centre of focal length as possible. Then the unit have to be calibrated with observed view by camera and then blocked repositioning.

This solution could allow to speed-up the camera set-up by one person. The camera repositioning and focussing lens onto the calibration grid centre do not require monitoring the camera's view at all. Thus, the video tracking system could be turned off during set-up. This facility formulated suggestion of laser pointer will speed up calibration and setting up of the camera video tracking system. This idea was not implemented but is believed to be beneficial.

5.6 Safety implementation against stepper motors overheating

The final modernisation suggested was the "hard" switch implementation to the power supply of the logical card.

This idea was caused by a state of the stepper motor when it was stopped. To stop the motor the last sequence was sent continuously, so in fact the motor worked constantly (current flow through inductor) just without movement. As a result the motor temperature increased. It was therefore required to turn off the unit power supply manually when the movement was not in use.

This model of control was required by the electronic construction of the phantom drive and particularly by the signal coding and decoder built into power supply unit. However, it was found that switching off the voltage of the logical card gives no power to the motor.

Thus the idea of the "hard" switch implementation to the logical card seems to be necessary. As a "hard" switch is suggested a transistor key use. It could be controlled by DO of LabVIEW program and stop action in the code could cut off

source of the current. There is believed that in this case ratio of the gearbox and static friction will block the rotation of the motor. Hence the stepper motor overheating could be eliminated.

Chapter 6

Conclusions and future work

Motion management for cancer located in the thorax e.g. lung cancer, is still an area of active research. It is possible to use phantoms to evaluate the effectiveness of new research procedures without harming patients.

There were a number of aims, objectives and requirement set in this project. Most of these were achieved and are indicated in the following paragraph as Section number followed by p and a letter e.g. (Section 1.4 point 1 would correspond to the deliverable 1 presented in Section 1.4).

A review of existing phantoms was carried out in Chapter 2 highlighting the drawback and advantages of current solutions, including the MAESTRO phantom, which is the object of this research work.

The main focus of the work was to evaluate and propose alternative implementation of the control system to control the stepper motors in open loop using LabVIEW. Two alternative methods of control have been investigated. The first is based on the methods implemented at the start of the project involving the sending of step sequences in the correct order to drive the phases of the motors (Section 1.4 p.1). The second approach involved the use of bi-polar drive to control the motor velocity using frequency and motor direction (Section 1.4 p.2).

The complexity and performance issues of the existing code developed by PhD student Imke Land led to the development of a new set of programs. The new code provided the user with the means to change parameters on-line (Section 3.2.2 p.H) as opposed to pre-calculating all the motion in advance. A calibration mode was programmed (Section 3.2.2 p.F). The new program was simplified and made more efficient by removing unnecessary operations and automating the process to reduce the amount of user intervention. The phantom position parameter was saved each time the program was stopped programmatically to avoid performing a re-

calibration. A new improved and more user-friendly interface was designed (Section 3.2.2 p.I). However, the code is not fully working and still needs modifications. Its parts work separately but the complex code resulted in shaking and buzzing of the stepper motors (Section 3.2.2 p.A) if the motion trajectory replicates any of Data File/ Sinusoidal/ Lujan/ Irregular breathing pattern (Section 3.2.2 p.B). The undertaken trials for sequence motion replication in a pseudo real time met several difficulties not solved up to now. A basic code (Appendix 1) that was shown to work was to generate linear movement with a step interval depending on the program frequency.

The other idea of the phantom motion control was to use a bi-polar drive and in consequence there had to be a new control software that worked using frequency modulation. The code (Appendix 2) was able to produce any previously listed breathing pattern with fluent movement and acceleration regulator. Moreover the program was equipped with position calibration mode. This motion control by frequency modulation code met all the aims for proper and fluent motion. The only drawback was caused by hardware and large current flow. The observed side effect was motor overheating leading to the rejection of this solution.

LabVIEW programming was not a trivial task and became more difficult as the project progressed. Constant access to the real device to test code was found to be necessary as simulation does not reflect actual issues that may be faced when using the actual hardware.

The second area of work was to become familiar with existing image tracking software developed by Mathieu Leibel, an ENIM placement student, and improve its characteristic by increasing the frequency of the measurements to 30 frames per second (Section 1.4 p.3). In reality, depending on environmental conditions the program was able to run mostly with 22 up to 30 [frames/s]. The research of the code allows identifying the most time consuming VI and simplification of the program by the reducing or replacing VI. The outcome of the work was a speed up of the frame rate able to be processed between 31 to 40 frames per second.

Other duties were to assist other members of the research team when performing tests requiring the use of the phantom and or operate the camera video tracking system.

Finally the last part of the work was to participate at ICSE 2009 conference (Section 1.4 p.8) where the paper entitled 'LabVIEW Motion of Radiotherapy Phantom' (Appendix 10) was presented also as a poster (Appendix 11).

The aim for future work should be looking for innovations and modernisations with existing thorax phantom.

This phantom's project involved a multitude of tests at UHCW culminating with a final positive result (Section 1.4 p.9) recorded in a YouTube video produced by Coventry University and entitled: Fighting Cancer with Control Theory - Control Theory Applications Centre (CTAC). I appear in this video in my role as the person in charge of the image tracking system.

My main contribution in terms of effort has been the development of LabVIEW code to control the stepper motors. The tuning of the image tracking system was also difficult as it was not possible to reproduce the conditions encountered inside the radiotherapy bunker at the University. I made several suggestions to improve the experimental set up and two of these were adopted: the simplified camera support and the new rod design. Other suggestions regarding the expansion of the rib motion require further development before being realised.

In terms of further work, the LabVIEW program for motion control could be further developed. Ideally the code should be simplified and the function for home position should be implemented. In addition, synchronising the phantom with signals from the spirometer in real time could be beneficial.

Whilst the control by frequency encountered technical difficulty it is believed that it has potential, being limited only by the number of counters available on the data acquisition interface.

It is considered that this Thesis represents a valuable resource for a person attempting to work with LabVIEW programming in engineering field, and for someone interested in novel issue in radiotherapy and undertaken action against cancer.

Chapter 7

References

1. Alasti, H., Cho, Y.B., Vandermeer, A.D., Abbas, A., Norrlinger, B., Shubbar, S., Bezjak, A. (2006). *Physics In Medicine And Biology*, 51(12), 3251-3267.
2. Benchetrit, G. (2000) *Breathing pattern in humans: diversity and individuality. Respiration Physiology*. 122(2-3), 123-129
3. Bolton, W. (1974). *Patterns in physics*, 571-581. McGraw-Hill, ISBN 83-01-01957-3.
4. Buchgeister, M. and F. Nusslin (1998). *Startup performance of the traveling wave versus standing wave linear accelerator. Med. Phys.*, **25**(4), 493-495.
5. Cancer Research in UK. (2011). Cancer Help UK. www.cancerhelp.org.uk
6. Cancer Research in UK. (2011). Cancer mortality - UK statistics. <http://info.cancerresearchuk.org/cancerstats/mortality>
7. Cancer Research in UK. (2011). Cancer treatments. www.cancerresearchuk.org
8. CIRS. (2010). *IMRT Thorax Phantom. Complete QA from CT imaging to dose verification.* www.cirsinc.com
9. Coventry University website – www.coventry.ac.uk
10. CTAC website: <http://www.coventry.ac.uk/CTAC>
11. D'Souza, W. and McAvoy, T. (2006). *An analysis of the treatment couch and control system dynamics for respiration-induced motion compensation. Med. Phys.*, **33**, 4701-4709.
12. Demanes DJ, Rodriguez RR, Schour L, Brandt D, Altieri G. (2005). *High-dose-rate intensity-modulated brachytherapy with external beam radiotherapy for prostate cancer: California endocurietherapy's 10-year results.* *Int J Radiat Oncol Biol Phys*, 2005; 61:1306–1316.
13. Depuydt, T., Verellen, D., Haas, O.C.L., Gevaert, T., Linthout, N., Duchateau, M., Tournel, K., Reynders, T., Leysen, K., Hoogeman, M., Storme, G. De Ridder, M., (2011) *Geometric accuracy of a novel gimbals based radiation therapy tumor tracking system*, *Radiotherapy and Oncology*, **98**, 365–372.
14. Dietrich, L., Tcking, T., Nill, S., Oelfke, U. (2003). *Physics In Medicine And Biology*, 50(10), 2405-2414.
15. dSPACE. (2011). DS1104 R&D Controller Board (2010). <http://www.dspace.de/en/ltd/home/products/hw/singbord/ds1104.cfm>

16. Duan, J., Shen, S., Fiveash, J.B., Brezovich, I.A., Popple, R.A., Pareek, P.N. (2003). *Medical Physics*, 30(8), 2241-2252.
17. Fitzpatrick, M., Starkschall, G., Balter, P., Antolak, J.A., Guerrero, T., Nelson, C., Keall, P., Mohan, R. (2005). *Journal of Applied Clinical Medical Physics*, 6(1):13-21.
18. FOCULUS 124: www.net-gmbh.com
19. French, Anthony Philip. (1968). *Special relativity*. Norton, W. W. & Company, Inc.
20. George, R., Chung, T. D., Vedam, S. S., Ramakrishnan, V., Mohan, R., Weiss, E., Keall, P. J. (2006). *Int J Radiat Oncol Biol Phys* 65, 924-933.
21. Haas, O.C.L., Paluszczyszyn, D., Gillot, G. and Mills, J.A. (2010). *Combined patient motion compensation and dose rate variation to improve radiotherapy treatment dosimetric accuracy. Proceedings of the UKACC International Conference on CONTROL 2010, 07-10 Sep 2010 in Coventry, UK.* 355-360
22. Haas, Olivier C.L., (2010). *Fighting Cancer with Control Theory - Control Theory Applications Centre (CTAC), CUTV, YouTube*, uploaded, 15 Mar 2010: <http://www.youtube.com/watch?v=aUVmGoLEpCI>
23. Herk, M. Van (2004). Errors and margins in radiotherapy. *Semin. Radiat. Oncol.*, 14, 52-64.
24. Hoogeman, M., Prevost, J-B., Nuytens, J., Poll, J., Levendag, P., Heijmen, B. (2009). Clinical accuracy of the respiration tumor tracking system of the CyberKnife: *Assessment by analysis of log files*. *Int J Radiat Oncol Biol. Phys.*, **74**, 297-303.
25. Hugo, D.G., Agazaryan, N., Solberg, T.D. (2002). *Medical Physics*, 29(11), 2517-2525.
26. Jiang, S.B., Pope, C., Jarrah, K.M.A., Kung, J.H., Bortfeld, T., Chen, G.T.Y. (2003). *Physics In Medicine And Biology*, 48, 1773-1784.
27. Keall, P.J. , Cattell, H., Pokhrel, D., Dieterich, S., Kenneth H. Wong, K.H., Murphy, M.J., Vedam S.S., Wijesooriya, K., Mohan, R. (2006). *Geometric accuracy of a real-time target tracking system with dynamic multileaf collimator tracking system*. *Int J Radiat Oncol Biol Phys*, **65**, 1579-1584.
28. Keall, P.J., Starkschall, G., Shukla, H., Forser, K.M., Ortiz, V., Stevens, C.W., Vedam, S.S., George, R., Guerrero, T., Mohan, R. (May 2004). *Physics In Medicine And Biology*, 49(10), 2053-2067.
29. Land I., Mills J., Haas O.C.L., Burnham K.J., Wilson A. (2006). WP1.2 Preliminary dynamic phantom with a limited number of degree of freedom. *Deliverable No D20*.
30. Land, I. (2009). *The Delivery Limitations of Adaptive Radiotherapy Systems*. PhD dissertation. University of Warwick.
31. Land, I., Mills, J.A., Young, K., Wilson. A., Haas, O.C.L., Burnham, K.J. (2006). Clinical perspective on the application of margins and tracking for adaptive radiotherapy
32. Lujan, A.E., Larsen, E.W., Balter, J.M., Haken, R.K.T. (1999). A method for incorporating organ motion due to breathing into 3D dose calculations. *Medical physics*, 26(5), 715-720.

33. MAESTRO thorax phantom (2010). *US patent application number 61/295106*, filled on 14 January 2010.
34. MAESTRO project website. (2010).
www.coventry.ac.uk/researchnet/ctac/projects/maestro
35. MAESTRO. Coventry University. (2009). *Methods and Advanced Equipment for Simulation and Treatment in Radiation Oncology*. www.coventry.ac.uk/maestro
36. Manfrotto camera tripod. (2011). <http://www.manfrotto.com>
37. Mathworks. (2011). *Matlab® and Simulink®*. <http://www.mathworks.com>
38. McArdle, W.D., Katch F. I., Katch, V.L. (2006) *Exercise Physiology: Energy, Nutrition, and Human Physiology*. Lippincott Williams & Wilkins, ISBN 0781749905.
39. McLennan Servo Suppliers Ltd. (2009). 23 HSX hybrid series stepper motor: www.mclennan.co.uk/datasheets/european/stepper/hsxsteppermotors.pdf
40. Modus Medical Devices Inc. (2009). www.quasarphantoms.com/quasar
41. Murphy, J.M. (2004). Tracking moving organs in real time. *Semin. Radiat. Oncol.*, 14, 65-75.
42. National Cancer Institute: <http://www.cancer.gov/cancertopics/types/lung>
43. National Instruments Corporation. (2011). *NI USB-6229 data acquisition module*. <http://sine.ni.com/ds/app/doc/p/id/ds-10/lang/en>
44. National Instruments Corporation. (2011). www.ni.com
45. National Instruments. (2011). www.ni.com/labview (2009).
46. Nioutsikou, E., Symonds-Taylor, J.R.N., Bedford, J.L., Webb, S. (Jul 2006). *Physics In Medicine And Biology*, 51(14), 3359-3374.
47. Paluszczyszyn, D. (2009). *Real time implementation of a new control system utilising the model predictive control and the Kalman filter predictor for the radiotherapy patient support system*. MSc thesis, Coventry University.
48. Putra, D., Haas, O.C.L., Mills, J.A. and Burnham, K.J. (2008). *A multiple model approach to respiratory motion prediction for real-time IGRT*. *Phys. Med. Biol.*, 53, 1651-1663
49. Radiological Physics Center. (2010).
http://rpc.mdanderson.org/rpc/services/Anthropomorphic_%20Phantoms/Anth_TLP.htm
50. Rassiah, P., Tanyi, J., Cheng, C., Varchena, V., Fuss, M., Salter, B. (2004). *AAPM PO-T-143 Poster*.
51. RS Components Ltd. (2011). <http://uk.rs-online.com>
52. Sahih, A. (2010). *Respiratory motion modelling and predictive tracking for adaptive radiotherapy*. PhD Thesis, Coventry University.
53. Saracen, M.J. (2005). *Respiration phantom for quality assurance*.
54. Sawant, A., Venkat, R., Srivastava, V., Carlson, D., Povzner, S., Cattell, H., Keall, P. (2008). *Management of three-dimensional intrafraction motion through real-time DMLC tracking*. *Med. Phys.*, 35, 2050-2061
55. Schaefer, M., Mnter, M.W., Thilmann, C., Sterzing, F., Haering, P., Combs, S.E., Debus, J. (Jun 2004). *Physics In Medicine And Biology*, 49(12), N175-N179.
56. Schneider, U., Pedroni, E., Lomax, A. (Jan 1996). *Phys Med Biol* 41(1), 111-124.

57. Schueler, B.A. (2000). *The AAPM/RSNA Physics Tutorial for Residents* 20:1115-1126.
58. Shimizu, S., Shirato, H., Ogura, S., Akita-Dosaka, H., Kitamura, K., Nishioka, T., Kagei, K., Nishimura, M., and Miyasaka, K. (2001). *Int J Radiat Oncol Biol Phys.* 51(2), 304-3010
59. Shirato, H., Suzuki, K., Sharp, G.C., Fujita, K., Onimaru, R., Fujino, M., Kato, N., Osaka, Y., Kinoshita, R., Taguchi, H., Onodera, S., and Miyasaka, K. (2006). *Int J Radiat Oncol Biol Phys.* 64(4), 1229-1236
60. Siemens (2010). *ONCOR. Digital Medical Linear Accelerator Specifications. Fighting cancer – fast and focused.* www.siemens.com/healthcare
61. Skworcow, P. (May 2006). *Tracking Control Applied to Radiation Therapy.* MPhil Transfer.
62. Skworcow, P., (2008). *Modelling and predictive control of radiotherapy treatment machines*, PhD Thesis, Coventry University.
63. Skworcow, P., Putra, D., Sahih, A., Goodband, J., Haas, O.C.L., Burnham, K.J., Mills, J.A., (2007). *Predictive tracking for respiratory induced motion compensation in adaptive radiotherapy*, *Measurement and Control*, **40(1)**, 16-19.
64. Tacke M., Nill S., Krauss A., Oelfke, U. (2010). *Real-time tumour tracking: Automatic compensation of target motion using the Siemens 160 MLC.* *Med. Phys.*, **37**, 753-761.
65. Texas Instruments. (1981). *The TTL Data Book for Design Engineers.*
66. The Radiology Support Device, Inc. (2008). *The RPC thoracic phantom.* http://www.rsdphantoms.com/rt_breathing.htm
67. Webb, S. (1997). *The physics of conformal radiotherapy - Advances in technology.* Institute of Physics Publishing Bristol and Philadelphia
68. White, D. R., Martin, R. J., Darlison, R.Br. J. (Nov 1977). *Radiol* 50(599), 814-821.
69. Wideröe, R. (1928). *Archiv Elektronik und Uebertragungstechnik* **21**: 387.
70. Wikipedia, the free encyclopaedia. (2010) – <http://en.wikipedia.org>
71. Wilbert, J., Meyer, J., Baier, K., Guckenberger, M., Herrmann, C., Hess, R., Janka, C., Lei Ma, Mersebach, T., Richter A., Roth, M., Schilling, K., Flentje, M. (2008). *Tumor tracking and motion compensation with an adaptive tumour tracking system (ATTS): system description and prototype testing.* *Med. Phys.*, **35(9)**, 3911-21.
72. Zhou, T., Tang, J., Dieterich, S., Cleary, K. (2004). *A robotic 3-D motion simulator for enhanced accuracy in CyberKnife stereotactic radiosurgery.* *International Congress Series*, 1268, 323-328.

Chapter 8

Appendices

The majority of the practical work involved the participation to parts of the MAESTRO project development. The tasks carried out were to set-up the systems during the experimental tests and programming, with NI LabVIEW, the stepper motors of the thorax phantom, and the camera video tracking system.

Because the LabVIEW software, for data acquisition were basically exploited the National Instruments devices. Presented and mostly used hardware for latest experimental set-up, it was:

- for the motion control of the MAESTRO thorax phantom : Appendix 3, Appendix 4, Appendix 5, Appendix 6, Appendix 7, Appendix 8,
- for video tracking system : Appendix 9, Appendix 5, Appendix 7, Appendix 8

The particular specifications were attached as appendices below:

Appendix 3 High performance size 23 hybrid stepper motors of the HSX series:

23HSX 102

23HSX 312

www.mclennan.co.uk/datasheets/european/stepper/hsxsteppermotors.pdf

Appendix 4 MSE570 Evo2; Bi-polar 3.5 [A] stepper motor drive

www.mclennan.co.uk/datasheets/european/stepper/mse570evo2iss002.pdf

Appendix 5 NI M Series multifunction DAQ for USB 6229

<http://sine.ni.com/nips/cds/view/p/lang/en/nid/203482>

Appendix 6 NI DAQ Card PCI-6229

<http://sine.ni.com/nips/cds/view/p/lang/en/nid/14136>

Appendix 7 NI DAQ Card 6024E (for PCMCIA)

<http://sine.ni.com/nips/cds/view/p/lang/en/nid/10969>

Appendix 8 NI SC 2075 Connector Card

<http://sine.ni.com/nips/cds/print/p/lang/en/nid/10806>

Appendix 9 IEEE1394a Digital CCD Camera FOculus FO124TB

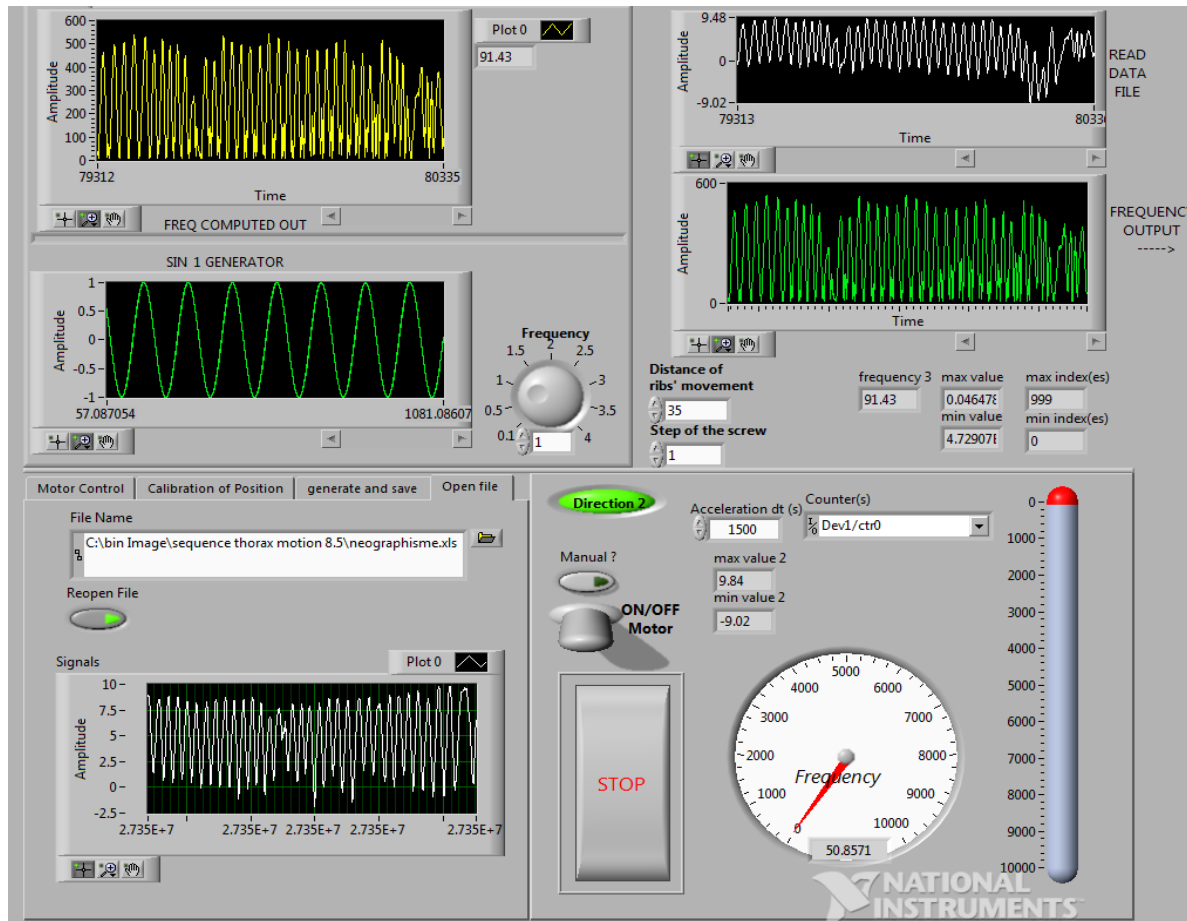
www.net-usa-inc.com/attachments/FOculus_IEEE1394_2010.pdf

There were also several other devices used for the tests and MAESTRO project development. The hardware model and its specifications source where shown by website addresses below:

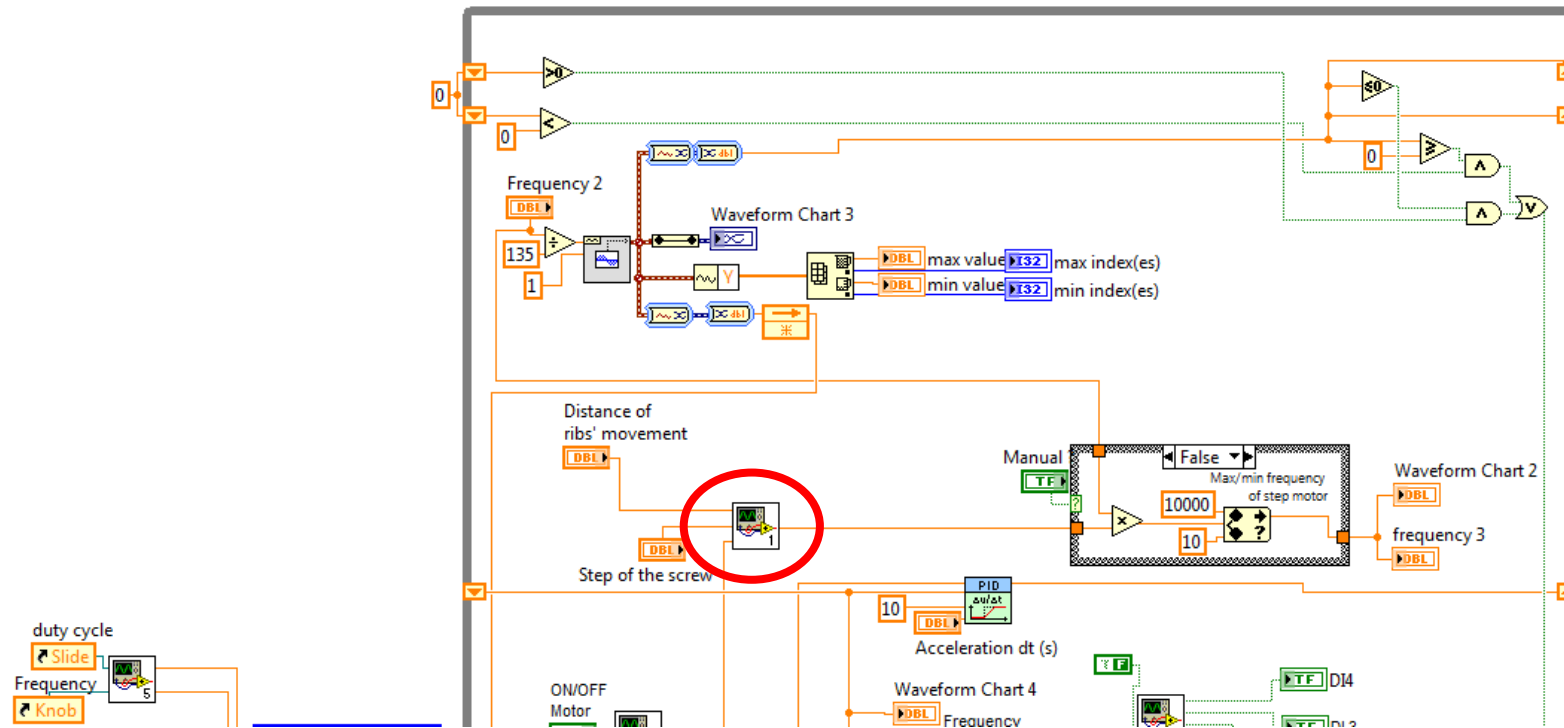
- NI DAQ Card PCIe-6259
<http://sine.ni.com/nips/cds/view/p/lang/en/nid/201814>
- NI BNC-2111 Connector Block
<http://sine.ni.com/nips/cds/view/p/lang/en/nid/201731>
- NI SCC-68 Connector Block
<http://sine.ni.com/nips/cds/view/p/lang/en/nid/202603>
- IEEE1394a Digital CCD Camera FOculus FO323TB
www.net-usa-inc.com/attachments/FOculus_IEEE1394_2010.pdf
www.net-usa-inc.com/attachments/FOculus_IEEE1394_2010.pdf
- Canon XL2 Professional Camcorder
www.canon.co.uk/For_Home/Product_Finder/Camcorders/professional/XL2/
- Panasonic Security CCD Camera
- Logitech Quickcam Express - Digital video camera – USB
http://www.amazon.co.uk/Logitech-Quickcam-Express-Digital-camera/dp/tech-data/B000225K5G/ref=de_a_smttd/275-9189272-0781604
- HUCO model FO15.Shaft Mounted Clutch.
<http://docs-europe.electrocomponents.com/webdocs/0080/0900766b800802ae.pdf>

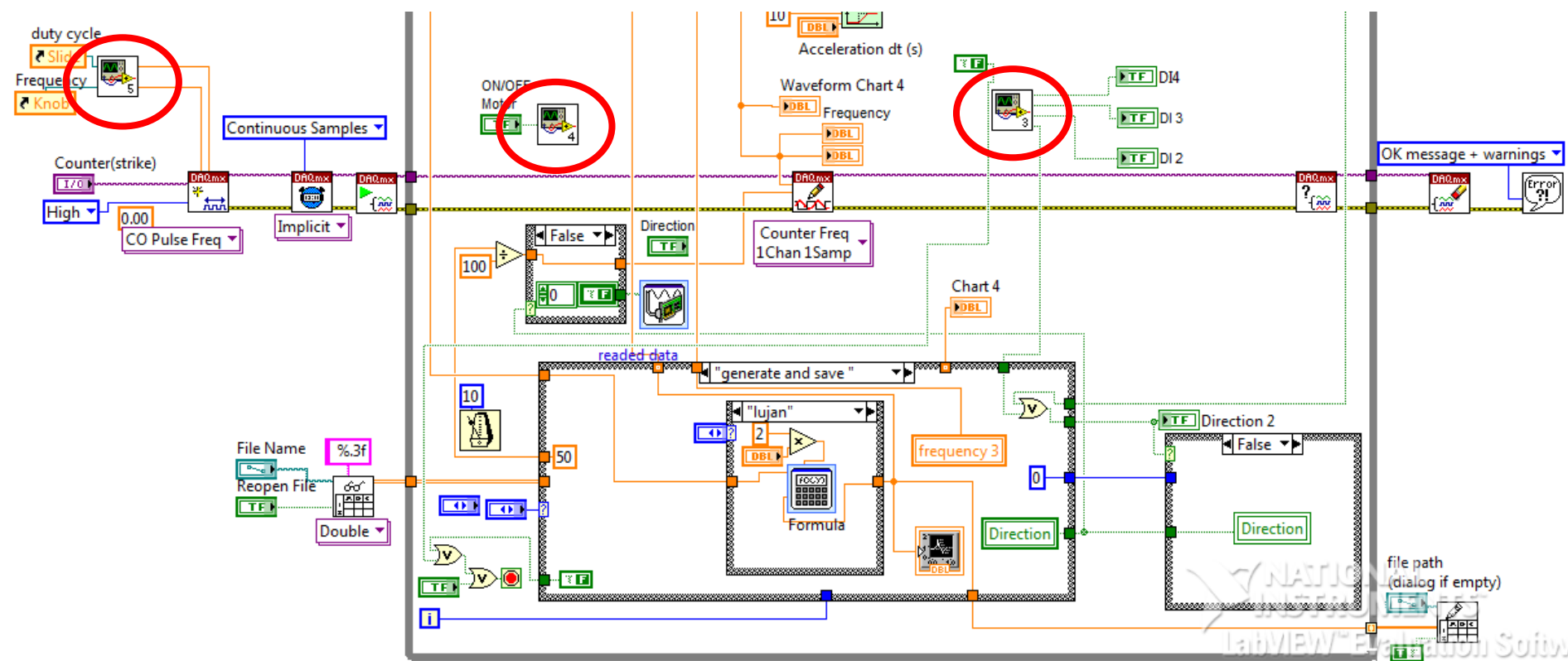
Appendix 1. Program code – motion control by frequency modulated signal

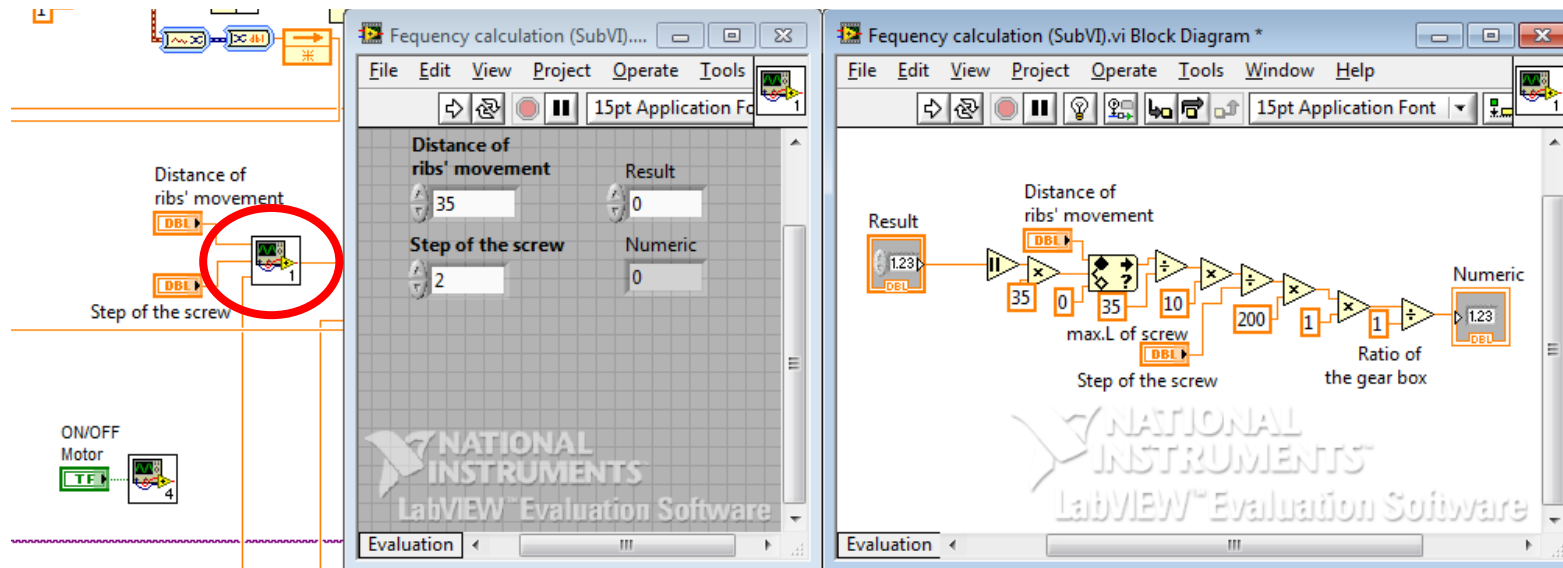
Front panel

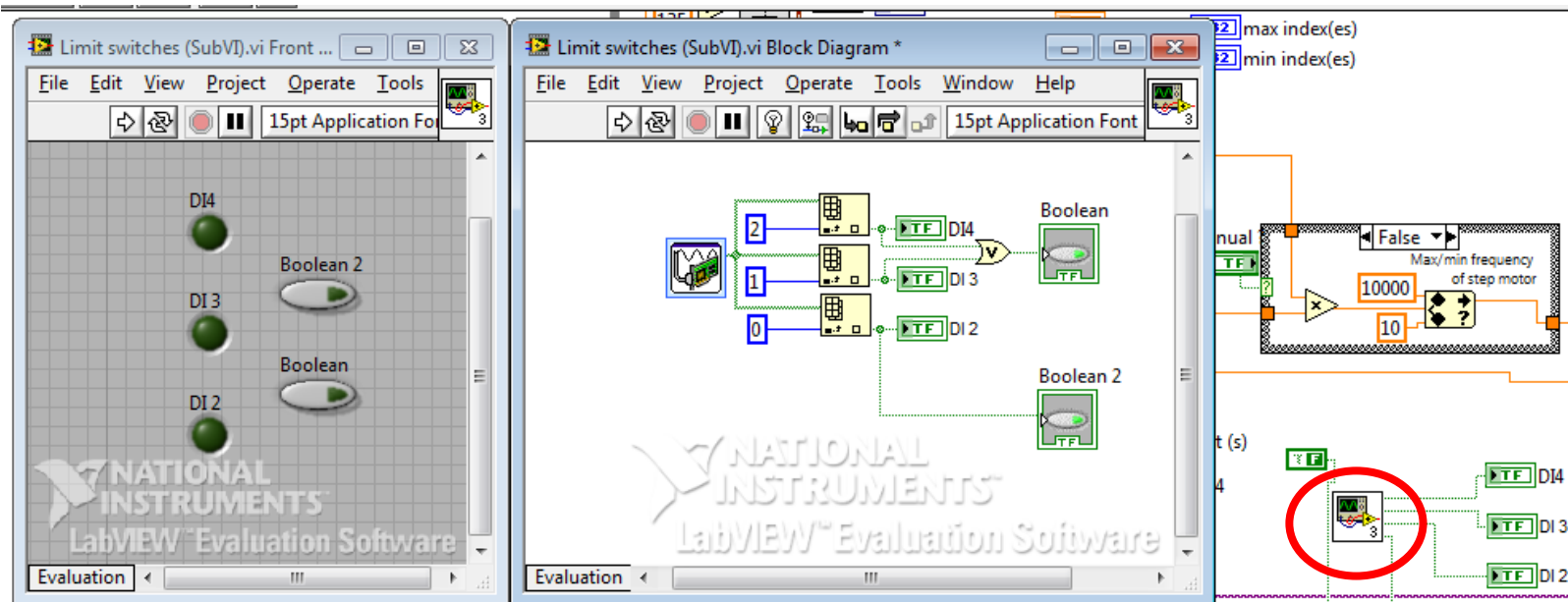


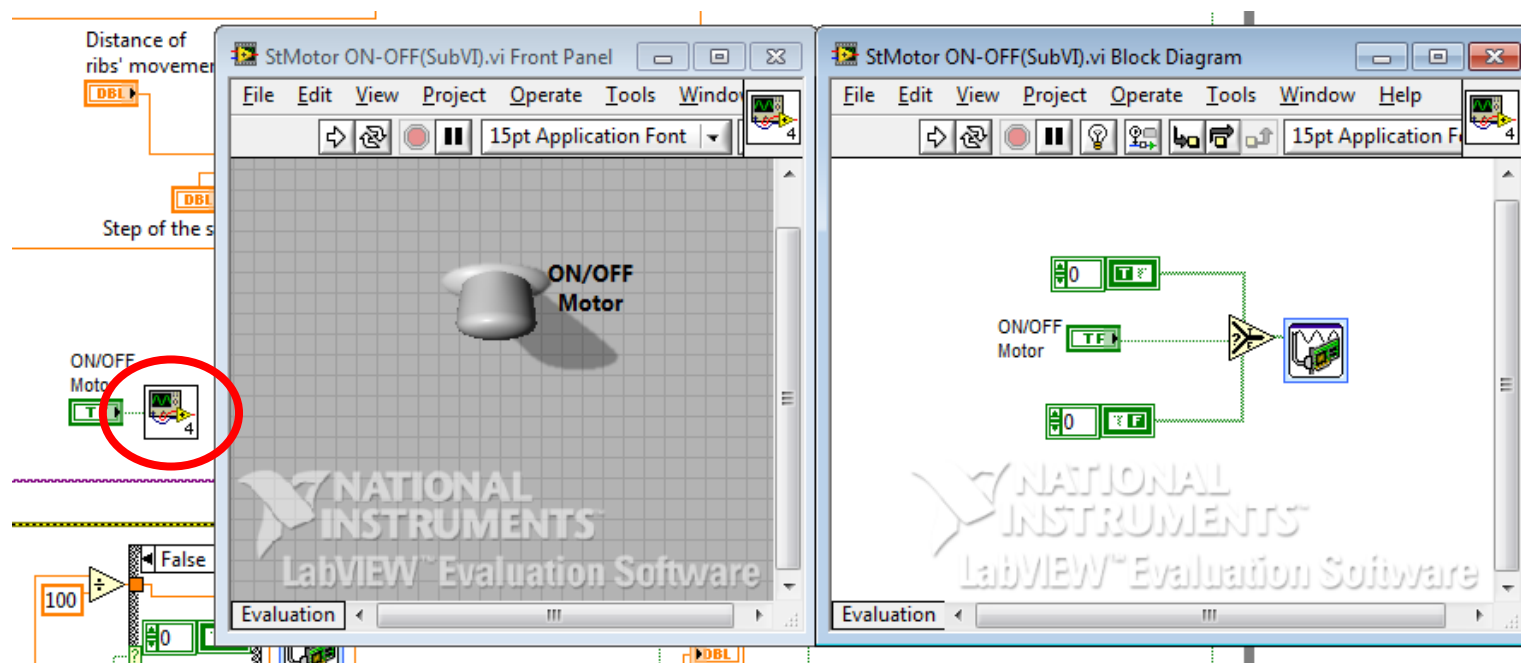
Block diagram

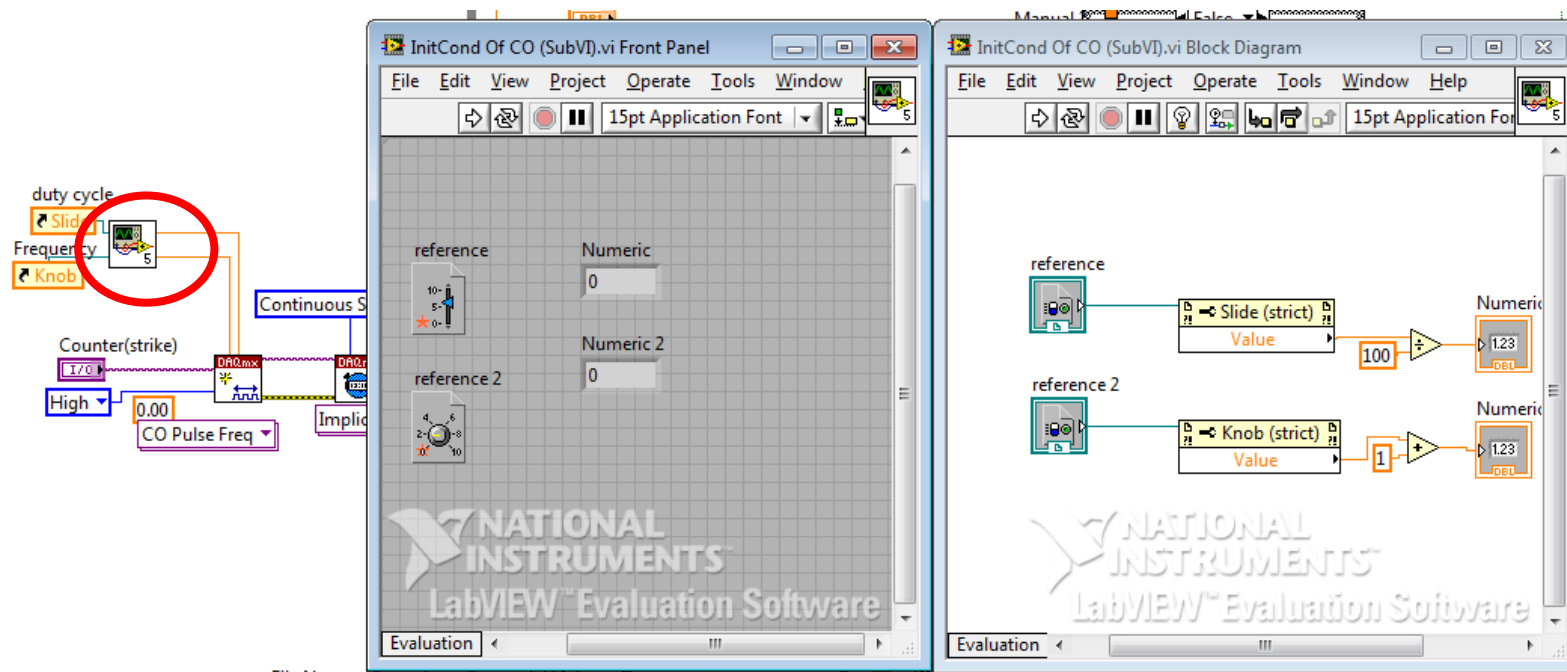






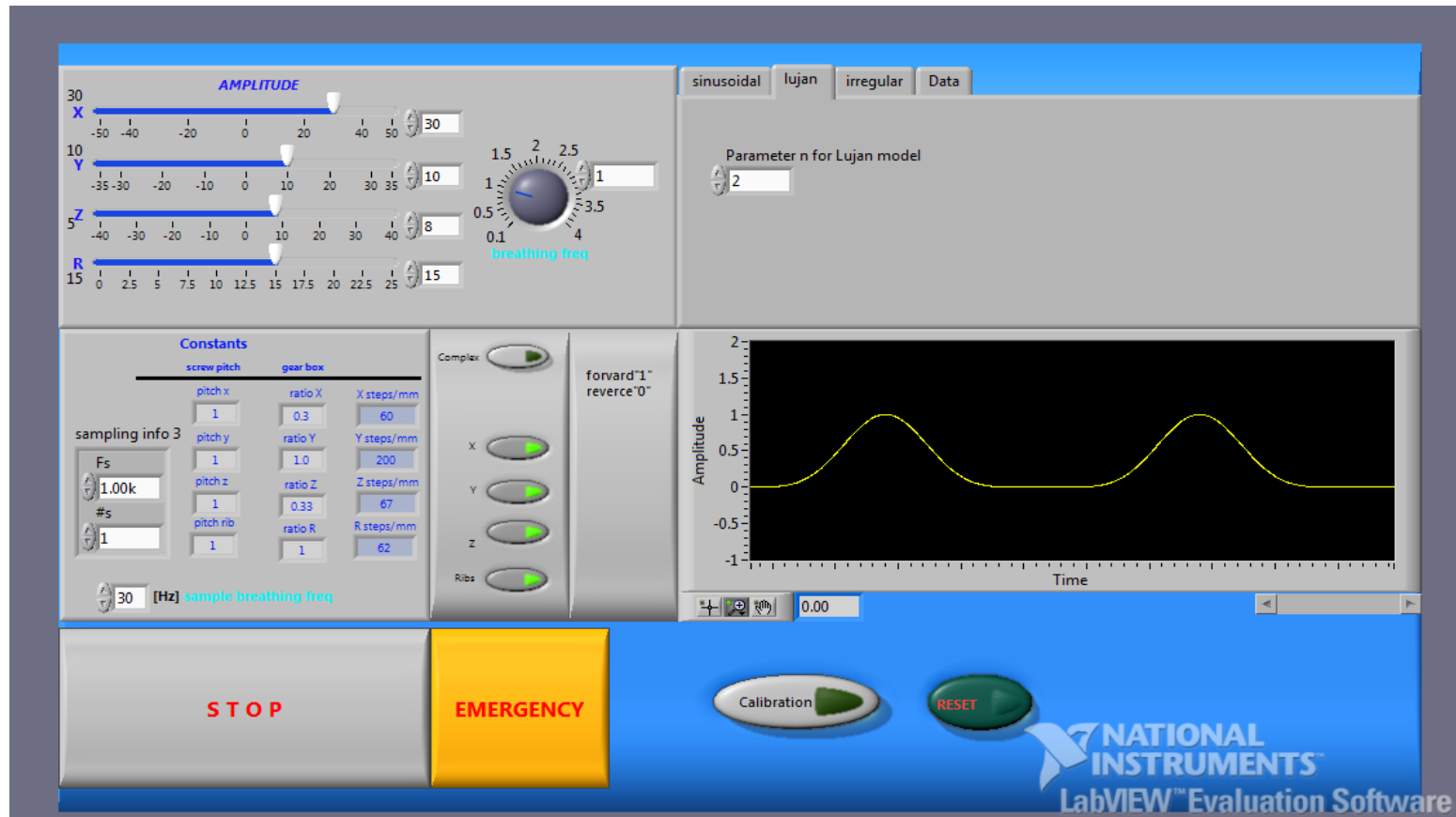




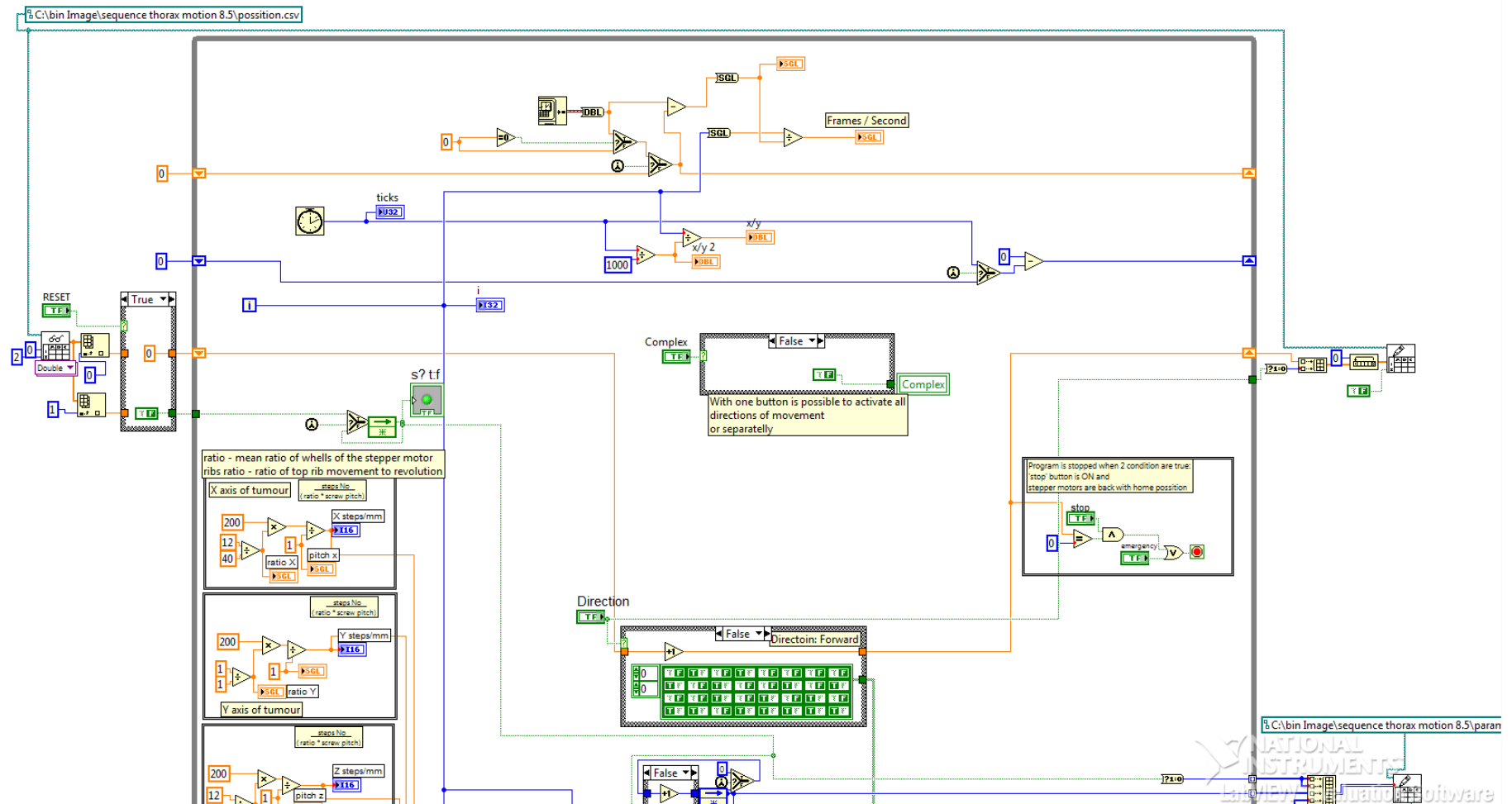


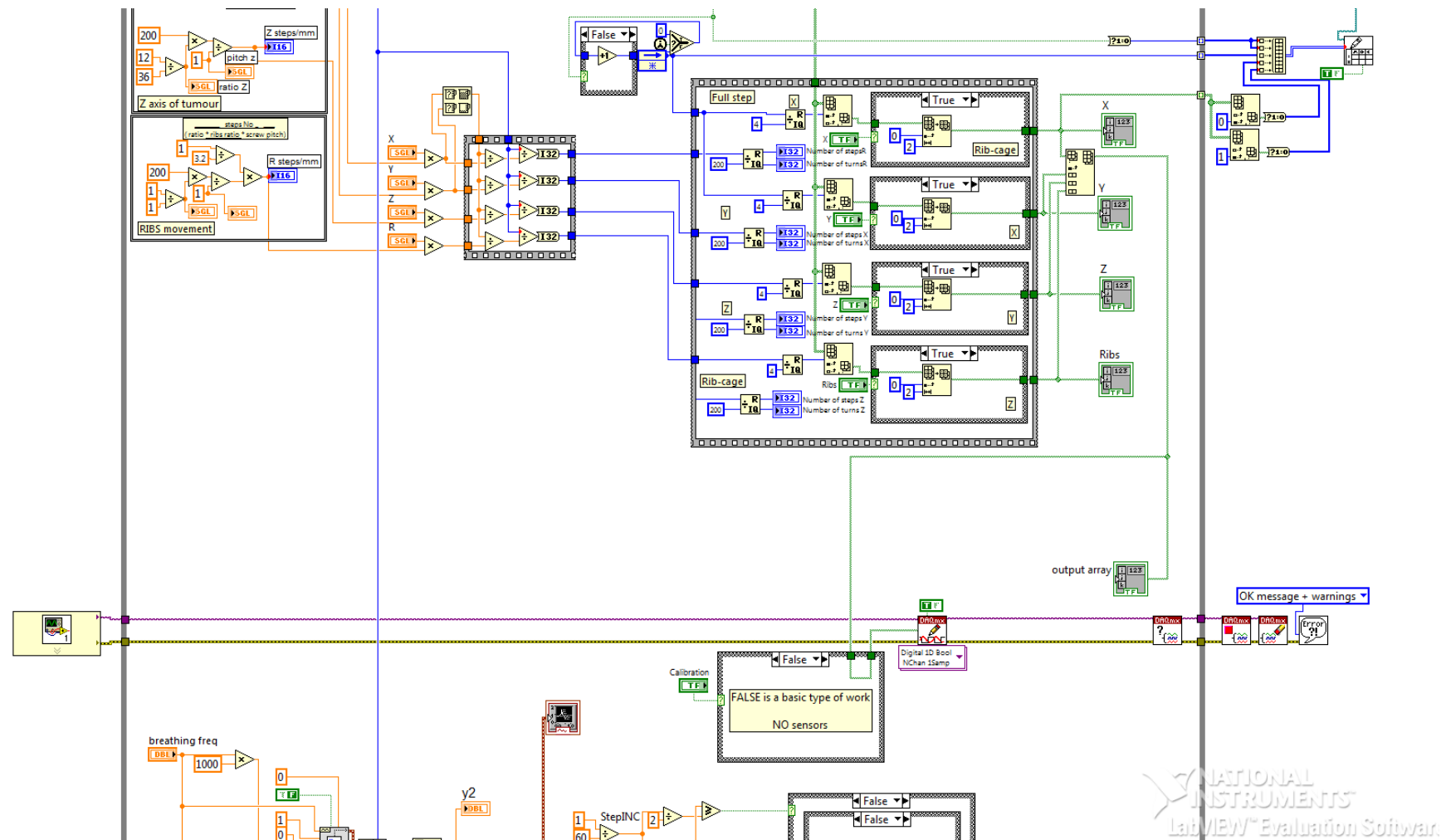
Appendix 2. Program code – motion control by sequence signal

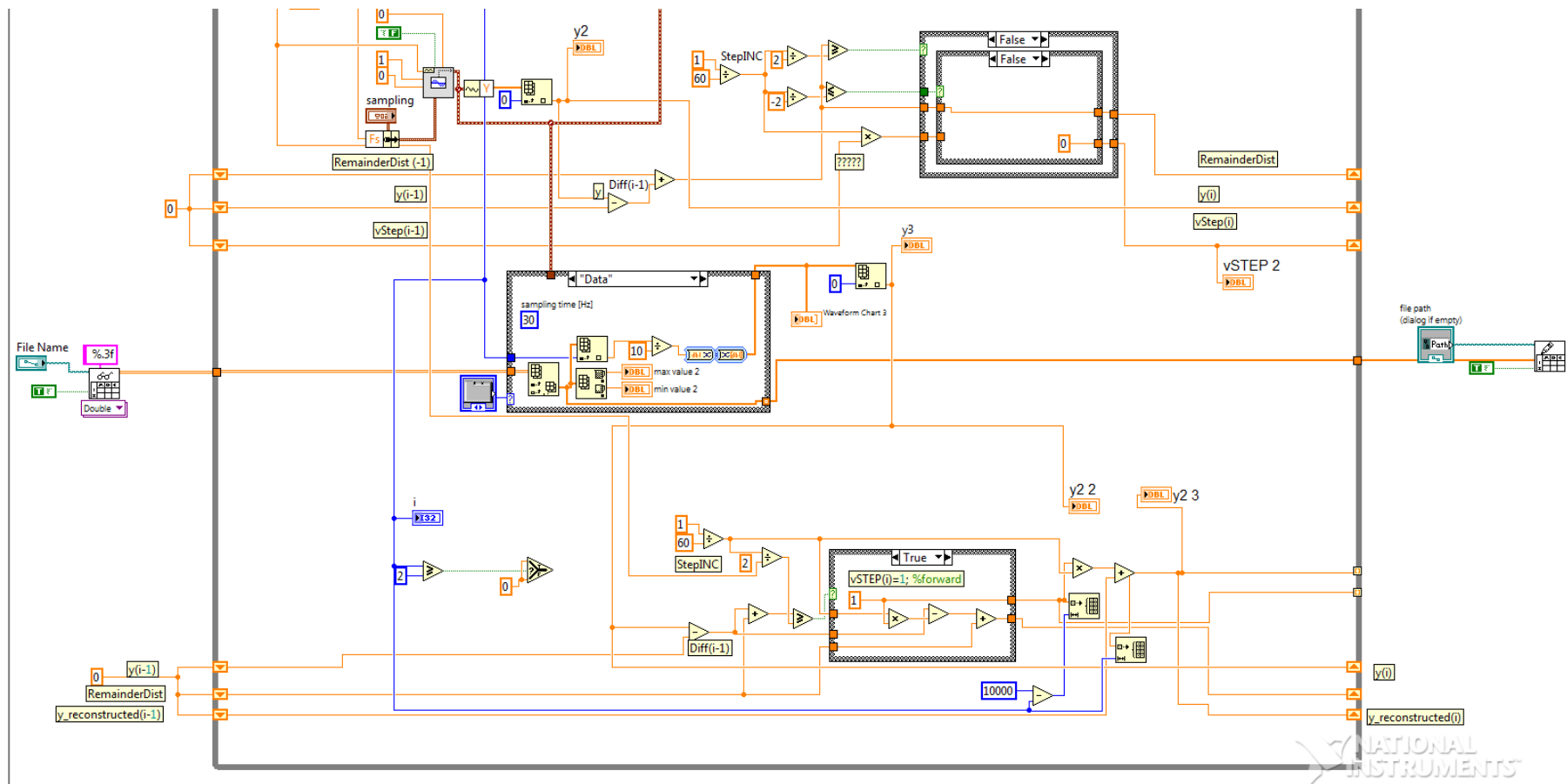
Front panel

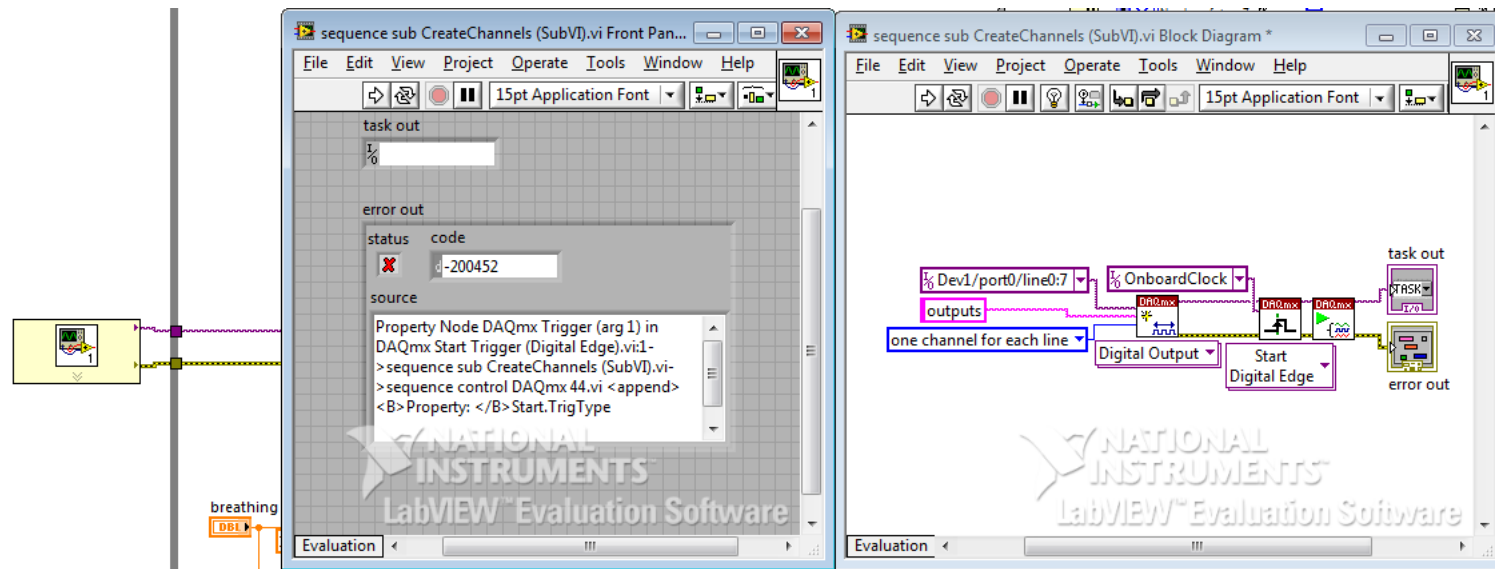


Block diagram









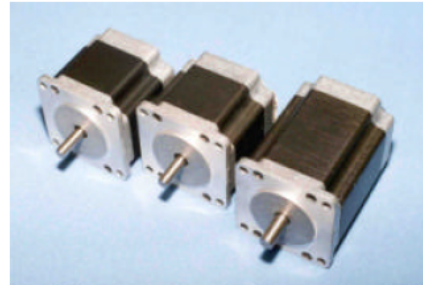
Appendix 3.

High performance size 23 hybrid stepper motors of the HSX series

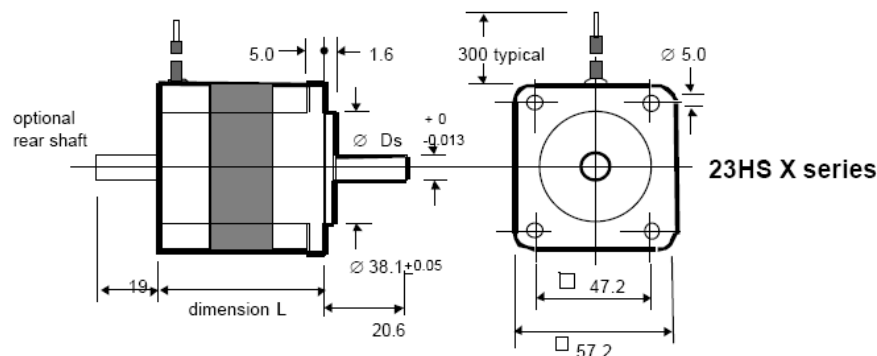
The high performance 23HSX series hybrid stepper motors conform to the international NEMA standard, and provide 200 steps/rev when used with full step drives or 400 steps per revolution in the preferred half step drive mode.

Features:

- High energy Neodymium magnets for increased performance
- 50% more torque than conventional hybrid types
- Choice of single or double shaft options
- Optional encoder or parking brake.
- High quality & Economical prices
- Available with a choice of precision planetary gearheads for increased torque and resolution at reduced speed.
- 8 leads provide the choice of Uni-polar or Bi-polar operation
- Non-standard customised executions available to special order
- Wide range of matched drives and control modules enable complete systems to be economically constructed based on 'in-service proven' technology.



Dimensions mm



Mechanical Specification: 1.8 degree high performance stepper motors

motor type	length 'L' mm	Shaft diameter 'Ds' mm	number of leads	mass Kg	Uni-polar Holding Torque Ncm	Bi-polar Holding Torque Ncm	Rotor Inertia Kgcm ²
23HSX-102	41	6.35	8	0.5	37	47	0.077
23HSX-202	55	6.35	8	0.7	75	98	0.22
23HSX-206	78.5	8.0	8	1.0	125	163	0.34

Electrical Specification:

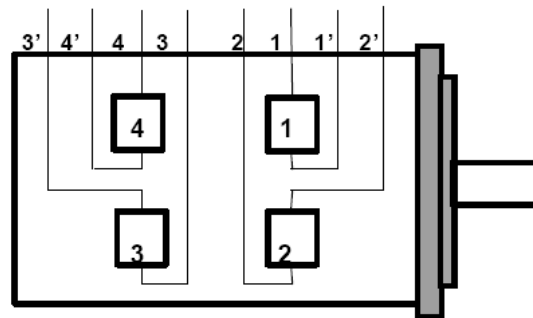
Uni-polar operation				Bi-polar operation	
motor type	Resistance per phase ohms	Current per phase Amps	Inductance per phase mH	Current / phase Series connection Amps	Current / phase Parallel connection Amps
23HSX-102	4.6	1.0	4.6	0.7	1.4 max.
23HSX-202	6.2	1.0	8.8	0.7	1.4 max.
23HSX-206	0.7	3.0	0.9	2.1	4.2 max.
23HSX-306	1.1	3.0	1.7	2.1	4.2 max.

Note Rear shaft may be specified by adding 'E' to part number EXAMPLE: 23HSX-206E

Mclennan Servo Supplies Ltd. Tel: +44 (0)8707 700 700 www.mclennan.co.uk

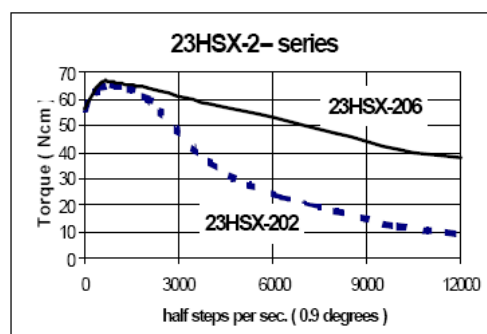
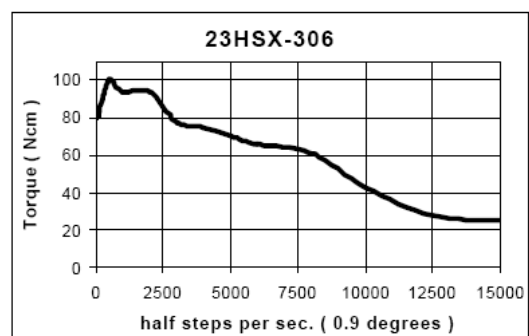
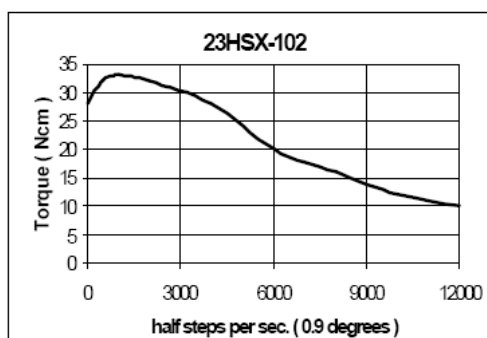


23HSX stepper motor lead colours:



Motor Types	lead or terminal identification							
Lead identity	1	1'	2'	2	3	3'	4'	4
23HSX 102 23HSX 202 23HSX 206 23HSX 306	Red	Red/ White	Yellow/ White	Yellow	Orange	Orange/ White	Brown/ White	Brown

Typical performance



Performance Curves

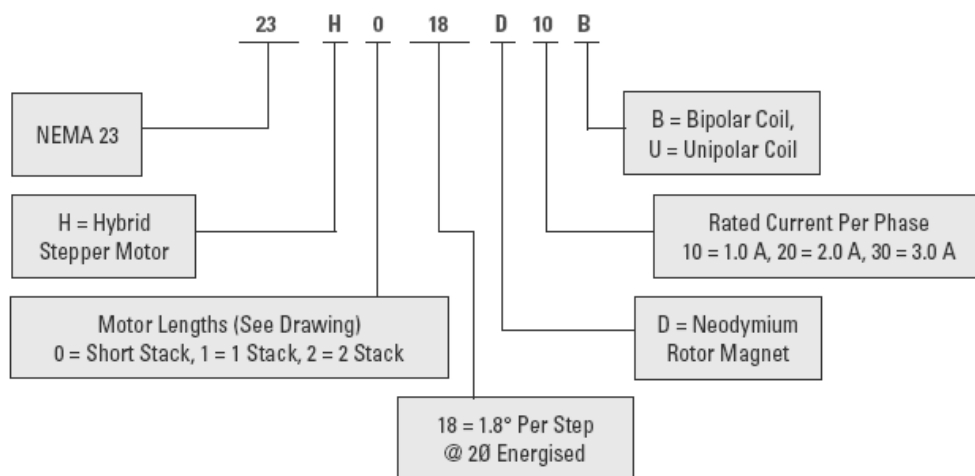
Bi-polar operation, coils in parallel

Motor	Current Per phase (Amps)	Rail Voltage (Vdc)
23HSX-102	1.4	36
23HSX-202	1.4	36
23HSX-206	4.0	70
23HSX-306	4.0	70

Motor Types	Lead or terminal identification							
Permanent Motor type	1	1'	2'	2	3	3'	4'	4
23HSX 1-- 23HSX 2-- 23HSX 3--	Red	Red / white	Yellow / white	Yellow	Orange	Orange / white	Brown / white	Brown
34HSX 1-- 34HSX 2-- 34HSX 3--	Red	Red / white	Yellow / white	Yellow	Black	Black / white	Orange / white	Orange

McIennan Servo Supplies Ltd.

Tel: +44 (0)8707 700 700



Appendix 4.

MSE570 Evo2; Bi-polar 3.5 [A] stepper motor drive

3.5 Amp Bi-polar stepper motor drive

MSE570 Evo 2

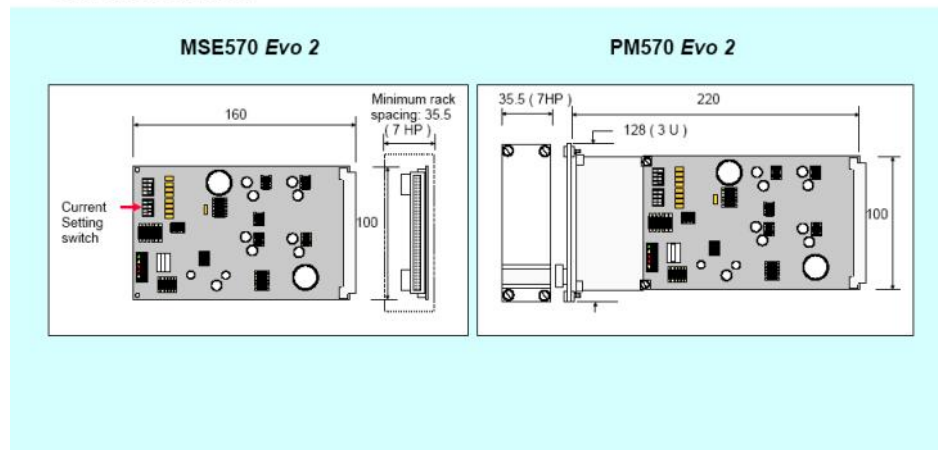
Features

- Bi-polar drive with pre-set drive currents up to 3.5 Amps per phase
- Increased operating voltage up to 48 V
- ½ step drive option for improved damping
- suitable for size 17, 23 & 34 frame size hybrid stepper motors
- Increased efficiency
- No heatsink required
- Reduced width (7HP)
- Single rail supply for both logic and motor
- Standard Thermal protection & condition monitoring
- Operates from external clock & direction signals
- Optional on-board oscillator circuit can be added for simple manual or PLC interfaced control
- Optional matched motherboards (MSB630 & MSB870) for connection via solder free terminals



Models:	Standard unit	Version with front panel kit
	MSE570 Evo 2	PM570 Evo 2
Motherboard options See motherboard data for connections	Version for clock / direction signal input	Version for use with PM600 controller
	MSB630	MSB870

Dimensions: mm



3.5 Amp Bi-polar stepper motor drive

MSE570 Evo 2

The MSE570 is a low cost high performance Eurocard Bi-polar drive designed for mounting in 3U high Euro-racks. Ideally suited for use with Nema size 17, 23 & 34 stepper motors, the unit provides a wide range of current options. Designed for use by original equipment manufacturers, the unit provides a reliable and economic in-service proven' drive solution. Furthermore, the MSE570 design enables users to customise the unit to meet their exact requirements by providing a series of up-grade options which can easily be implemented.



Improved Output stage efficiency

The MSE570 Evo 2 features a chopped constant current output stage with on-board current settings from 0.5 to 3.5 Amps per phase to meet the requirements of virtually any 2 or 4 phase hybrid stepper motor in the Nema 17, 23 & 34 frame sizes. The use of chopped constant current drive techniques combined with the latest developments in power stage technology results in significant advances in efficiency. Furthermore, the output current may be reduced via an external input when the motor is at standstill to reduce temperature rise in the drive and the motor. The drive is designed for use with rail voltages from 15 to 48 Vdc such as MSE173 when up to 7 drives can be incorporated in a single rack together with the power supply. For high speed operation the Power supplies type MSE562 & MSE875 are recommended for single and multi axis applications depending on motor current settings.

New Features

- Increased efficiency
- No heatsink required
- Reduces width
- Increased operating voltage
- Single rail supply for both logic and motor
- Standard Thermal protection & condition monitoring

Choice of full or half step drive

The MSE570 may be set to operate in full step or half step drive. Half step drive is recommended since it provides increased resolution (400 steps/rev. using conventional hybrid stepper motors) together with improved smoothness and damping of motor resonance.

Thermal Protection

A thermal sensor is fitted to prevent overheating of the output stages. The drive may be automatically disabled on over-temperature by setting switch SW1-1 on.

Status LED's for condition monitoring

The MSE570 drive board has five status LEDs. The status LEDs provide a visual indication of drive condition. The function of each indicator is shown in the table. Surface-mount types are fitted as standard, with provision for the user to fit through-board types. These may be soldered into locations at the front edge of the board.

LED 1	Green	Power in on
LED 2	Yellow	Output is disabled
LED 3	Red	Over-temperature fault detected
LED 4	Red	Overload fault detected
LED 5	Yellow	Home phase output

Customising the MSE570 to meet individual application requirements

Choice of external or internal step control

In most applications MSE570 will be operated in conjunction with an external control source consisting of a clock pulse train to determine rate and distance together with a direction signal. Where operation off line from a control processor is required a print on the circuit board is provided for the user to add a simple voltage controlled oscillator to facilitate manual control of the motor drive system.

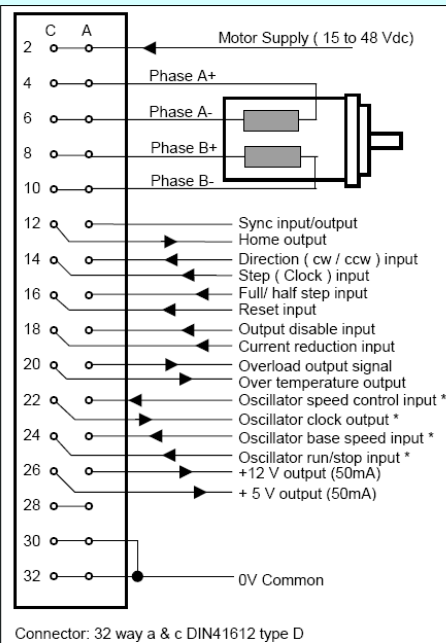


Specification

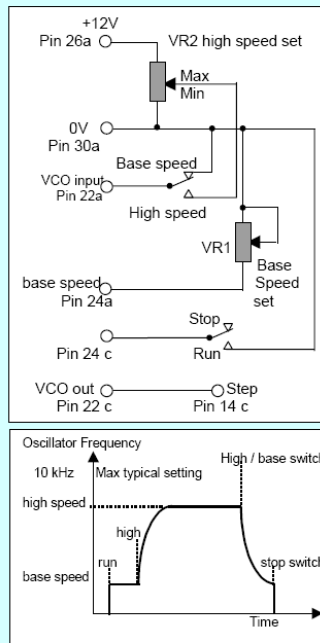
MSE570

Type without front panel		MSE570 Evo 2	Notes
Type with front panel		PM570 Evo 2	
Supply Voltage	Vdc	15-48 + 10% max.	Max ripple: 3 V peak/Peak
Current consumption	Amps	1-2.7 A	Depending on motor selected
Logic Supply Voltage	Vdc	No separate supply required	Use motor supply
Output Stage		2 Phase Bi-polar	Chopped constant current
Output current per phase	Amps	2 Phase Bi-polar	Chopped constant current
		0.5 to 3.5	Set by on-board DIP switch
Step logic		Full step / half step	Open circuit for full step
Control signals		CMOS Schmitt trigger	@ 12V with 10KΩ pull-up resistors
Logic 0: (Low)	Volts	0 to 2	& diode isolation
Logic 1: (high)	Volts	9V to 30V max.	or contact closure to 0V
Monitor Outputs		Open collector NPN transistor	Referenced to 0V
Low Level	Volts	1 max.	@ 30mA max.
High Level	Volts	Open Circuit	+ 24V max.
Auxiliary outputs	Vdc	Regulated +12V @ 50mA max.	For use with on-board oscillator
	Vdc	Regulated +5V @ 50mA max.	
Thermal Protection		Standard	Automatic shutdown protection
Condition monitoring		Standard	Via 5 way LED display + outputs
Up-grade options			User fit options: refer to manual
On board Oscillator		Optional	
Dimensions	mm	100 high x 160 long x 35.5	Std. Eurocard : Use 7HP wide panel

Typical Connections



External Oscillator connections *



Note* Oscillator connections when circuit is fitted to MSE570 Printed circuit board

Stepper motor drive current settings

MSE570

The motor phase current can be set to suit the motor to be driven by the use of the on-board DIP switch fitted to the MSE570. The table below shows the nominal phase currents for each setting

Switch Setting				Nominal Current per phase (Amps)	Typical Motor	Motor Connections	Typical Power Supply consumption @ 36 Vdc (Amps)
SW2-1	SW2-2	SW2-3	SW2-4				
off	off	off	off	0			
off	off	off	on	0.5			1.0
off	off	on	off	0.9	17HS-020	4 lead	1.1
off	off	on	on	1.2	23HS-102	parallel	1.2
off	on	off	off	1.3	23HSX-102	parallel	1.3
off	on	off	on	1.6			1.4
off	on	on	off	1.85	17HS-240	4 lead	1.4
off	on	on	on	2.1	23HS-104	parallel	1.4
on	off	off	off	2.3	23HS-304	parallel	1.7
on	off	off	on	2.5	34HS-109	series	1.8
on	off	on	off	2.7	23HSX-202	parallel	1.9
on	off	on	on	2.9	34HS-106	parallel	2.0
on	on	off	off	3.0	34HS-209	series	2.1
on	on	off	on	3.1	23HS-309	series	2.1
on	on	on	off	3.3	34HS 109	series	2.3
on	on	on	on	3.5	23HSX-206 23HS-309 23HSX-306 34HS-109 34HS-209 34HSX-108 34HSX-208 34HSX-312	parallel parallel parallel parallel parallel parallel parallel series	2.7

Recommended motor-drive-connection combinations shown in **BOLD**

Rack mounting power supply

MSE562

The MSE562 is designed for mounting in a 3U high Eurorack and is ideal for use with the MSE570 drive card. The unit will power up to 2 small motor axes or a single axis using a 34HS size motor. For applications requiring multi-axis operation using a combination of motors requiring high current settings the MSE173 Power supply or MSE875 units are recommended to drive up to 4 motors.

MSE562 provides a 35 Vdc motor rail for high speed operation using the MSE570 Evo 2 drive.

Alternatively, where a motor is to be used at ultra high speed, the MSE562's 70 Vdc rail can be utilised in conjunction with a PM546 Drive



Specification

Width	142.2 mm (28E)	
Depth	220 mm	
Mounting	3U high rack installation	
Connector	DIN41612 type D (32 way a & c)	
AC Supply	230 / 115 Vac 50 or 60 Hz.	

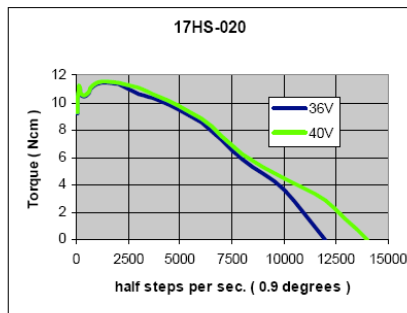
Outputs:

5V \pm 0.25 V	1.5A Max	100mV ripple max.
24V \pm 2.0 V	1.0 A Max.	2.5 V ripple max.
35V \pm 3.0 V	3.0A Max	4.0 V ripple max.
70V \pm 3.0 V	2.0 A Max	14.0 V ripple max.

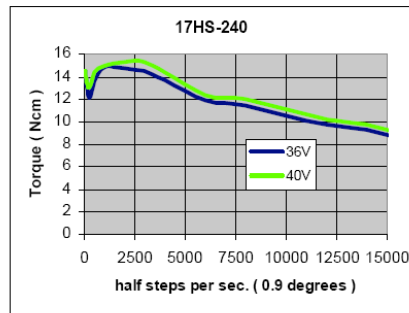
Connections: Refer to handbook

Performance using MSE570 with alternative supply voltages

Size 17 hybrid motors:

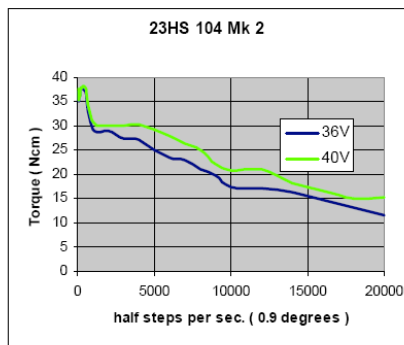


0.9 amps per phase

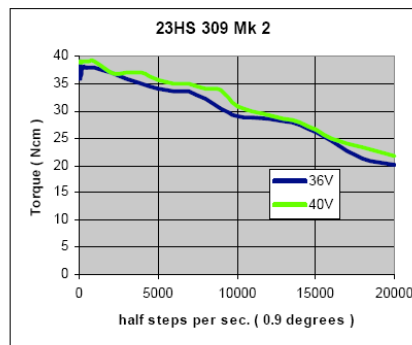


2.3 amps per phase

Size 23 high speed hybrid motors:



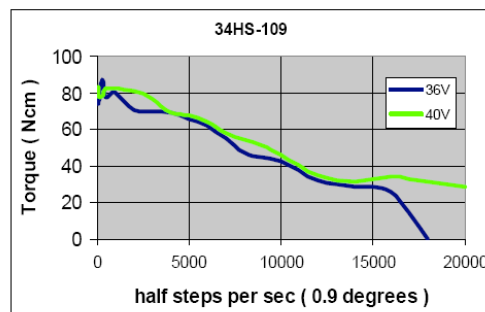
Coils in parallel . 2.1 amps per phase



Coils in parallel, 3.5 amps per phase

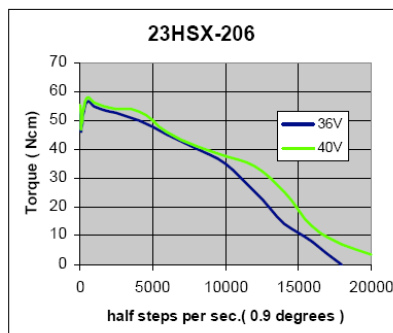
Size 34 high speed hybrid motor:

Coils in parallel, 3.5 amps per phase

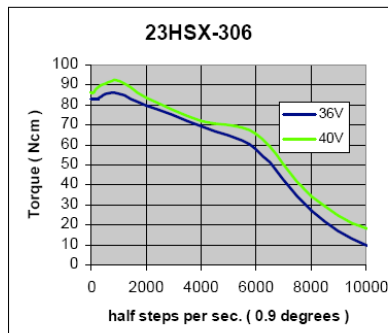


Performance using MSE570 with alternative supply voltages

Size 23 high torque hybrid motors:

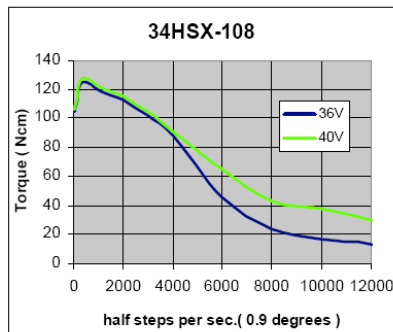


Coils in parallel, 3.5 amps per phase

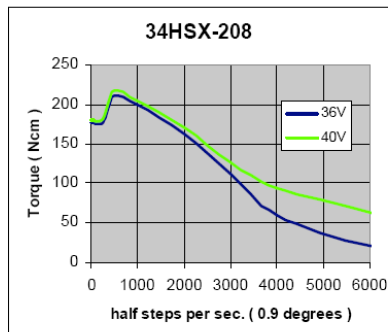


Coils in parallel, 3.5 amps per phase

Size 34 high torque hybrid motors:



Coils in parallel, 3.5 amps per phase



Coils in parallel, 3.5 amps per phase

Quick reference motor guide:

Size 17 motors							
Motor	Frame size	Length	Max Working torque *	Motor	Frame size	Length	Max Working torque *
17HS-020	42 mm	34 mm	8 Ncm				
17HS 240	square	46 mm	12 Ncm				
Size 23 high speed stepper motors				Size 23 high torque stepper motors			
23HS-104	Ø 57 mm	52 mm	20 Ncm	23HSX-206	57 mm square	55 mm	40 Ncm
23HS-309		67 mm	30 Ncm	23HSX-306		78.5 mm	60 Ncm
Size 34 high speed stepper motor				Size 34 high torque stepper motors			
34HS-109	Ø 86 mm	62.3 mm	50 Ncm	34HSX-108	Ø 86 mm	67 mm	80 Ncm
				34HSX-208		94 mm	125 Ncm

Note* Maximum recommended working torque to allow adequate reserve for acceleration

Appendix 5.

NI M Series multifunction DAQ for USB 6229



Technical Sales
United Kingdom
01635 523545
info.uk@ni.com

NI USB-6229

Legacy USB DAQ Device

- 32 analog inputs (16-bit, 250 kS/s)
- 4 analog outputs (16-bit, 833 kS/s), 48 digital I/O (32 at up to 1MHz), and 32-bit counters
- **National Instruments recommends the X Series USB-6343 for all new applications**



Overview

This is a legacy device. National Instruments recommends the X Series USB-6343 multifunction DAQ device for all new applications.

The National Instruments USB-6229 is a USB high-performance M Series multifunction data acquisition (DAQ) module optimized for superior accuracy at fast sampling rates.

The National Instruments USB-6229 is designed specifically for mobile or space-constrained applications. Plug-and-play installation minimizes configuration and setup time, while direct screw-terminal connectivity helps keep costs down and simplifies signal connections.

Each module also features an OEM version. Check the resources tab or use the left navigation to get pricing and technical information.

Driver Software

NI-DAQmx driver and measurement services software provides easy-to-use configuration and programming interfaces with features such as DAQ Assistant to help reduce development time. Browse the information in the Resources tab to learn more about driver software or download a driver. M Series devices are not compatible with the Traditional NI-DAQ (Legacy) driver.

Application Software

Every M Series data acquisition device includes a copy of NI LabVIEW SignalExpress LE so you can quickly acquire, analyze, and present data without programming. In addition to LabVIEW SignalExpress, M Series data acquisition devices are compatible with the following versions (or later) of NI application software – LabVIEW 7.1, LabWindows™/CVI 7.x, or Measurement Studio 7.x. M Series data acquisition devices are also compatible with Visual Studio .NET, C/C++, and Visual Basic 6.

Specifications

Specifications Documents

- Specifications (2)
- Data Sheet

Specifications Summary

General	
Product Name	USB-6229
Product Family	Multifunction Data Acquisition
Form Factor	USB
Part Number	779810-01 , 779810-02 , 779810-03 , 779810-04 , 779810-06 , 779810-07
Operating System/Target	Windows
DAQ Product Family	M Series
Measurement Type	Quadrature encoder , Voltage
RoHS Compliant	Yes
Analog Input	
Channels	32 , 16
Single-Ended Channels	32
Differential Channels	16
Resolution	16 bits
Sample Rate	250 kS/s
Max Voltage	10 V
Maximum Voltage Range	-10 V , 10 V
Maximum Voltage Range Accuracy	3100 μ V
Maximum Voltage Range Sensitivity	97.6 μ V
Minimum Voltage Range	-200 mV , 200 mV
Minimum Voltage Range Accuracy	112 μ V
Minimum Voltage Range Sensitivity	5.2 μ V
Number of Ranges	4
Simultaneous Sampling	No
On-Board Memory	4095 samples

Analog Output	
Channels	4
Resolution	16 bits
Max Voltage	10 V
Maximum Voltage Range	-10 V , 10 V
Maximum Voltage Range Accuracy	3230 μ V
Minimum Voltage Range	-10 V , 10 V
Minimum Voltage Range Accuracy	3230 μ V
Update Rate	833 kS/s
Current Drive Single	5 mA
Digital I/O	
Bidirectional Channels	48
Input-Only Channels	0
Output-Only Channels	0
Number of Channels	48 , 0 , 0
Timing	Software , Hardware
Max Clock Rate	1 MHz
Logic Levels	TTL
Input Current Flow	Sinking , Sourcing
Output Current Flow	Sinking , Sourcing
Programmable Input Filters	Yes
Supports Programmable Power-Up States?	Yes
Current Drive Single	24 mA
Current Drive All	896 mA
Watchdog Timer	No
Supports Handshaking I/O?	No
Supports Pattern I/O?	Yes
Maximum Input Range	0 V , 5 V
Maximum Output Range	0 V , 5 V

Counter/Timers	
Counters	2
Buffered Operations	Yes
Debouncing/Glitch Removal	Yes
GPS Synchronization	No
Maximum Range	0 V , 5 V
Max Source Frequency	80 MHz
Minimum Input Pulse Width	12.5 ns
Pulse Generation	Yes
Resolution	32 bits
Timebase Stability	50 ppm
Logic Levels	TTL
Physical Specifications	
Length	26.67 cm
Width	17.09 cm
Height	4.45 cm
I/O Connector	Screw terminals
Timing/Triggering/Synchronization	
Triggering	Digital

Appendix 6. NI DAQ Card PCI-6229



Technical Sales
United Kingdom
01635 523545
info.uk@ni.com

NI PCI-6229

16-Bit, 250 kS/s, 32 Analog Inputs

- Four 16-bit analog outputs (833 kS/s)
- 48 digital I/O; 32-bit counters; digital triggering
- Correlated DIO (32 clocked lines, 1 MHz)
- NIST-traceable calibration certificate and more than 70 signal conditioning options
- Select high-speed M Series for 5X faster sampling rates or high-accuracy M Series for 4X resolution.
- NI-DAQmx driver software and NI LabVIEW SignalExpress interactive data-logging software



Overview

The National Instruments PCI-6229 is a low-cost multifunction M Series data acquisition (DAQ) board optimized for cost-sensitive applications. Also consider the high-speed M Series devices for 5X faster sampling rates or the high-accuracy M Series devices for 4X resolution and superior measurement accuracy.

Low-cost M Series devices incorporate advanced features such as the NI-STC 2 system controller, NI-PGIA 2 programmable amplifier, and NI-MCal calibration technology to increase performance and accuracy. To learn more about M Series technologies, device specifications, and information on recommended cables and accessories, please refer to the data sheet and specifications.

Driver Software

M Series devices work with multiple operating systems using three driver software options including NI-DAQmx, NI-DAQmx Base, and the Measurement Hardware DDK. Browse the information in the Resources tab to learn more about driver software or download a driver. M Series devices are not compatible with the Traditional NI-DAQ (Legacy) driver.

Application Software

Every M Series data acquisition device includes a copy of NI LabVIEW SignalExpress so you can quickly acquire, analyze, and present data without programming. In addition to LabVIEW SignalExpress, M Series data acquisition devices are compatible with the following versions (or later) of NI application software – LabVIEW 7.x, LabWindows™/CVI 7.x, or Measurement Studio 7.x; or LabVIEW with the LabVIEW Real-Time Module 7.1. M Series data acquisition devices are also compatible with Visual Studio .NET, C/C++, and Visual Basic 6.

Specifications

Specifications Documents

- Specifications
- Data Sheet

Specifications Summary

General	
Product Name	PCI-6229
Product Family	Multifunction Data Acquisition
Form Factor	PCI
Part Number	779068-01
Operating System/Target	Windows , Real-Time , Linux , Mac OS
LabVIEW RT Support	Yes
DAQ Product Family	M Series
Measurement Type	Voltage , Digital , Frequency , Quadrature encoder
RoHS Compliant	Yes
Analog Input	
Channels	32 , 16
Single-Ended Channels	32
Differential Channels	16
Resolution	16 bits
Sample Rate	250 kS/s
Max Voltage	10 V
Maximum Voltage Range	-10 V , 10 V
Maximum Voltage Range Accuracy	3100 μ V
Maximum Voltage Range Sensitivity	97.6 μ V
Minimum Voltage Range	-200 mV , 200 mV
Minimum Voltage Range Accuracy	112 μ V
Minimum Voltage Range Sensitivity	5.2 μ V

Number of Ranges	4
Simultaneous Sampling	No
On-Board Memory	4095 samples
Analog Output	
Channels	4
Resolution	16 bits
Max Voltage	10 V
Maximum Voltage Range	-10 V , 10 V
Maximum Voltage Range Accuracy	3230 μ V
Minimum Voltage Range	-10 V , 10 V
Minimum Voltage Range Accuracy	3230 μ V
Update Rate	833 kS/s
Current Drive Single	5 mA
Digital I/O	
Bidirectional Channels	48
Input-Only Channels	0
Output-Only Channels	0
Number of Channels	48 , 0 , 0
Timing	Hardware , Software
Max Clock Rate	1 MHz
Logic Levels	TTL
Input Current Flow	Sinking , Sourcing
Output Current Flow	Sinking , Sourcing
Programmable Input Filters	Yes
Supports Programmable Power-Up States?	Yes
Current Drive Single	24 mA
Current Drive All	448 mA
Watchdog Timer	No

Supports Handshaking I/O?	No
Supports Pattern I/O?	Yes
Maximum Input Range	0 V , 5 V
Maximum Output Range	0 V , 5 V
Counter/Timers	
Counters	2
Number of DMA Channels	2
Buffered Operations	Yes
Debouncing/Glitch Removal	Yes
GPS Synchronization	No
Maximum Range	0 V , 5 V
Max Source Frequency	80 MHz
Minimum Input Pulse Width	12.5 ns
Pulse Generation	Yes
Resolution	32 bits
Timebase Stability	50 ppm
Logic Levels	TTL
Physical Specifications	
Length	15.5 cm
Width	9.7 cm
I/O Connector	68-pin VHDCI female
Timing/Triggering/Synchronization	
Triggering	Digital
Synchronization Bus (RTSI)	Yes

Appendix 7.

NI DAQ Card 6024E (for PCMCIA)



Technical Sales

United Kingdom

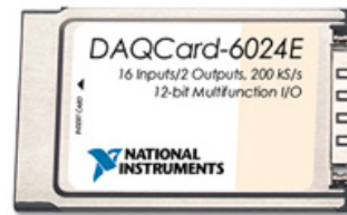
01635 523545

info.uk@ni.com

NI DAQCard-6024E (for PCMCIA)

200 kS/s, 12-Bit, 16 Analog Input Multifunction DAQ

- Consider the NI USB-6251 for 1.25 MS/s, 16-bit analog input; built-in connectivity; and more
- Two 12-bit analog outputs, 8 digital I/O lines, two 24-bit counters
- Use with the LabVIEW PDA Module for handheld data acquisition applications
- NIST-traceable calibration and more than 70 signal conditioning options
- Superior LabVIEW, LabWindows™/CVI, and Measurement Studio integration for VB and VS .NET
- Included NI-DAQmx driver software and additional measurement services



Overview

For laptop-based measurements, National Instruments recommends the NI DAQPad-6015 for USB and NI-DAQmx driver software.

The National Instruments DAQCard-6024E delivers low-cost, high-performance E Series technology to laptop and handheld devices that have a PCMCIA (PC Card) slot. You get up to 200 kS/s, 12-bit resolution on 16 single-ended analog inputs. Depending on your system, the NI DAQCard-6024E can stream to disk at rates up to 200 kS/s. It has digital triggering; two 12-bit analog outputs; two 24-bit, 20 MHz counter/timers; and eight digital I/O lines.

Note for Windows Vista Users

DAQCard (PCMCIA) support for Windows Vista is not available for NI data acquisition devices. For laptop-based measurements with 16-bit resolution, please consider NI M Series for USB.

The mark LabWindows is used under a license from Microsoft Corporation.

Specifications

Specifications Documents

- Specifications
- Data Sheet

Specifications Summary

General	
Product Name	DAQCard-6024E
Product Family	Multifunction Data Acquisition
Form Factor	PCMCIA
Part Number	778269-01
Operating System/Target	Windows , Pocket PC
DAQ Product Family	E Series
RoHS Compliant	No
Analog Input	
Channels	16 , 8
Single-Ended Channels	16
Differential Channels	8
Resolution	12 bits
Sample Rate	200 kS/s
Max Voltage	10 V
Maximum Voltage Range	-10 V , 10 V
Maximum Voltage Range Accuracy	19.112 mV
Minimum Voltage Range	-50 mV , 50 mV
Minimum Voltage Range Accuracy	0.119 mV
Number of Ranges	4
Simultaneous Sampling	No
On-Board Memory	2048 samples

Analog Output	
Channels	2
Resolution	12 bits
Max Voltage	10 V
Maximum Voltage Range	-10 V , 10 V
Maximum Voltage Range Accuracy	10.568 mV
Minimum Voltage Range	-10 V , 10 V
Minimum Voltage Range Accuracy	10.568 mV
Update Rate	1 kS/s
Current Drive Single	5 mA
Current Drive All	10 mA
Digital I/O	
Bidirectional Channels	8
Input-Only Channels	0
Output-Only Channels	0
Number of Channels	8 , 0 , 0
Timing	Software
Logic Levels	TTL
Input Current Flow	Sinking , Sourcing
Output Current Flow	Sinking , Sourcing
Programmable Input Filters	No
Supports Programmable Power-Up States?	No
Current Drive Single	24 mA
Current Drive All	192 mA
Watchdog Timer	No
Supports Handshaking I/O?	No
Supports Pattern I/O?	No
Maximum Input Range	0 V , 5 V
Maximum Output Range	0 V , 5 V

Counter/Timers	
Counters	2
Buffered Operations	Yes
Debouncing/Glitch Removal	No
GPS Synchronization	No
Maximum Range	0 V , 5 V
Max Source Frequency	20 MHz
Minimum Input Pulse Width	10 ns
Pulse Generation	Yes
Resolution	24 bits
Timebase Stability	100 ppm
Logic Levels	TTL
Physical Specifications	
Length	8.56 cm
Width	5.4 cm
Height	0.5 cm
I/O Connector	68-pin VHDCI female
Timing/Triggering/Synchronization	
Triggering	Digital
Synchronization Bus (RTSI)	No

Appendix 8.

NI SC 2075 Connector Card



Technical Sales

United Kingdom

 01635 523545 

info.uk@ni.com

SC-2075

- 3.75 by 5.25 in. breadboard size
- BNC connectors for analog inputs/outputs and digital trigger
- Breadboard connector compatible with E Series and legacy 1200 DAQ devices
- Built-in 15 V power (15 V or adjustable 0-5 V)
- Cost-effective device that is ideal for academic laboratories
- Spring terminals for access to inputs/outputs and timing signals featured



Overview

The SC-2075 is a connector accessory for constructing circuits and connecting them conveniently to virtual instruments. It is compatible with both the E Series and legacy 1200 Series data acquisition boards. A ± 15 V power supply is available to build op-amp circuits. You can choose the power source from the board or external power supply. The breadboard is detachable for replacement after repeated use. The SC-2075 features three binding posts for 15 V outputs, two binding posts for 0-5 V outputs, and two binding posts for analog inputs.

Appendix 9.

IEEE1394a Digital CCD Camera FOculus FO124TB

FOculus – Always a new perspective

Product overview

NET's FOculus product family

With the cameras of the FOculus product line the step into the world of digital image processing becomes very easy and cost effective. Two different housing versions support cameras in monochrome and color, allowing a large selection of different resolutions, frame rates and CCD image sensors. In order to complete the IEEE1394a FOculus family additional 6 models with CMOS image sensors have been added. This diversity provides a solution for a wide variety of vision applications.

General features

FOculus comes in a robust and compact industrial metal housing (29 x 29 x 39mm *Tiny models*, 44 x 29 x 63mm *Small version*) with C/ CS-mount connection, equipped with high-sensitive, high-quality CCD / CMOS image sensors to perform best image quality. The large selection of different sensors (1/3", 1/2", 1/1.8", 2/3") with resolutions of (VGA, WVGA, SVGA, XGA, SXGA, UXGA, QXGA) used within FOculus will provide the best camera for individual applications.

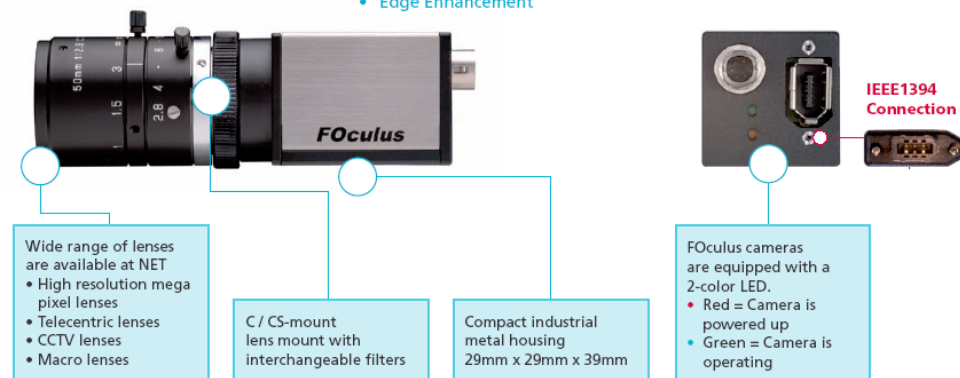
Control features

FOculus offers features acc. to IIDC 1.31 like Trigger & Strobe, Shutter, Gain, White Balance, Brightness, Gamma:

- **Partial Scan**
 - ROI
 - Format 7 free selectable
- **Trigger**
 - Software / ext. Trigger
 - Mode 0 ~ 5
 - Mode 14 – preset multiple shutter mode with a single trigger
 - Mode 15
 - One-Shot / Multi-Shot functionality
- **Binning**
 - Vertical 1x2
 - Full 2x2
- **Video Modes / Formats**
 - Format 0, 1, 2, 7
 - Mode 0 - 7
- **Time Stamp**
- **Multi Camera Auto-Sync**
- **Serial I/O Interface (RS232)**
- **Frame Save Function**
- **LUT (Look up table)**
- **One Pixel Snow Noise Remove**
- **Edge Enhancement**

IEEE1394 interface

The interface cable is tightly secured by the screw lock of the IEEE1394 connector even under a harsh environment.



MACHINE VISION

FACTORY

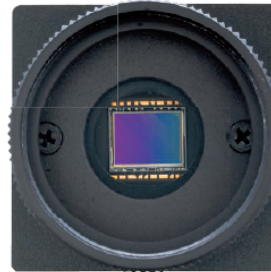
FOculus – Always a new perspective

Technical Data - T-series CCD image sensor

Tiny CCD Features

The Tiny-Series is the smallest camera of the FOculus Family. The robust housing with dimensions of 29 x 29 x 39mm is especially designed to meet the requirements of rough industrial environment.

The FOculus Tiny CCD series consists of 5 mono-chrome and 5 color models with SONY sensors and resolutions from VGA to UXGA and frame rates at full resolution from 16 to 60fps. Besides all standard features of an industrial camera the FOculus tiny cameras also offer some special features like auto white balance and a special overlapping shutter mode.



Tiny CCD



		FO124TB	FO124TC	FO134TB	FO134TC	FO323TB	FO323TC	FO432TB	FO432TC	FO531TB	FO531TC
Image Sensor		1/3" IT CCD ICX244AL/AQ		1/2" IT CCD ICX414AL/AQ		1/3" IT CCD ICX204AL/AK		1/2" IT CCD ICX267AL/AQ		1/1.8" IT CCD ICX274AL/AQ	
Effective Pixel		659 (H) x 494 (V) VGA		659 (H) x 494 (V) VGA		1034 (H) x 779 (V) XGA		1388 (H) x 1040 (V) SXGA		1628 (H) x 1236 (V) UXGA	
Data Path		8bit or 12bit BW/Raw RGB + YUV422									
Pixel Size		7.40 x 7.40 μm		9.90 x 9.90 μm		4.65 x 4.65 μm		4.65 x 4.65 μm		4.40 x 4.40 μm	
Frame Rate		60 fps 86 fps (format7)		60 fps 86 fps (format7)		30 fps 36 fps (format7)		15 fps 20 fps (format7)		15 fps 16 fps (format7)	
Scanning System		Progressive Scan									
Binning		Pixel Binning BW & FO531TC									
Synchronization		Internal									
Trigger	Edge	Rising Edge or Falling Edge									
	Mode	Mode 0 ~ 5; 14, 15									
	Source	External Trigger or Software Trigger									
Strobe		Active High, Support Normal Mode or Trigger Mode									
SIO(RS-232)		IIDC V. 1.31 version : Pass through or NET Command									
Digital Interface/Transfer Rate		IEEE1394.1 port(6pin) / 400Mbps									
Gain Control		Manual: 0 ~ 25 dB; Auto Gain				Manual: 0~27 dB Auto Gain	Manual: 0~25 dB Auto Gain	Manual: 0 ~ 27 dB; Auto Gain			
Shutter		Manual: 1μs ~ 3600s / Auto Shutter									
Gamma		0.4 ~ 2.5									
S/N Ratio		56 dB or better									
Advanced Features		ROI; One Shot & Multi Shot; Multi Camera Auto Sync; High Speed Up Trigger Framerate, LUT, Frame Save									
Lens Mount		C- / CS-mount									
Dimension		29 (W) x 29 (H) x 39 (D)mm									
Operating Temperature		- 5°C to + 45°C									
Regulations		FCC, CE, RoHS									
Camera Specifications		IIDC 1394-based Digital Camera Specification v1.31									

CESSING

QUALITY CONTROL

Appendix 10.

ICSE 2009 conference paper.

3. Graduate Student Papers

LabVIEW Motion of Radiation Therapy Phantom

Marek Augusciak, Olivier C.L. Haas, Imke Land

*Control Theory and Application Centre (CTAC), Engineering and Computing Faculty, Coventry University,
Priory Street, CV1 5FB, Coventry, UK
Tel, Fax: +44(0)24 76888052, E-mail: ctac@coventry.ac.uk*

Abstract: This paper is describing new dynamic thorax phantom for adaptive radiation therapy (ART), which will be used for lung cancer treatment. This model was manufactured from tissue equivalent materials to human body parts to be able absorb and scatter ionising radiations in a way that is identical to bones or blood. This thorax phantom and its tumour are moving in three directions 3D and have got independent and different types of motion.

This Methods and Advanced Equipment for Simulation and Treatment in Radiation Oncology (MAESTRO) project was developed by CTAC with cooperation of University Hospital Coventry and Warwickshire (UHCW) and its period was 5 years, since 2004 to 2009.

Keywords: Image guided radiation therapy (IGRT), Computer aided control system design, Frequency control, Linear estimation, Medical systems, Simulation

This item has been removed due to third party copyright. The unabridged version of this thesis can be viewed at the Lanchester library, Coventry University.

3. Graduate Student Papers

This item has been removed due to third party copyright. The unabridged version of this thesis can be viewed at the Lanchester library, Coventry University.

3. Graduate Student Papers

This item has been removed due to third party copyright. The unabridged version of this thesis can be viewed at the Lanchester library, Coventry University.

This item has been removed due to third party copyright. The unabridged version of this thesis can be viewed at the Lanchester library, Coventry University.


3. Graduate Student Papers

This item has been removed due to third party copyright. The unabridged version of this thesis can be viewed at the Lanchester library, Coventry University.

This item has been removed due to third party copyright. The unabridged version of this thesis can be viewed at the Lanchester library, Coventry University.

Appendix 11.

ICSE 2009 conference – poster

LabVIEW Motion Control of Radiation Therapy Phantom	
Marek Augusciak, Olivier C.L. Haas	
Control Theory and Applications Centre (CTAC), Engineering and Computing Faculty, Coventry University, Priory Street, CV1 5FB, Coventry, UK Tel, Fax: +44(0)24 76888052, E-mail: auguscim@coventry.ac.uk , o.haas@coventry.ac.uk	
	
Project objectives:	Improve LabVIEW program to generate the phantom motion Implement frequency based motion control for stepper motor

This item has been removed due to third party copyright. The unabridged version of this thesis can be viewed at the Lanchester library, Coventry University.